RSC Advances

ROYAL SOCIETY OF CHEMISTRY

www.rsc.org/advances

Thiophene-based push-pull chromophores for small molecule organic solar cells (SMOSCs).

Volodymyr Malytskyi,[a, b] Jean-Jacques Simon [b], Lionel Patrone*[b] and Jean-Manuel Raimundo*[a]

Received (in XXX, XXX) Xth XXXXXXXXX 20XX, Accepted Xth XXXXXXXXX 20XX
DOI: 10.1039/b000000x

The last decade has witnessed a rapid progress of organic photovoltaics boosted by the design and synthesis of novel π-conjugated small donor-acceptor molecules (mainly thiophene-based chromophores) and by the control and optimization of both device processing and fabrication. Although some important progress has been reached, current challenges remain to further improve their efficiency, durability and cost-effectiveness in order to compete with silicon-based solar cells. The review will provide to the scientific community both general and deep information on the structure-properties relationships related to the photocurrent efficiencies comprising a detailed I/V characteristics. It will highlight guidelines for designing new efficient and emerging alternatives to conjugated polymers on the basis of thiophenic chromophores representing, to date, the most widely used class of organic materials for such purpose) as well as important information on device processing or fabrication factors that could influence their performances.

Introduction.

Organic solar cells (OSCs) constitute the third generation solar cells technology and are nowadays of crucial interest because they can offer a good alternative to high cost solar cells based on silicon. Indeed, organic materials display several advantages compared to their inorganic counterpart, such as for instance a lighter weight, a facile chemical tailoring to fine tune their optoelectronic properties and an ease of processability, opening thus the possibilities of developing large-area and cost-effective solar cells based on ecofriendly technologies.

The first attempts to fabricate organic solar cell were described in the early 80's by Chamberlain from thin organic layers sandwiched between two dissimilar electrodes. Such devices have shown very low solar power conversion efficiency up to 0.3% (PCE)[1] that strongly depends on the nature of the electrodes. A major breakthrough was achieved in 1986 by Tang[2] with the possibility of producing efficient solar cells based on organic semiconductors. A two-layer device fabricated from a copper phthalocyanine (CuPc, as donor material) and perylene tetracarboxylic derivate (PV, as acceptor), end-capped respectively by an ITO and Ag electrodes, led to a PCE value near 1%. Interestingly, in such devices, the charge generation efficiency was found to be relatively independent of the bias voltage. The donor-acceptor interface (p-n junction) provides efficient exciton dissociation in comparison to single layer solar cells. These findings stimulated new works in the field of organic and polymer-based solar cells. A new milestone was reached with the discovery of C_{60} as a highly efficient acceptor.[3] Although the development of new acceptor materials is strongly requested and seems to be promising[4], fullerenes C_{60}, C_{70} and their analogues $PC_{61}BM$, $PC_{71}BM$ ([6,6]-phenyl-C_{61}-butyric acid methyl ester) and [6,6]-phenyl-C_{71}-butyric acid methyl ester respectively) are readily used and became a traditional acceptor part in OPV cells.

In spite of achieving good photovoltaic conversion efficiencies with the so-called planar heterojunction cells (PHJ), their performances are rather limited due to the small area (interface) contributing to the photovoltaic effect. To circumvent this dilemma, researchers have turned out their attention to the development of bulk heterojunction (BHJ). In such structures the p-type and n-type materials are co-deposited, in a determined ratio, to ensure a greater dissociation irrespectively to the thickness. Nevertheless, despite to be a very attractive solution, numerous problematic originate and need to be solved to ensure perfect reproducibility of the devices structures.

Among them, batch-to-batch reproducible synthesis is somewhat difficult to implement, that is why since very recently scientists have paid more and more attention in the use of small organic molecules.[5] Using this approach new OPV devices have been fabricated and fast-optimized leading to power conversion efficiency (PCE) values as high as 11%.[6]

For characterizing overall performance of solar cells devices it is appropriate to use few parameters. First of them is an open-circuit voltage, V_{OC}, which shows the maximum possible voltage which could be extracted from a device. In first approximation V_{OC} is determined by an energy difference between LUMO level of an acceptor molecule and HOMO of donor one. Keeping in mind that in most cases fullerene derivatives are used as an acceptor, a low HOMO level of donor is responsible for high V_{OC}. The maximum current delivered by a device in short circuit conditions, I_{SC}, characterize the possibility of charge generation by the cell. In consequence, it depends from other factors, namely light absorption properties and effectiveness of exciton separation. While amelioration of optical properties usually demands a low bandgap of a donor component, the effective charge separation could not occur if LUMO of donor is less than ≈0.3 eV higher than LUMO of acceptor. So, obviously, there is a competition to find an optimal donor molecule with a low enough HOMO level, a high enough LUMO and at the same time not a large bandgap between them. In OC or SC conditions photovoltaic cell do not produce any power ($W = V \times I$). The operating point is a condition with the maximum power and values of V_m and I_m lower then V_{OC} and I_{SC} respectively. A ratio between products $V_m \times I_m$ (means maximum achieved power) and $V_{OC} \times I_{SC}$ (means maximum possible power) is called a fill factor, FF, and in generally characterizes the efficacy of the cell structure. It could depend on very various factors among which the active layer morphology and charge carrier mobilities are very important. So, solubility properties of active compounds and their solid state electrical properties should also be taken in

consideration during a molecular engineering of new organic materials for photovoltaic application.

In this article, we will focus on various criteria that influence power conversion efficiencies in small organic molecules, mainly based on the thiophene skeleton, used in organic solar cells from a chemist's viewpoint with the aim to introduce both a variety of exotic organic materials and insights that are potentially applicable to small molecule organic solar cells.

D-A type.

Despite their extensive uses as key–components in the field of Graëtzel solar cells (*i.e.* DSSC), D-A structures have gained only recently a strong interest for OPVs devices.

Among them, triarylamine-based conjugated chromophores end-capped with acceptors, such as di- or tri-cyanovinyl groups, are some representatives' D-A structures that have been largely tested.[7,8] Elongation of the π-conjugated system between the donor and the dicyanovinyl acceptor edge substituents by the increment of thiophene units (from 3 to 6 units) does not affect significantly the λ_{max} on such structures. Interestingly unexpected, the highest molar extinction coefficient was attained for the tetrathiophene (4T) analogous derivative. As anticipated consecutive change of the acceptor moiety from di- to tri-cyanovinyl (DCV, TCV) leads to a significant bathochromic shift, due to an increase of the electron withdrawing strength, (from 514 to 629 nm and 524 to 643 nm for 2T and 3T derivatives, respectively)[9] associated with a reduced molar extinction coefficient. Modification of the donor unit with a fluorene or heterofluorene such as carbazole constitutes an attractive way to tailor and enhance optical properties. Thus, the substitution of a benzene ring on the triphenylamine (TPA) fragment by a fluorene leads to a slight bathochromic shift with a concomitant increase of the PCE values (Scheme **1**).

Scheme 1

Modification of the donor part by a dendritic-like structure based on two TPA units (**3a** and **3b**) has a dramatic effect on electrochemical properties. It was shown that such changes reduce the HOMO energy level to 0.15-0.16 V as well the LUMO to 0.11-0.13 V compared to their linear analogs **3a** relied on the donor strength. This fact results in a higher energy band gap estimated from cyclic voltammetry and correlates well with the observed optical gap. The highest PCE value (2.67 %) was obtained for the device based on the compound **1c** prepared by bilayer vacuum deposition and annealed for 20 min at 100°C.

Further substitutions on the TPA part were envisioned by Ko et al.[10,11] in order to fine tune the optical and electrochemical properties of the donating part (Scheme **2**).

Scheme 2

It can be noticed herein that shorter π-conjugated spacer lengths provide, in that case, comparable conversion efficiencies up to 2.46 % for **5c**, which can be attributed to higher J_{SC} value (8.91 $mA \cdot cm^{-2}$) compared to **1a** (4.92 $mA \cdot cm^{-2}$) due to an optimized performance architecture in the BHJ blend with $PC_{71}BM$ compared to the PHJ with C_{60} for **1a**. Further optimization, of the phase segregation upon addition of 1-chloronaphthalene (CN) as an additive, leads to a significant enhancement of the conversion efficiency up to 3.66 %.

Additional improvement of the photophysical properties has been achieved with the fused benzothiophene **6** (Scheme **3**) instead of 2-thienylbenzene as spacer.[12] Therefore, compared to **5c**, better optical and hole-mobility properties are attained. Subsequent device made from a blend of **6** and $PC_{71}BM$ (1:3) with TiO_x layer affords 4% conversion efficiency.

Scheme 3

Silole bridged bithiophene (DTS) spacer has been used in order to gain further insights for the design of SMOSCs in the above TPA compounds series.[13] Thus, introduction of the DTS moiety along the π-conjugated spacer (**7**) does not change significantly the optical properties (λ_{max} = 537 nm ε = 45 800 M^{-1} cm^{-1}) compared to **5c** (λ_{max} = 536 nm ε = 32 174 M^{-1} cm^{-1}) but results in a refinement of the HOMO and LUMO energy levels which are lowered by almost 0.5 V. (Scheme **4**).

Scheme 4

Fabrication of a planar-mixed heterojunction (PMHJ), by vacuum deposition, with **7** and fullerenes derivatives in the molar ratio (1:1) achieves conversion efficiency up to 2.69 % and 3.82% with C_{60} and C_{70} respectively. The higher PCE originates from the high V_{OC} potentials achieved in these devices (0.88 V and 0.83 V respectively compared to 0.774 V for **5c**) as a consequence of the energy levels optimization.

Besides the common covalent bridging strategy, the design of "dwarf" chromophores (*i.e.* minimizing the size of the chromophore) has recently emerged to be a possible alternative for controlling the batch-to-batch reproducibility as well as to get low cost systems associated with high purity and optimized photophysical properties.[14, 15] Therefore, both Roncali's group and Würthner's group have demonstrated the validity of this concept throughout the synthesis of the smallest push-pull dyes based on thiophene rings (Schemes **5** and **6**).

Scheme 5

Optimized chemical structures have been obtained by varying only the acceptor edge substituent. On the basis of this series the best performances were achieved with the compound **8c** leading to PCE up to 3.0% in blended films with $PC_{61}BM$ 55 wt %. Further devices optimizations were made, for instance replacing $PC_{61}BM$ by $PC_{71}BM$, and the hole-collecting PEDOT: PSS layer by MoO_3, and using a Ba/Ag metal electrode leading to attain remarkable PCE value of 4.5%.

Scheme 6

However, by changing the donor part from dialkylamino to TPA, Roncali et al. have obtained a reasonable value of 2.53 % of conversion efficiency on un-optimized architectures devices (Scheme **6**). In furtherance of their continuous efforts on the understanding of structure-properties relationships, the covalent bridging strategy was applied on the acceptor part in order to optimize the light harvesting properties (Scheme **7**). Thus

substitution of the dicyanovinyl (**9**) by the thieno-fused-dicyanoindene (**10**) moiety leads to a 110 nm red shift, as expected. Although this bathochromic shift is accompanied by a two-fold decrease of the molar extinction coefficient an enhanced PCE (2.97 %) was clearly evidenced. Additional work on fine-tuning properties of the donating group has been done in order to give a better accuracy of the HOMO levels and bandgap control as well as to gain further information on the design of such chromophores (Scheme **7**).[15] Shortening the π-conjugated spacer results in a 55 nm hypsochromic shift (from **9** to **11**) while an average shift of 27 nm was observed for compounds **12** to **13** because of the lower resonance energy of the thienyl ring. As a consequence, higher FF and J_{SC} characteristics were obtained beside a decrease of the V_{OC} leading to an increase of the photocurrent (1.60–1.70 %). Interestingly, the best performances were obtained for compound **14** evidenced by the highest J_{SC} (6.80 mA.cm^{-2}) and PCE (1.92 %) values, whereas the bridged carbazole analogous **15** did not improve the photocurrent.[16]

Scheme 7

Additionally it has been demonstrated that **16,** a structural isomer of **10**, exhibits a higher dihedral angle leading to a less planar π-conjugated system. According to the structural modification of the chromophores general behaviors can be deduced that are consistent with the optical and electrochemical experiments (Scheme **8**).[17] For instance, bridging the dicyano group leads to a positive shift of the reduction potential (from **9** to **10** and **16**-**19**) due to a better stabilization of the radical anion upon reduction attributed to the formation of the cyclopentadienyl anion radical on those structures. Replacement (from **10** to **17**-**18**) of the phenyl ring by thienyl or introduction of methoxy groups significantly increases the HOMO levels. Optical observations were in agreement with the cyclic voltammetry experiments, thus the narrow bandgap for **17** and **18** compared to **10** is related to an increase of the HOMO level. Evaluation of the performances of these chromophores has been achieved using a bilayer planar heterojunction with the following architecture ITO/PEDOT: PSS (40nm)/**10**,**16**-**19** (35nm)/C_{60} (30nm)/Al (100nm). The highest performance give a PCE of 2.97% for **10** (V_{OC}= 0.97 V, J_{SC}= 5.32 mA.cm^{-2} and FF= 0.52) while **16** exhibits the lowest PCE according to the optical and electrochemical data (0.57%, V_{OC}= 0.71 V, J_{SC}= 2.07 mA.cm^{-2} and FF= 0.35).

Scheme 8

Further interesting insights were obtained from the previous D-A series by the insertion of a second acceptor along the π-conjugated spacer. The elegant combination of two different acceptors give rise to chromophores with the D-A-A configuration.[18, 19, 20] These D-A-A structures exhibit both narrow bandgap and lower HOMO levels compared to their D-A counterparts (Scheme **9**). Thus, insertion of the benzothiadiazole (BT) unit in the D-A structures fosters the creation of quinoidal mesomeric forms over the π-conjugated skeleton resulting to a bathochromic shift of the maximum of absorption. Moreover, judicious choices of the substituents as well as the aromatic rings over the π-conjugated backbone are key parameters to control both energy levels and bandgap. For instance, substitution of the phenyl ring by a thienyl leads to a substantial red shift of 90 nm of the maximum of absorption (*i.e.* **22a**→**20a** and **22b**→**20b**). Effective PMHJ solar cells (AM 1.5-100 mW/cm^2) have been obtained by vacuum-deposition of compounds **20** to **22** as donors and C_{70} as acceptor (blended films in ratio 1:1.6) with photocurrent characteristics ranging from 5.00 to 6.60 %. By varying the nature of the inserted acceptor from BT to pyrimidine (**20a**→**21**) a lowered HOMO level and an increased V_{OC} where attained. Hence, solar cell performances of PMHJ devices (**21**: C_{70}, in ratio 1:1) have shown enhanced efficiency up to 6.40 %.

Precise adjustments of electrical parameters can be also implemented to improve the generated photocurrent. Therefore, accurate balance control between the photovoltage and the photocurrent causes a notable enhancement of the PCE up to 6.80 % for **22b**. Optimization of the cell structure is also critical for boosting cells performances. As exemplified hereby it was shown that an ultrathin layer of 1 nm of Ca before the Ag cathode leads to an increase of the conversion efficiency from 4.41 to 5.28 % for a PMHJ solar cell based on **20b** and $PC_{61}BM$.[21]

Scheme 9

A_3D type

Optimization of the light harvesting properties of the chromophores is a crucial point that needs to be addressed in order to improve the conversion efficiencies. An elegant solution to tackle this problem has been developed by several groups, from 3D-structures mainly based on the TPA core. Indeed, TPA structures are of peculiar interest for this problematic, as they have already demonstrated their ability to generate efficient linear chromophores and allow the possibility to introduce various acceptor edge groups on the same skeleton. Hence, through an iterative pathway, a star-shaped series of TPA has been synthetized by Roncali et al. in which the π-conjugated arms offer variability in term of length, nature and acceptor edge groups. Using this strategy, dissymmetric structures are therefore attainable with both a controlled acceptor load and morphology structures (Scheme **10**).

Scheme 10

As demonstrated on bulk heterojunction devices, from the structures **23** to **25**, a noticeably linear improvement in power conversion efficiencies is observed ranging from 0.46 to 1.17 % respectively.[22] Explanations of this observation originate from (*i*) the fact that there is a linear dependency of the intramolecular charge transfer (ICT) with the number of acceptors present over the π-conjugated backbone and (*ii*) an enhanced V_{OC} (**23**: 0.48 V; **24**: 0.72 V; **25**: 0.89 V; *i.e.* lower HOMO levels). Moreover increasing the number of acceptor groups promotes different spatial arrangement in the solid-state with strong intermolecular D-A interactions that can affect also the PCE. As expected, the highest V_{OC} (0.96 V) was obtained for the compound **26** containing three dicyanovinyl end-groups, however, reduced PCE (1.02 %) is achieved due to a lower filing factor compared to **25**. Furthermore, optimizations of these rudimentary devices were undertaken to boost the power conversion efficiencies. For instance, addition of a thin film of LiF between the C_{60} acceptor

layer and the Al electrode provides an impressive increase of the PCE from ~ 1% to 1.85 % (with V_{OC}= 1.15 V and I_{SC} = 4.59 mA.cm^{-2})[23] for the device made from **26**.

Taking into account these aspects the strategy is valid and worth pursuing as the observed synergistic effects lead to considerable improvement of the PCE.

With the aim to enhance the photovoltaic output signals, several structural modifications have been conducted on the TPA derivatives based on the previous obtained results. Interestingly, contrary to polymeric or polycrystalline organic structures, amorphous TPA based chromophores have the advantage not to require control of the molecular orientation. First attempts have been focused basically on the hole-transport properties by engineering TPA derivatives with linear p-type organic semiconductors acting as the donor material in PV devices. Thus, structure-like **28** (Scheme **11**) has been synthetized and tested as donor material in a bilayer heterojunction with C_{60} as the acceptor. PCE not exceeding 0.32 % (V_{OC}= 0.67 V; J_{SC}= 1.70 mA.cm^{-2})[24] has been attained with such compound as mainly a consequence of a low filing factor. Although low PV efficiency has been obtained, **28** demonstrated good hole-mobility properties up μ_h = 1.10 10^{-2} cm^2 V^{-1} s^{-1} which is very promising for PV applications.

Scheme 11

Subsequent replacement of one or two arms by unit end-capped with DCV (**29** and **30** respectively, Scheme **12**) as acceptor has led to a drastic improvement of the PCE (1,80 % and 2,02 % respectively) due to a large increase of the short-circuit current density and V_{OC} (**29**: V_{OC}= 0.85 V; J_{SC}= 5.30 mA.cm^{-2}; **30**: V_{OC}= 1.07 V; J_{SC}= 5.83 mA·cm^{-2}) that are intrinsically correlated to the ICT.[25]

Scheme 12

To achieve improved results and gain further insights into structure-properties relationships, bridged-thienyl spacers have been introduced in the TPA molecular skeleton. Covalently bridged-spacers are well-known to exalt photophysical properties compared to their un-bridged analogues.[26] For instance, Li[27] and co-workers used 3,6-dihexyl-thieno[3,2*b*]thiophene as electron relay between the TPA donor part and the dicyanovinyl end groups for the construction of star-shaped structures (Scheme **13**). Devices made from a blend of **31** and $PC_{61}BM$ or $PC_{71}BM$ in weight ratio 1:2 with a Al/Ca as cathode leads to high-performance devices under standard illumination conditions (respectively 1.63 % and 2.87 %) associated with exceptional high J_{SC} values (4.66 to 6.80 mA.cm^{-2}) and V_{OC} (0.90 V and 0.96 V) that are among to the best reported in literature.

Scheme 13

To achieve readily processable active materials, Lin et al. have synthetized star-shaped structures based on the TPA scaffold using alkyl-cyanoacetate (ACA) as acceptor.[28] Incorporation of ACA aims at introducing simultaneously solubilizing and acceptor groups on the molecular π-conjugated backbone and avoids tedious multistep reactions. As a result, successful synthesis of **32** has been achieved associated with a good solubility in common solvents and high molar extinction coefficient (7.3 10^4 M^{-1} cm^{-1}) (Scheme **14**). Absorption maximum is red-shifted by 65 nm compared to the unsubstituted analogue **28** because of the intramolecular charge transfer. Additionally, **32** retains relatively high hole-mobility, measured by the space charge limited current (SCLC) method, up to 1.5 10^{-3} cm^2 V^{-1} s^{-1} guarantied effective charge carrier transport and reduced photocurrent loss. Optimized BHJ solar cells made from **33** in conjunction with $PC_{71}BM$ (best weight ratio 1:2 respectively) as the electron acceptor gave under standard illumination condition AM1.5 a power conversion efficiency, without any post-treatments, of 3.60% (V_{OC}= 0.89 V, J_{SC}= 7.30 mA.cm^{-2}). Furthermore, the photophysical properties of the star-shaped chromophores **32** were compared with linear and 2D analogous chromophores (**33**–**34** Scheme **15**) in order to investigate the structural effects on the above properties.[29]

Scheme 14

As expected, on the linear analogous derivatives, increment of the number of thiophene unit from 1 to 3 (**33a** to **33c**) led to a 20 nm red shift of the maximum of absorption whereas increasing the number of arms around the TPA core it remains almost unchanged (**32**, **33c** and **34** 494, 498, 494 nm respectively). In addition, the energy differences between the HOMO levels of the chromophores and the LUMO level of $PC_{71}BM$ are sufficient to ensure the exciton dissociation and lead to a high V_{OC} (from 0.87 to 0.99 V). Relative to **33a**-**33c**, chromophores **34** and **32** exhibit the highest PCEs (at same weight ratio with $PC_{71}BM$ 1:2), attaining 4.03% for **34** (J_{SC}= 9.03 mA.cm^{-2}), due to stronger absorption and higher mobilities.

Scheme 15

Replacing the thienyl unit by an ethylenic bond can be used to reduce the aromatic character of the π-conjugated arms in order to design more efficient chromophores. The ternary substituted TPA-based compound **35**, end-capped with an octyl cyanoacetate (CA) group, was synthesized and evaluated by Li et al. in BHJ solar cells and compared to its analogue **32** (Scheme **16**).[30] Due to the less aromatic character of the arms better charge transfer occurs between the central donor and external acceptor groups. As expected, compound **35** possesses broad and strong visible absorption band which is red-shifted by 24 nm related to **32** and lower HOMO energy level. The photovoltaic performance was collected from a BHJ solar cell device with the following architecture ITO/ PEDOT: PSS (30nm)/ **35**: $PC_{71}BM$ (70nm)/ Ca/ Al (120 nm). The performances were recorded after a thermal annealing of the photosensitive layer at 80°C (10min.) at different blend weight ratios (from 1:1 to 1:3, w/w) under AM1.5 conditions. The best device, based on a blend at 1:3 ratio, exhibited a PCE of 2.1% (V_{OC}= 0.91V, J_{SC}= 4.64 mA.cm^{-2} and FF= 0.50). The reduced photoconversion compared to **32** was ascribed to a decrease of the short-circuit current due to lower hole-mobility (μ_h = 2.03·10^{-4} cm^2 V^{-1} s^{-1} *vs* μ_h = 1.5·10^{-3} cm^2 V^{-1} s^{-1}).

Scheme 16

Motivated by the obtained results and continuing their efforts on the structure-properties relationships of star-shaped chromophores Li et al. investigated a novel class of trisubstituted TPA. Those are based on 5-vinyl-4,4'-dihexylbithiophene as π-conjugated spacer, in order to afford efficient solution-processable OSCs materials associated with good film forming properties and are end-capped with a dicyanovinyl group.[31] Compared properties of **36** *vs* **37** show that the latter displays enhanced photophysical properties caused by the insertion of the vinyl group onto the π-conjugated backbone. For instance **37** exhibits red shift by 40 nm of the maximum of absorption and lower HOMO level (-5.03 *vs* -5.22 eV for **36**) likewise the bandgap (1.61 *vs* 1.88 eV for **36**). Consequently, spin-coated films of either **36** or **37** were used to fabricate BHJ with $PC_{71}BM$ as acceptor (with ratio 1:2 w/w respectively). Improved performances devices were obtained as anticipated for **37** exhibiting a power conversion efficiency of 3.00% (V_{OC}= 0.88 V, J_{SC}= 7.76 mA.cm^{-2}) which is twofold higher than **36** (Scheme **17**).

Scheme 17

Besides processability, stability of chromophores is a crucial parameter that needs to be considered. Regarding dicyanovinyl acceptors, acidic hydrogen could be problematic for long-term stability of the active layers. In this context, Min et al.[32] have designed a new star-shaped TPA **38** possessing an ethyl-dicyanovinyl group as acceptor (Scheme **18**), which avoids the presence of acidic hydrogen. Additionally, **38** shows reduced torsional interactions compared to **36** because of lack of steric hindrance of the hexyl chains (leading consequently to lower HOMO level) and presents good solubility. Thus, BHJ made from **38** and $PC_{71}BM$ has resulted in a twofold improvement of the PCE (3.10%) relative to **36** (1.40%) even without post-treatments. Moreover, as already stated, device performances could be enhanced by optimizing the processing conditions such as thermal annealing methods or solvent additives. Therefore, the previous device treated, during the processing step, with 2% of 4-bromoanisole as additive has attained a remarkable efficiency of 3.60% (V_{OC}= 0.96 V, J_{SC}= 7.60 mA·cm^{-2}) related to morphology optimization and larger sized-domains.

Scheme 18

Additional improvements have been achieved regarding the absorption properties compared to **28** by insertion of benzothiadiazole (BT) moieties into the π-conjugated systems of the TPA starburst molecular structures. Indeed, introduction of BT lead, not only, to a broadening absorption spectrum and also to an increase of the thermal stability probably due to the S-N intramolecular bondings.[33] Moreover, **39** displayed typical p-type semiconductor behavior in air associated with a hole-mobility of μ_h= 4.90 10^{-4} cm^2 V^{-1} s^{-1} which is almost 50 times higher than the reported analog **28**.

All these features, associated to good solubility properties, make **39** to be a donor of choice for fabricating solution-processed OSCs. Consequently, a blend of **39** and $PC_{71}BM$ has been deposited by spin coating exhibiting a PCEs as high as 4.3% without any post-treatment (device structure: ITO/PEDOT: PSS/ **39**: $PC_{71}BM$ (1:2, w/w)/Ca/Al, (V_{OC}= 0.87 V, J_{SC}= 9.51 mA.cm^{-2})). The high value obtained has been correlated to the surface morphology displaying nano-aggregated domains that are suitable and beneficial to the charge separation. In order to expand the scope of this compounds family, He et al. have developed and tested in BHJ OSCs the derivatives **40a** and **40b** (**40a** or **40b**: $PC_{71}BM$ (1:3, w/w).[34] Extended π–conjugated backbone was obtained by inserting the vinylene groups and TPA end-groups in order to achieve broader absorption. Although similar optical properties to **28** were gained lower photovoltaic performances (PCEs of 1.90% and 1.23% with V_{OC}= 0.75 V, J_{SC}= 6.41 mA.cm^{-2}; V_{OC}= 0.71 V, J_{SC}= 5.41 mA.cm^{-2} respectively) were attained mainly due to poorer film-forming properties (large molecular size, lower solubility) and weaker ICTs.

Scheme 19

As was demonstrated for structure-like **39**, thiophene or polythiophene structures can play not only a linker role but can also act as a donor. The **41a** star-shaped conjugated molecule possesses a D–A structure with TPA as the donor core unit, benzo[1,2,5]thiadiazole (BT) as the acceptor unit and terthiophene (TT) donor end groups.[35] Comparatively to the corresponding star-shaped molecules **41b**[36] and **41c**[37], **41a** shows a red-shifted absorption with a maximum at 538 nm and an absorption edge extending to 650 nm associated to higher hole mobility up μ_h= 1.1 × 10^{-4} cm^2 V^{-1} s^{-1}. The BHJ solar cells based on the device structure ITO/PEDOT: PSS/ **41**: $PC_{71}BM$ (70nm)/Ca/Al, with a blend **41**: $PC_{71}BM$ at a 1:3 ratio (w/w), exhibited a power conversion efficiency of 2.28% (V_{OC}= 0.82V, J_{SC}= 6.39 mA.cm^{-2} and FF= 0.43) under standard illumination AM1.5 conditions. Compounds **41b** and **41c** exhibit lower efficiencies, 0.61% (V_{OC}= 0.91V, J_{SC}= 1.54 mA.cm^{-2} and FF= 0.43, with a Ba (10nm)/Al (100nm) cathode) and 1.33% (V_{OC}= 0.81V, J_{SC}= 4.18 mA.cm^{-2} and FF= 0.39) respectively incriminated to lower hole-mobility as well as less π-π interactions in the solid state due to the less planar TPA scaffold related to TT.

Scheme 20

Replacing benzothiadiazole by benzoselenadiazole (BS) into TPA star-shaped skeleton was described recently (Scheme **21**).[38] Selenium atom was used because of its more electron rich character compared to sulfur and induced a red shift in π-conjugated systems relative to their sulfur counterparts. Thereby, compound **42** was designed and synthesized displaying both a good solubility and a broad absorption from 300 to 650 nm similar to that of **39**. BHJ OSCs based on blend films of **42** and $PC_{71}BM$ (1:2, w/w) have given rise to photovoltaic performances up to 1.54% (V_{OC}= 0.91 V, J_{SC}= 4.54 mA.cm^{-2}, FF=0.37).

Scheme 21

Due to their intrinsic attractive properties, diketopyrrolopyrrole (DPP) have been proven promising materials for the design of efficient OSCs. Thus changing BT or BS acceptors by a DPP moiety in TPA based-materials has led to the design of novel materials that can be used as non-fullerene acceptors for solution-processed OSCs. To this end, Zhan et al.[39] have synthesized a

soluble chromophore **43** and have therefore demonstrated its potential application in OSCs (Scheme **22**). A device structure ITO/PEDOT: PSS/P3HT: **43** (1:1, w/w)/Ca/Al leads to an impressive increase of the V_{OC}= 1.18 V (J_{SC}= 2.68 mA.cm^{-2}) associated to a conversion efficiency as high as 1.20%.

Scheme 22

Shi and co-workers have recently optimized the photophysical properties of the above DPP architectures by end-capping with substituted or unsubstituted benzene rings (compounds **44a-44c** – Scheme **23**).[40] The latter were investigated as π-conjugated donors in blend films with $PC_{61}BM$ as the acceptor at ratio 1:1 (w/w) (for (**44a** and **44b**) or 1:2 (for **44c**). Best performances were obtained after improving the films morphologies by adding 2% of DIO (1,8-diiodooctane) during the solution-process step. Generally, the synthesized chromophores exhibit roughly similar optical and electrochemical behaviors with slight differences relative to the endgroup that influences mainly the π-π stacking in the solid state. The device structures demonstrated that the highest PCE (2.98%) was obtained for **44a** and was correlated to its most efficient charge transport properties and higher hole-mobility among the others (**44a**: μ_h= 8.63 10^{-5} cm^2 V^{-1} s^{-1}, V_{OC}= 0.72 V, J_{SC}= 7.94 mA.cm^{-2} *vs* **44b**: μ_h= 2.42 10^{-5} cm^2 V^{-1} s^{-1}, V_{OC}= 0.76 V, J_{SC}= 5.14 mA.cm^{-2} and **44c**: μ_h= 4.43 10^{-5} cm^2 V^{-1} s^{-1}, V_{Oc}= 0.80 V, J_{SC}= 5.83 mA.cm^{-2}) as well as a smoother film morphology and an higher exciton dissociation efficiency.

Scheme 23

Expanding the π-conjugated system of **39** by embedding additional thienyl ring has demonstrated to be benefit to improve the light harvesting properties on the TPA-DPP based structures. Indeed, improvement of the photophysical properties were ascribed to an increase of the molecular ordering that inter alia impacts on the absorption properties and on the charge mobilities (Scheme **24**).[41] Consequently, a dramatic enhancement of the photovoltaic performances, more than two fold magnitude, was obtained in favor to **45** (2.95%, V_{OC}= 0.81 V, J_{SC}= 10.02 mA.cm^{-2}) compared to **39** (1.38%, V_{OC}= 0.77 V, J_{SC}= 5.08 mA.cm^{-2}) in conventional device structures with $PC_{71}BM$ as acceptor (at ratio 1:4 and 1:2 (w/w) respectively). Similar results were obtained when $PC_{61}BM$ was used as acceptor (1.81%, V_{OC}= 0.83 V, J_{SC}= 5.60 mA.cm^{-2} *vs* 1.13%, V_{OC}= 0.84 V, J_{SC}= 4.19 mA.cm^{-2}). Moreover, the HOMO (-5.13 eV) and LUMO (-3.32 eV) energy levels suggest that **45** could be used as an acceptor in blended films with P3HT yielding a PCE of 0.63% with an impressive V_{OC}= 1.14 V, (J_{SC}= 1.33 mA.cm^{-2}).

Scheme 24

Original star-shaped chromophores based on non-TPA cores, with a C_{3h} symmetry, are of interest due to the possibility to fine-tune the properties of such structures by modifying for instance the planarity and controlling the solid-state interactions. Based on these considerations, Xiao et al.[42] and Bo et al.[43] have envisioned the use of planar structures such as benzotrithiophene (BTT) and benzotrisindole (BTI) respectively to develop new star-shaped structures (Schemes **25-26**).

Fine-tuning the properties of molecules **46a-46c** by a selective increase of the thiophenic units leads to a control of the HOMO level while the LUMO level remains almost unaffected.

Compounds **46a-46c** exhibit broad optical absorption with similar behaviors; the main difference came from the highest energy band due to the increase of the number of thienyl units. BHJ solar cells were fabricated with the device structure ITO/PEDOT: PSS (45nm)/**46**: $PC_{61}BM$ or **46**: $PC_{71}BM$ /Ca (20nm)/Al (80 nm). Increasing the number of thienyl units led to a significant enhancement of the PCE from 0.16% for **46a** (V_{OC}= 0.54V, J_{SC}= 0.95 mA.cm^{-2} and FF= 0.31) to 0.74% for **46c** (V_{OC}= 0.69V, J_{SC}= 2.93 mA.cm^{-2} and FF= 0.7) at a **46**: $PC_{61}BM$ 1:1 ratio. Changing the blend to **46c**: $PC_{71}BM$ (1:2 ratio) improves the conversion efficiency up to 1.36% (V_{OC}= 0.72V, J_{SC}= 4.13 mA.cm^{-2} and FF= 0.46) due to a better intimate donor acceptor mixing and smoother surface.

Scheme 25

BTI core has been used for the synthesis of chromophores **47-48** and due to presence of the N-atom it should display a higher donor character relative to BTT. The films made from **47** and **48** display a broad absorption in the visible associated to an optical bandgap of 1.82eV and 2.07eV respectively. From the electrochemical experiments the HOMO and LUMO energy levels have been calculated to be -5.12eV and -3.30eV for **47** and -5.07eV and -3.00eV for **48** attesting their ability to be used as donors in BHJ in conjunction with $PC_{61}BM$ or $PC_{71}BM$ as acceptors. Hence, solar cells devices with the architecture ITO/PEDOT: PSS (40nm)/ **47-48**: $PC_{71}BM$ /LiF (0.5 nm)/Al (100 nm) were prepared and evaluated. The photovoltaic performances were found to be dependent to the ratio of donor to acceptor. The best results were obtained for a ratio of 1:3 with a thickness of the photoactive layer of about 105 nm. Under these conditions, PCEs of 1.95% for **47** (V_{OC}= 0.82V, J_{SC}= 5.31 mA.cm^{-2} and FF= 0.45) and 1.73% for **48** (V_{OC}= 0.65V, J_{SC}= 8.13 mA.cm^{-2} and FF= 0.33) were achieved. However, a post-deposition thermal annealing at 130°C for 5 min. for **48** increases the conversion efficiency up to 2.05% (V_{OC}= 0.72V, J_{SC}= 6.41 mA.cm^{-2} and FF= 0.44) while an improvement for **47** is obtained when 0.5% of CN is used as solvent additive leading to a PCE of 2.29% (V_{OC}= 0.82V, J_{SC}= 6.00 mA.cm^{-2} and FF= 0.47). The enhancement has been incriminated to marked changes of the film morphologies when the post-treatments were performed as attested by the surface and morphology analysis. The results obtained from these structures make them very promising candidates for the elaboration of SMOSCs and need to be further explored.

Scheme 26

Recently Wu et al. have envisioned the synthesis of cruciform-like structures originating from the link of two linear chromophores (Scheme **27**).[44] Thus, two new structures **49** and **50** have been designed and synthesized in order to be investigated as potential new efficient donor for organic solar cells. They differ one to each other by the length of the arms. As expected, **50** exhibiting the longest π-conjugated system led to the highest maximum absorption (λ_{max}= 525 nm). Interestingly, from solution (λ_{max}= 495 nm) to thin film (λ_{max}= 499 nm) **49** shown similar

spectra suggesting weak intermolecular contacts in the solid-state while **50** displays a 13 nm red shift due to better π-π interactions. From the solid-state spectra the optical bandgap can be deduced to be 2.07eV and 1.82eV respectively to **49** and **50**. The low-lying HOMO energy levels of **49** and **50** are appropriate to generate large V_{OC} in the devices.

Conventional structure of ITO/PEDOT: PSS (30 nm)/**49** or **50**: $PC_{71}BM$ (1:3, w/w, 90 nm)/Ca (15 nm)/Al (100 nm) have been used for the fabrication of BHJ solar cells. Photovoltaic performances were determined under standard illumination conditions AM1.5. Conversion efficiencies of 0.74% for **49** (V_{OC}= 1.09V, J_{SC}= 2.47 mA.cm^{-2} and FF= 0.27) and 3.14% for **50** (V_{OC}= 1.08V, J_{SC}= 6.75 mA.cm^{-2} and FF= 0.43) were obtained without any treatments. The significant differences of the PCEs in favor to **50** came from the improved short-circuit current and fill factor related to a better phase separation and broader absorption spectrum

Scheme 27

A – D – A type

Besides the recently developed TPA-based chromophores most efforts have been devoted to the linear oligomeric thiophene π-conjugated systems. On such derivatives the thiophene π-conjugated backbone, is routinely combined with selected acceptors in order to fine-tune their photophysical properties. From a given donor (D) and acceptor (A) different combinations are possible leading to several defined architectures namely D-A, A-D-A, D-A-D etc… Symmetric and dissymmetric structures can be easily obtained using iterative synthetic pathways and offer most advantages than polymers because of their higher solubility, monodisperse character and the possibility to better fine tune their properties.

In addition, as evidenced on TPA star-shaped structures, combination of a donor with a given strength acceptor broadens the absorption spectrum and optimizes the light-harvesting properties. Consequently a reduction of E_g was produced concomitantly with an increase of the V_{OC} due to a decrease of the HOMO level. All these phenomena are in favor of optimizing the photovoltaic performances.

In this context, association of a septithiophene with two different acceptors namely the dicyanovinyl (DCN) and the diethylthiobarbituric (DETA) acid affords two symmetrical (A-D-A) and one asymmetrical (A-D-A') structures (Scheme **28**). In those systems the oligothiophene π-backbone acts as the hole-transporting material whereas the acceptor expands the absorption spectrum to higher wavelengths, via an ICT, allowing a better match with the solar spectrum.

Scheme 28

As expected, the replacement of one DCN by DETA (**51** to **53**) leads to a 31 nm red shift and subsequent exchange of the second DCN by DETA (**51** to **52**) leads to another 21 nm red shift of the λ_{max}. Surprisingly, it can be noticed that from **51** to **52** a reduction of the band gap is attained while a concomitant diminution of the power conversion efficiency is obtained as the number of DETA increase in a PHJ configuration with a spin-coated donor layer and a vacuum deposited C_{60} layer (1.64% **51**, 1.21% **53** and 0.36% **52** respectively).[45] From these observations it appears that the molecule desymmetrization affects both the optical properties as well as the packing arrangement in the solid state, which has the dramatic effect on the PCE. Further investigations in BHJ solar cells based on a blend of **51** and $PC_{61}MB$ (in 1:1.4 (w/w) ratio) led to an improvement of the PCE value up to 2.45%[46] and 3.7%.[47]

Chen's group further studied an analogous series by changing the nature of the acceptor. Interestingly, it was found that the alkyl-cyanoacetate (ACA) end-group acts as a quite effective acceptor group with the benefit to improve the film morphologies qualities by changing the nature of the alkyl chain (Scheme **29**).

Scheme 29

Thus, compounds **54a**, **54b** and **54c** display similar optical properties in $CHCl_3$ (absorption maxima *ca.* 492 nm and absorption coefficients are 7.6×10^4, 6.3×10^4, 6.0×10^4 M^{-1} cm^{-1}, respectively). PCE were evaluated on a BHJ devices, made from a blend of each of these donors and $PC_{61}BM$ (1:0.5 w/w), leading to high efficiency, up to 4.46%, 5.08% and 4.52% for **54a**, **54b** and **54c** respectively.[48] The observed variations can be incriminated to the formation of different grain-sized domains organizations in the blend as evidenced by AFM. For instance, microphotographs of **54b**, exhibit well separated domains (assigned to the acceptor-rich and donor-rich parts) associated to a higher roughness (4.05 nm compared to 2.51 nm for **54a** and **54c**). Comparison of the volume occupied by the side chains (linear or hyperbranched alkyl chains) is of importance on the final properties (**54b** and **54c**) and has to be considered in the molecular design of linear systems.

Continuing their studies on the structure-property relationships modulation of the properties have been achieved by varying the nature of the acceptor on symmetrical structures[49, 50] (Scheme **30**).

Scheme 30

As expected the energy levels and bandgap can be easily fine-tuned on these architectures by changing the strength of the acceptors. Nonetheless, the nature of the terminal acceptors will affect not only the optical properties but also dramatically the solid-state packing as well as on the solubility. That might impact both on the hole and electron mobilities and on the grain size domains. Hence, hole-mobilities were measured by the space charge limited current method (SCLC) on films made from the compounds **55** to **58** giving the following mobilities $\mu_h = 0.47\cdot10^{-4}$ cm^2 V^{-1} s^{-1}, $\mu_h = 3.26\cdot10^{-4}$ cm^2 V^{-1} s^{-1}, $\mu_h = 1.50\cdot10^{-4}$ cm^2 V^{-1} s^{-1} and $\mu_h = 0.24\cdot10^{-4}$ cm^2 V^{-1} s^{-1} respectively. Bulk heterojunction devices fabricated with a blend of each donors and $PC_{61}BM$ in the ratio 1:0.5 (w/w) (except for **55**: 1:0.8 (w/w)) led moderate to high PCE as high as 4.05%, 5.08%, 6.10% and 2.46% for **55 – 58** respectively. The enhancement of PCE for **57** compared to **56** is attributed to the higher J_{SC} value (J_{SC}= 13.98 mA.cm^{-2} versus J_{SC} J_{SC}= 10.74 mA.cm^{-2}) due to a stronger red shift of the maximum of absorption.

Changing the previous acceptors by the 1,3-indanedione analogous in compound **61** leads to a reduced band gap and

should improve their photovoltaic conversion efficiencies (Scheme **31**). Nevertheless, the poor packing in the solid state (as revealed by XRD analysis) and its low LUMO level (-3.86 eV) provide a relatively low PCE for **60** that not exceed 0.66%. The rather low PCE could be assigned to the lack of solubility for those chromophores, which turns to be prohibitive for fabrication solution processes (*i.e* for **61**). However, considering the better solubility of **59**, the **59**-based structure gives rise to an efficient device with a PCE of 4.93% and I/V characteristics close to that of **56** and **57**.[51]

Scheme 31

Further modulations were achieved from these linear systems by inserting into the π-conjugated systems various unsubstituted or substituted rigid blocks (Schemes **32**-**33**) that can help to adjust the photovoltaic characteristics as well as their intrinsic optoelectronic properties. For instance, the dithienosilole derivative **62** demonstrated greater light harvesting efficiency. BHJ devices based on this chromophore showed a PCE of 5.84% along with a noticeably high fill factor of 0.64.[52] As an archetype structure benzodithiophene (BDT) **63** was first investigated and used for the preparation of an efficient BHJ cell (PCE = 5.44%) with a high V_{OC}= 0.93 V.[53] Encouraged by these results further optimization were achieved by changing the nature of the acceptors (to have greater light absorption) and also by increasing their solubility by the introduction of alkyl side chains (**64**-**65**).[54] Hence, an optimized BHJ device made from a blend of **65**, $PC_{71}BM$ and PDMS as additive in the active layer led to date to one of the highest PCE value (7.38%) with an average 7.18% obtained from a hundred devices

Scheme 32

Scheme 33

With the aim to enlarge the scope of this series, chromophore **65** was further optimized into 2D structures by expanding laterally the π-conjugated system with different thienyl substituents (**66a–66c**, Scheme **33**).[6] Solution-processed BHJ devices were fabricated from these chromophores and $PC_{71}BM$ as electron acceptor. Similarly to **65**, the optimal weight ratio D:A was selected to be 1:0.8, and the device performances were improved by addition of PDMS as an additive (0.2 mg mL^{-1}) (PDMS). Additionally, when other additives such as 1,8-diiodooctane and 1-chloronaphthalene were used no significant improvement was attained. For instance, optimized device performance based on **66a** showed an exceptional PCE value of 8.12% with a V_{OC}= 0.93V, J_{SC}= 13.17 mA.cm^{-2}) and a fill factor of 0.66.

Cui et al.[55] prepared the analogous 2D molecule **67** of derivative **64** with an A-D-A framework (Scheme **34**). Although optical properties were not modified significantly compared to **64**, the BHJ OSC device based on **67**: $PC_{71}BM$ (1:0.5, w/w) leads to an increase of the PCE 4.0% (which almost twofold magnitude higher than for **64**) associated to a notable fill factor of 0.63 without any specific treatments.

Scheme 34

The use of benzotrithiophene (BTT) as central core instead of BDT was investigated by Patra et al. (Scheme **35**).[56] The first attempts to make solar cells devices from **68b** and $PC_{71}BM$ (in 1:0.75 ratio (w/w)) led to a respectably power conversion efficiency of 3.61% with V_{OC}= 0.88V, J_{SC}= 7.39 mA.cm^{-2} and a fill factor of 0.57. Improvements during the fabrication process by adding 0.25 vol% of 1-chloronaphthalene, as an additive, during the formation of the blend film of **68b**: $PC_{71}BM$, increased significantly the PCE to 5.05% with V_{OC}= 0.86V, J_{SC}= 9.94 mA.cm^{-2} and a fill factor of 0.59. In such devices, the enhancement was attributed to the suppression of the nanophase molecular aggregation.

Scheme 35

Pursuing their efforts on the optimization of the molecular structures led Shen et al. to develop shorten derivatives of compounds **63**-**67** that are depicted in scheme **36**.[57] Thus, four new solution-processable A-D-A chromophores (**70**-**72**) were designed and synthetized with a BDT as central core end-capped with indenedione (ID) as acceptor and connected by thiophene or bithiophene as π-conjugated spacers. The photovoltaic conversion efficiencies were determined for each compound in presence of $PC_{71}BM$ (1.5:1 ratio (w/w)). The results indicate that in such structures the π-conjugated spacer is of importance, as well as the side chain on BDT, because the highest efficiencies were obtained for the longest spacer and correlate perfectly with the results for the series **63**-**67**. Indeed, the PCE are respectively 5.67% for **69**, 6.75% for **70**, 4.15% for **71** and 5.11% for **72**.

Scheme 36

Since recently new interesting acceptors have been commonly used for the synthesis of advanced chromophores in optoelectronic applications namely the diketopyrrolopyrrole core (DPP). Thus, Yao et al.[58] end-capped the previous DBT core with DPP and fabricate an efficient device with $PC_{71}BM$ as acceptor (Scheme **37**). Indeed, when compound **73** was deposited as a blend by spin-casting from an *o*-dichlorobenzene solution in presence of an optimized percentage of DIO (0.70%), used as additive, a continuous interpenetrating network film was formed associated to a photovoltaic efficiency up to 5.29% and gathering the following I/V characteristics V_{OC}= 0.72V, J_{SC}= 11.86 mA.cm^{-2} and a fill factor of 0.62. The lowest value obtained for **73** compared to **69** was incriminated to a reduction of the V_{OC}. Slight enhancements have been achieved, from the work of Zhian et al.,[59] by changing the nature of the acceptor, from $PC_{71}BM$ to $PC_{61}BM$, and applying a thermal annealing at 110°C during 10 min. Consequently a PCE of 5.79% was attained.

Scheme 37

Besides this example, the DPP unit has been used in conjunction with several others π-conjugated spacers in order to investigate the influence of the spacer on the electroptical properties of the synthetized chromophores. Thereby, Jo and Choi[60] have studied and compared the influence of electro-donating character and planarity of different spacers on the

properties (Scheme **38**).

Scheme 38

From this study it appears that the insertion of weak π-donating spacers, such as biphenyl (**76**) and naphthalene (**77**), contribute to higher V_{OC} inversely to stronger systems like dithienyl (**74**), or fused-bithiophene (**75**) due to a lower HOMO energy level. In addition, when more rigid and planar π-conjugated spacers were used it was observed an increase of the short-circuit current density J_{SC} (**75** and **77**) owing to a higher hole-mobility. Therefore the use of naphthalene in this series corresponds to the best compromise owing its enhanced V_{OC} and J_{SC} characteristics leading to a device with a power conversion efficiency of 4.40%.

Y. Li et al. have done further investigation by replacing the central core by other rigid and non-rigid nitrogen aromatic π-conjugated structures (Scheme **39**).[61] Owing their light harvesting properties and appropriate energy levels the new compounds have been tested in a device having the following structure ITO/PEDOT: PSS/**78**: $PC_{61}BM$/LiF/Al. Nevertheless among the examined structures only **78a** gave satisfactory performance with a PCE of 1.50%, along the I/V characteristics V_{OC}= 0.66V, J_{SC}= 4.12 mA.cm^{-2} and a FF of 0.44.

Scheme 39

Extension of the carbazole π-conjugated spacer of the compound **78a**, based on the two regioisomeric indolo[3,2-b]carbazoles cores (Compounds **79**-**80**, scheme **40**), has been carried out by Yagai et al..[62] Interestingly, depending on the regiochemistry of the backbone linkages (3,9- or 2,8-) two different solid-state behaviors are found (crystalline *vs* amorphous). As a result, significant dissimilarities in phase segregation are obtained from **79** and **80** blended films with $PC_{61}BM$ that affect dramatically the photophysical properties. For instance, compound **79** presents a linear structure (crystalline) whereas **80** displays a S-shape structure (amorphous). These differences imply that thermal annealing would decrease or increase respectively the degree of phase separation and would modify their molecular packing. Consequently, although the compounds display the same optical and electrochemical properties their PCE are quite different upon thermal annealing due to a difference on the degree of phase separation. The best results (PCE = 1.80%) were obtained for **79** after thermal annealing at 130°C (V_{OC}= 0.77V, J_{SC}= 5.91 mA.cm^{-2} and a FF of 0.40) while **80** presents under the same condition a PCE of 1.40% (V_{OC}= 0.72V, J_{SC}= 3.92 mA.cm^{-2} and a FF of 0.50).

Scheme 40

Thereafter, a novel series of bis-DPP derivatives bridged with various π-conjugated spacers were also investigated by Nguyen and co-workers in order to elucidate and understand more deeply the molecular features that can be helpful for the construction of novel effective molecular structures (Scheme **41**).[63] Additionally, their studies have been correlated with DFT calculations that have been proven to be very effective as an aide prediction tools. A rapid screening of compounds **81**-**88** has revealed that the structure **86d** constitutes one of the most promising structures and was chosen for further optimization. Therefore, the best performances (PCE up to 4.20% with V_{OC}= 0.85V, J_{SC}= 9.90 mA.cm^{-2} and FF= 0.49) for **86d** have been achieved for a blend of **86d**:$PC_{71}BM$ (1:1 w/w) annealed at 80°C in presence of chloronaphthlene (0.50%) as solvent additive.

Scheme 41

In a similarly work, R. A. J. Janssen et al.[64] have studied four novel tetrathiophene derivatives flanked with DKKP end-capped either with benzothiophene or benzofuran moieties (Scheme **42**). Interestingly, all structures (**89a**-**89d**) possess comparable electro-optical properties but display quite different solubility behaviors. During the device fabrication, careful adaptation of the processing conditions (concentration, solvent, temperature, additive) for each compounds in presence of $PC_{71}BM$ as acceptor have given cells performances ranking from 3.6 to 4.6%. This experiments point out that small structural changes will strongly affect the solubility properties and consequently the photovoltaic performances.

Scheme 42

An analogous derivative **90** (Scheme **43**) has been recently described by Zhu et al.[65] showing good optical properties and optimum energy levels for OPV applications. Solution processed BHJ solar cells have been fabricated from **90** and $PC_{71}BM$ (1:1.5, w/w) leading to devices with PCE of 2.82% after thermal annealing. The lowered values obtained from this device compared to the previous, based on tetrathiophene core, might be relied on a decrease of the molecular packing. More interestingly, compound **90** has been successfully used as an acceptor in a BHJ device in a blend film with P3HT (1:1.2, w/w respectively) yielding a PCE of 0.83% with a V_{OC}= 1.17V after thermal annealing. This evidences an ambipolar character for **90** with the possibilities to use such compounds either as donor or acceptor in the construction of solar cells.

Scheme 43

As already mentioned the possibilities to boost the photo-absorption properties as well as the electron and hole-mobilities can be achieved both by chemical design and engineering, but drive to more and more complicated structures. In addition, the aim to use solution-processed technologies requires the use of large solubilizing units that can affect at the meantime the solid-state arrangement. To circumvent such difficulties Bäuerle et al. studied, using vacuum deposition process, some oligothiophenic structures substituted with shorter alkyl-chains, based on the α-quinquethiophene core, and end-capped with dicyanovinyl groups (Scheme **44**) in OPV devices.

Scheme 44

Thus, optimized planar heterojunctions made from compounds **91** and C_{60} demonstrated PCE of 3,4% with V_{OC}= 0.98V and J_{SC}= 10.60 mA.cm^{-2}.[66] Based on those promising results a series of unsubstituted oligothiophene **92** (n= 1-6) end-capped with DCV was further investigated (Scheme **45**).[67]

Scheme 45

For instance **92a** showed a well-structured absorption band centered at 406 nm. Increasing the number of thiophene units leads to a bathochromic shift of the maximum of absorption from 406 nm (**92a**) to 532 nm for **92f** associated to a hyperchromic effect (**92a**: ε = 39 000 L mol^{-1} cm^{-1} to **92e**: ε = 73 300 L mol^{-1} cm^{-1}). Devices made by vacuum deposition of 15 nm of a C_{60} layer and 6 nm of **92d-92f**, showed a high values of PCE = 1,20%, 2,60% and 2,80% respectively. Beside, BHJ cells based on **92e** and C_{60} were also prepared leading to PCE as high as 5.2% after device fabrication optimizations.

Solid-state packing was also studied on the methyl substituted derivatives **92e** along the π-conjugated backbone. Methyl groups were introduced at different positions of the π-conjugated skeleton (Scheme **46**). These modified oligomers (**93-95**) were incorporated by vacuum deposition process in BHJ solar cells exhibiting PCEs ranking from 4.80 to 6.10%.

Subsequent optimization of the deposition process and changes of the fabrication conditions have led to an enhanced PCE up to 6.90%.[68] This result suggested the existence of strong specific intermolecular interactions within the organic layer associated to effective π–π overlap and multidirectional electronic coupling evidenced by single-crystal X-ray structure analysis of **94**.

Scheme 46

Replacement of thiophene units by analogous selenophene or ethylenedioxythiophene (EDOT) core were also investigated (Scheme **47**).[69]

Scheme 47

Nevertheless, despite a broader and more intense absorption properties selenium-containing oligomers (**96-98**) have shown lower performances compared to **92e** with PCEs ranging from 2.50 to 3.10%. The lowest obtained values might be attributed to lowered solid-state packing due to the longer alkyl chains used along the π-conjugated backbone. In addition increasing the number of selenophene decreases also the photovoltaic characteristics. Later on Palomares et al. have changed the thiophene or selenium containing oligomers by a more electron rich unit such as EDOT (**99**). A BHJ device structure based on **99**:$PC_{70}BM$ gave rise to an enhancement of the PCE up to 3.75% associated to good annealing properties and high open-circuit voltage and fill-factor (V_{OC}= 1.01V, J_{SC}= 6.00 $mA.cm^{-2}$ and FF= 0.63).[69b]

Benzothiadiazole derivatives have been also examined as terminal acceptors in oligothiophene. Thus compounds **100** and **101** have been synthetized (Scheme **48**) using a terthiophene as electron relay between the acceptors.

Scheme 48

Combination of the dyes **100** or **101** with C_{60} have been tested both in PHJ and BHJ solar cells.[70] The obtained devices showed high V_{OC} values (V_{OC}= 0.98-1.05V), and the performances of a PHJ device based on **101** and C_{60} bilayer have given rise to a PCE up to 3.15%.

Combination of benzothiadiazole with 2,7-carbazole end-capped with oligothiophene have been explored par Li et al.[71] in order to readjust HOMO levels compared to molecules **100** or **101** and optimized the band gap (Scheme **49**). Thus, solution processed organic solar cells based on a blend **102a**/$PC_{71}BM$ exhibit a PCE of 2.26% associated with a high open-circuit voltage close to that of **101** (V_{OC}= 0.98-1.05V). Expanding the terminal π-conjugated system by an oligothiophene moiety (**102b** and **102c**) leads to a slight decrease of the V_{OC} (V_{OC}= 0.92 and 0.86V respectively) on devices having the same configuration accompanied with higher PCE values up to 3.44% and 3.90% respectively without any post-treatment due to an enhancement of the J_{SC} and FF.

Scheme 49

Different type of s-tetrazine derivatives have been investigated and tested as end-groups in a oligothiophene series synthetized by Tu et al..[72] Thus, active solar cells obtained from the series of the compound **103** (Scheme **50**) show, by AFM and TEM experiments, that on blended films of **103**: $PC_{61}BM$ (1:1 w/w ratio) well-ordered packing structure of **103** in the crystalline state leads to higher photovoltaic performances. In addition, replacement of $PC_{61}BM$ by $PC_{71}BM$ in presence of 1% of DIO as additive affords a device with a power conversion efficiency reaching 3.24% (J_{SC}= 7.87 $mA.cm^{-2}$).

Scheme 50

The strategy has been applied toward the synthesis of extended A-D-A-D-A chromophores incorporating two different acceptors at central and terminal positions along the π-conjugated backbone namely the benzothiadiazole and trifluoroacetyl (Scheme **51**). Using vacuum deposition technique PHJ solar cells were prepared from the compounds **104-106**. The presence of these acceptors lower the HOMO level, providing an unusually high V_{OC} (V_{OC}= 1.17V (**105**) and 1.10V (**106**)) associated to moderate PCE of 1.56% and 1.45% respectively.[73]

Scheme 51

Similar studies have been conducted by Y. Chen et al.[74] on the solution processable chromophore **107** incorporated in BHJ solar cells (Scheme **52**) through a spin coating process. An optimized donor/acceptor weight ratio was found to be 1:0.8 for **107**:$PC_{61}BM$ affording a PCE of 2.43% without any post-treatment (V_{OC}= 0.76V, J_{SC}= 5.20 $mA.cm^{-2}$ and FF= 0.61) and using LiF/Al as cathode. Thermal annealing at 150 °C for 10 min improved the PCE up to 3.07% (V_{OC}= 0.78V, J_{SC}= 7.10 $mA.cm^{-2}$ and FF= 0.55), suggesting that the enhancement can be attributed to a better molecular packing at the solid state associated with an improvement of the absorption intensity and hence the shunt current circuit density from 5.20 to 7.10 $mA.cm^{-2}$

Scheme 52

Thienothiadiazole and thienopyrazine have been also examined as central acceptors in oligothiophene series end-capped with DCV or trifluoroaceyl groups (Scheme **53**). Insertion of such central acceptors leads to a red shift of the maximum of absorption compared to their analogous parent compounds with

benzothiadiazole (707 nm, 675 nm, 620 nm for **108**, **109** and **110** respectively). Nevertheless, the different attempts to optimize the solar cells during the process of fabrication have not permitted to enhance efficiently the photovoltaic characteristics. Indeed, only moderate PCE values were attained in the range of 0.8% to 1.3% ascribed to the lack of transport of the photo-generated electrons and holes (J_{sc} are not exceeding 3.20 mA.cm^{-2}), the low molar absorptivity and the low-lying LUMO energy levels of the donor.[75]

Scheme 53

With the aim to enhance the electron withdrawing efficiency properties of DCV and to reduce the optical band gap, a nitrobenzene ring can be used in place of one of the cyano groups. Mikroyannidis et al. have successfully applied this strategy during the synthesis of the phenylenevinylene-based chromophore **111** (Scheme **54**).[76] Replacement of one of the cyano groups leads to a reduction of the optical band gap, with a maximum of absorption around 640 nm, compared to the unsubstituted DCV compound. BHJ solar cells device were fabricated using **111**: PCBM as active material sandwiched between ITO/Al electrodes. The low PCE, 1.36%, is mainly attributed to the low J_{SC} (V_{OC}= 0.73V, J_{SC}= 0.056 mA.cm^{-2} and FF= 0.31) due to the small exciton diffusion lengths as well as low mobility of hole. Thermal annealing of the blend affords an improvement of the PCE up to 2.33% induced by an increase of the packing density facilitating both the exciton dissociation and charge transportation.

Scheme 54

In addition, changing the $PC_{61}BM$ acceptor by perylene diimide PDI in the previous device leads to a remarkable PCE of 1.87%. Further improvement, notably by insertion of ZnO in between the active layer and the Al-cathode followed by a thermal annealing (5min., 100°C) gives rise to an exceptional PCE of 3.17%.[77]

With the aim to enhance the light-harvesting abilities and optimize the optical bandgap compared to A-D-A counterparts, Wong et al. have envisioned the combination of two strong electron-withdrawing groups leading to the A-A-D-A-A structures.[78] Hence, in the following examples **112-113** (Scheme **55**) the dithienosilole (DTS) core has been selected as *p*-type building block in respect with its better packing abilities and higher hole-mobilities compared to their carbon-based homologues.

Scheme 55

Elaboration of planar mixed heterojunction devices based on **112** and fullerene acceptors (C_{60} or C_{70}) leads to decent power conversion efficiencies from 2,3% to 3.7% respectively (V_{OC}= 1.05V, J_{SC}= 5.80 mA.cm^{-2} and FF= 0.38, V_{OC}= 1.01V, J_{SC}= 9.79 mA.cm^{-2} and FF= 0.38) after tuning the donor: acceptor ratio (from 1:1 to 1:1.5) without any post-treatments such as thermal of solvent annealing processes.

Further investigations have been done with the DTS core incorporating solubilizing chains (Scheme **56**). The roles of such chains are to improve the solubility of chromophores in organic solvents for solution casting processes as well as their packing structure and their solid-state miscibility with fullerenes. A careful attention on the molecular design, chain position, and electron density has to be paid to ensure the best properties. In this context, Wang et al. described in a recent work the impact of such molecular modification on the photoconversion properties.[79]

Scheme 56

The best results were obtained for **116** and $PC_{61}BM$ (1:0.8 ratio) with a PCE up to 3.81% (V_{OC}= 0.92V, J_{SC}= 8.73 mA.cm^{-2} and FF= 0.49). AFM microphotographs of spin-coated films from chloroform solutions show better interpenetrating network for **116** compared to **114-115** associated to higher roughness and better optical absorption properties. These results highlight again the importance to control the size, nature, length and position of the alkyl chains that strongly impact the optical absorption, energy levels, packing and film morphology.

To gain further insights, Kim et al. have introduced on the terminal alkyl substituents an amide function (compounds **118**) that would favor intermolecular interactions via a hydrogen bonding network[80] compared to **117** structures (Scheme **57**). This hydrogen bonding will affect dramatically the interfacial interactions, optical properties, the film morphology and therefore the photovoltaic properties. Thus, it has been demonstrated in this work that the introduction of intermolecular interaction induces well-ordered molecular packing that is not suited for the optimization of the photovoltaic performance. Indeed, the best result was obtained for **117b** with a PCE exceeding 4.30% (V_{OC}= 0.82V, J_{SC}= 9.79 mA.cm^{-2} and FF= 0.54) while its counterpart **118b** leads only a PCE of 3.22% under the same conditions (V_{OC}= 0.87V, J_{SC}= 7.94 mA.cm^{-2} and FF= 0.47).

Scheme 57

An analogous strategy was adopted by Lam and co-workers but using a terminal acid group (CO_2H) (Scheme **58**).[81] Interestingly, in this case an improvement of the photovoltaic efficiency was observed for the derivative **119b** compared to its ester analogue (**119a**). The enhanced PCE value was mainly attributed to a better hydrogen-bonding network that induces strong π-π interactions and highly ordered films with a vertical alignment. This behavior leads to higher hole-mobilities in favor of **119b** as measured by the SCLC method (μ_h = 2.83 10^{-5} cm^2 V^{-1} s^{-1} (**119b**) μ_h = 6.91 10^{-6} cm^2 V^{-1} s^{-1} (**119a**)) that directly impact on the photovoltaic conversion efficiency (0.91% (V_{OC}= 0.71V, J_{SC}= 2.86 mA.cm^{-2}, FF= 0.45) and 0.06% (V_{OC}= 0.53V, J_{SC}= 0.45 mA.cm^{-2}, FF= 0.26) respectively). In addition, it is noted that the formation of nanofibers as-cast films prevents the use of post-treatments or solvent additives.

Scheme 58

D – A – D

Besides the A-D-A structures, several groups have developed in parallel D-A-D architectures with the same aim. For instance, one can cite the work of Li[86] who has widely used the

benzo[1,2,5]thiadiazole core as central acceptor part flanked with TPA donors and connected together by thiophenic linkers (Scheme **59**).

Scheme 59

Preliminary studies based on the derivative **120** have been performed with different devices architectures made from pristine **120**, a PHJ structure (**120** and C_{60}) and a BHJ from a blend of **120** and $PC_{61}BM$. In a typical device, the active layer was sandwiched between a ITO/PEDOT: PSS as anode and LiF/Al as cathode. From the obtained results it has been demonstrated herein that the configuration BHJ shows the highest photovoltaic performances with a PCE 0,19%. Further optimization of cathode material by using Ba/Al instead of LiF/Al gave rise to an enhancement of the PCE up to 0,26%.[82]

In order to increase the photovoltaic performances of such derivatives, multi-arms architectures were built up as shown in scheme **60** and compared with their linear D-A-D counterparts.[83]

Scheme 60

All structures are well soluble in dichlorobenzene, which makes them suitable to elaborate organic solar cells by spin-coating processes. Thus, in devices with structure of ITO/PEDOT: PSS/active layer/LiF/Al and optimized conditions (thickness (70-90 nm), donor: acceptor ($PC_{71}BM$) ratio 1:3 (w/w)) the highest PCE was obtained for the four-arms derivatives **122c** (1.80%, V_{OC}= 0.92V, J_{SC}= 4.90 mA.cm^{-2} and FF= 0.41). Nevertheless for all compounds tested the PCE values are comprised between 1,10 to 1.80% demonstrating that other parameters have to be controlled and taken into account to optimize the devices.

Further investigations were done on compounds **123** and **124** (Scheme **61**). To ensure sufficient solubility alkyl chains have been introduced along the π-conjugated backbone (**123**) or at the terminal position (**124**). The derivative **123** is crystalline while its counterpart **124** is amorphous, this difference will certainly affect the performances of the devices. As expected, **124** exhibits a bathochromic shift (λ_{max}=456 nm and λ_{max}=353 respectively) and a higher HOMO level compared to 125 due to its extended π-conjugated system. Organic solar cells were fabricated and the device based on **123**:$PC_{61}BM$ (1:3 ratio (w/w) exhibits higher V_{OC} and PCE than that for **124**:$PC_{61}BM$ (0.56% (V_{OC}= 0.80, J_{SC}= 1.80 mA.cm^{-2}, FF= 0.39) and 0.42% (V_{OC}= 0.62V, J_{SC}= 1.89 mA.cm^{-2}, FF= 0.36) respectively) attributed to the lower HOMO energy level of **123**. Changing the nature of the acceptor (**123**: $PC_{71}BM$) yielded to a higher PCE up to 1.23% (V_{OC}= 0.86, J_{SC}= 3.50 mA.cm^{-2}, FF= 0.41), which is not improved by thermal annealing.[84]

Scheme 61

In the following example Zhen et al. have investigated the star-shaped bis-(tri-substituted)TPA **125**[85] end-capped at two of its extremities by an hexyl-thiophene and connected through a benzothiadiazole core (Scheme **62**). Organic solar cells based on **125**: $PC_{71}BM$ (donor: acceptor ratio 1:3) yielded, without any solvent additives or thermal post-treatments, a PCE of 3.18% (V_{OC}= 0.96V, J_{SC}= 6.83 mA.cm^{-2}, FF= 0.48). This example demonstrates that the connection pathway of the different building blocks along the π-conjugated system is of crucial of importance to control the photoconversion efficiencies.

Scheme 62

The nature of the π-conjugated linker plays also an essential role in the achieved properties. In this context, Li and coll. have structurally modified the archetype chromophore **120** in order to improve its efficiency in BHJ solar cells (Scheme **63**).[86] Thus the insertion of hexyl side chains (**126**) helps in getting better blend morphology. As a consequence a PCE up to 1,44% was attained. (**126**: $PC_{71}BM$ (1:3 ratio) V_{OC}= 0.79V, J_{SC}= 4.84 mA.cm^{-2}, FF= 0.37). Extending the π-conjugated system with thieno[3,2-b]thiophene (**127**) instead of thiophene allows significantly to broaden the absorption spectra. However, even if an increase of the shunt current circuit density is noticed (from J_{SC}= 4.84 mA.cm^{-2} to J_{SC}= 5.71 mA.cm^{-2}) the PCE for **126** still the same (1.44%) as the V_{OC} has decreased (from V_{OC}= 0.79V to V_{OC}= 0.74V) due to a higher HOMO energy level. The introduction of bulky alkyl chains at the periphery (**128**) reduced significantly the PCE from 1.44% to 0.75% related to poorer miscibility with $PC_{71}BM$ as evidenced by the AFM microphotographs and the lower hole-mobilities (from μ_h = 1.48 10^{-4} cm^2 V^{-1} s^{-1} (**127**) to μ_h = 2.78 10^{-5} cm^2 V^{-1} s^{-1} (**128**)) determined by the SCLC (space-charge-limited-current) method.

Scheme 63

The results demonstrate that broadening the absorption spectra with remaining the lower HOMO energy level have to be considered in the synthesis and design of high performance organic chromophores.

Pursuing their efforts in the understanding and in the design/synthesis of efficient chromophores for photovoltaic applications, Li et al. have replaced the benzothiadiazole core by a (dicyanomethylene)-pyran unit in chromophores **129** to **131** (Scheme **64**). Organic solar cells based on **128**: $PC_{71}BM$ (1:3 ratio w/w) exhibits a PCE of 1.40% (V_{OC}= 0.71V, J_{SC}= 5.07 mA.cm^{-2}, FF= 0.38) which corresponds to almost twice the value obtained from that based on **129**: $PC_{61}BM$ (PCE= 0.79%) due to the stronger absorption properties of $PC_{71}BM$ in the wavelength range 350-550nm. Modifying the linker from benzene (**129**) to thiophene (**130**) alters the photophysical properties. For instance a red shift of the maximum of absorption was observed as well as a lower bandgap. Therefore, under the same conditions an improvement up to 2.06% of the photovoltaic efficiency was attained with **129**: $PC_{71}BM$ (V_{OC}= 0.79V, J_{SC}= 5.94 mA.cm^{-2}, FF= 0.44). Introduction of solubilizing chains along the π-conjugated system (**131**) leads to a better miscibility with $PC_{71}BM$, without altering the optical properties, associated to an enhancement of the PCE to 2.10% (V_{OC}= 0.78V, J_{SC}= 6.74 mA.cm^{-2}, FF= 0.39).[87]

Scheme 64

Further work has been done Zhan and coll. with other central acceptors such as thieno[3,4-c]pyrrole-4,6-dione (**132a-c**)[88] and bisthiazole (**133a-c**)[89] that are widely used to synthetize low-

bandgap polymers due to their strong electron withdrawing abilities (Scheme **65**).

Scheme 65

Photovoltaic cells were fabricated with a structure of ITO/ PEDOT: PSS/**132a-c**: $PC_{71}BM$/Al. Interestingly the use of thieno[3,4-c]pyrrole-4,6-dione in **132** as acceptor appears to be a promising candidate as its photovoltaic efficiency was higher than its counterparts **121a** or **123**. Indeed, under identical conditions **121a** and **123** have a PCE of 1.30% (V_{OC}= 0.71V, J_{SC}= 4.80 mA.cm^{-2}, FF= 0.38) and 1.70% (V_{OC}= 0.87V, J_{SC}= 4.80 mA.cm^{-2}, FF= 0.40) respectively while **132** exhibits values of PCE ranking from 1.91% to 2.41% (V_{OC}= 0.85V, J_{SC}= 5.52 mA.cm^{-2}, FF= 0.41 and V_{OC}= 0.86V, J_{SC}= 6.51 mA.cm^{-2}, FF= 0.43). By changing the donor: acceptor ratio from 1:3 (w/w) to 1:4 (w/w) enhanced the PCE up to 2.87% (V_{OC}= 0.94V, J_{SC}= 6.94 mA.cm^{-2}, FF= 0.44) and 2.90% (V_{OC}= 0.88V, J_{SC}= 7.73 mA.cm^{-2}, FF= 0.43) respectively. Finally, thermal annealing of the blend **132b**:$PC_{71}BM$ (1:4 w/w) led to a PCE of 3.31% (V_{OC}= 0.91V, J_{SC}= 7.70 mA.cm^{-2}, FF= 0.47). Substitution of thieno[3,4-c]pyrrole-4,6-dione by bisthiazole leads to the chromophores **132a-c.** Increasing the π-conjugated system from **133a** to **133c** provides better intermolecular interactions in the solid-sate and generates strong tendency to absorb the low energy photons as evidenced by the UV-Vis spectroscopy. The chromophores show typical p-type semi-conductor behavior in air with hole-mobilities as high as μ_h = 3.60 10^{-4} cm^2 V^{-1} s^{-1} (**133c**). BHJ solar cells based on **133a-c**: $PC_{71}BM$ (1:4; w: w) blend films showed increasing PCE (up to 2.61%) due to broader and stronger absorption as well as higher hole-mobility as expanding the π-conjugated system (spin-cast solutions: **133a**: V_{OC}= 0.71V, J_{SC}= 3.42 mA.cm^{-2}, FF= 0.30, **133b**: V_{OC}= 0.81V, J_{SC}= 4.69 mA.cm^{-2}, FF= 0.33 and **133c**: V_{OC}= 0.84V, J_{SC}= 7.72 mA.cm^{-2}, FF= 0.40).

A narrow band gap chromophore **134** based on triphenylamine and isoindigo was further investigated by Yang and coll. (Scheme **66**).[90a] due its efficiency previously demonstrated in DSSCs devices.[90b] AFM microphotographs evidenced a good miscibility between **134** and $PC_{61}BM$ with interpenetrating structures, which would facilitate charge separation in the solid state, associated to a broad absorption spectrum from 300 to 750 nm. BHJ OSCs devices with a layered structure of ITO/PEDOT: PSS/**134**: $PC_{61}BM$ (1:1 ratio w/w)/(80nm)/Ca(10nm)/Al(100nm) were fabricated and led to a PCE of 0.61% (V_{OC}= 1.00V, J_{SC}= 2.35 mA.cm^{-2}, FF= 0.26). V_{OC} is among the highest values in all-small molecules or polymers highlighting the importance of such acceptor in future development of SMOSCs due to the high V_{OC} attained.

Scheme 66

A α-heptathiophene series of D-A-D-type oligomers **135**, **136**, and **137** based on TPD (thieno[3,4-**c**]-pyrrole-4,6-dione), TPN (thienoperylene naphthalene) and TIN (thienoimidazole naphthalene) as central acceptor core respectively have been developed by H.-Y. Wang and coll. (Scheme **67**).[91] Modification of the diimide unit of **135** by perylene or imidiazole analogues in **136** and **137** has the benefits to enhance the coplanarity and to tune the energy levels due to a better intermolecular stacking in the solid-state. The photovoltaic performances were determined by fabricating BHJ devices (ITO/PEDOT: PSS/**135-137**: $PC_{71}BM$/LiF/Al) with a donor: acceptor ratio (2:1, w/w). The device **135**: $PC_{71}BM$ blends showed the best PCE of 1.87% (V_{OC}= 0.87V, J_{SC}= 4.93 mA.cm^{-2}, FF= 0.44) while **136**: $PC_{71}BM$ and **137**: $PC_{71}BM$ blends in the same conditions led only to PCE of 0.77% and 0.11% respectively (V_{OC}= 0.76V, J_{SC}= 2.22 mA.cm^{-2}, FF= 0.45, V_{OC}= 0.75V, J_{SC}= 0.58 mA.cm^{-2}, FF= 0.25). However, for **136** and **137** efficiencies can be improved in blends device structures with a weight ratio of 1:1 (w/w) respectively to 1.24% and 0.34% (V_{OC}= 0.77V, J_{SC}= 2.75 mA.cm^{-2}, FF= 0.59, V_{OC}= 0.69V, J_{SC}= 1.91 mA.cm^{-2}, FF= 0.26). The lower PCE are mainly attributed to the different morphology of the blend films and the presence of high crystalline domains.

Scheme 67

By comparison of the work done by Zhan (Scheme **65**), Suh et al. have developed a new series **138a-b** based on the bithiophene imide (BTI) as an electron deficient unit. (Scheme **68**).[92] The BTI is unit of choice due to its strong electron-withdrawing character, planar architecture, good solubility, and close π-π stacking in the solid state. In addition, BTI presents the advantage to decrease the steric hindrance between the alkyl chains of the electron rich unit and the imide group and changes the shape of the oligomers (as banana-like structure) compared to the **132** analogues. *J-V* characteristics obtained from devices with the geometry ITO/PEDOT: PSS (40 nm)/**138**: $PC_{71}BM$ (80 nm)/Al (100 nm) led to the best performances in favour of **138a** with a PCE of 1.36% (1:3 ratio, V_{OC}= 0.91V, J_{SC}= 3.93 mA.cm^{-2}, FF= 0.38) after a thermal annealing a 130°C. Extension of the π-conjugated system for **138b** didn't induced any improvement of the photovoltaic characteristics, as the best PCE attained is only of 1.08% (1:4 ratio, thermal annealing at 120°C, V_{OC}= 0.80V, J_{SC}= 3.79 mA.cm^{-2}, FF= 0.36) even after addition of solvent additives such as 1,8-octanedithiol (ODT) or 1,8-diiodooctane (DIO).

Scheme 68

Cao et al. have investigated the influence of the extension of the π-conjugated system of the chromophores **121**, using fused fluorenyl TPA-based units, on the photovoltaic properties (Scheme **69**).[93, 94] BHJ solar cells were fabricated with the device configuration ITO/PEDOT: PSS/**139**: $PC_{61}BM$ or **140**: $PC_{61}BM$/Ba/Al. Several weight ratios were studied to improve the efficiencies (1: 1, 1: 2 and 1: 4). As demonstrated improvement of the device characteristics were obtained by increasing the $PC_{61}BM$ content in the blend films. In both examples the best PCE achieved were 0.75% and 0.22% (1:4 ratio, V_{OC}= 0.75V, J_{SC}= 1.95 mA.cm^{-2}, FF= 0.34, 1:4 ratio, V_{OC}= 0.70V, J_{SC}= 1.59 mA.cm^{-2}, FF= 0.22) respectively. Despite an extended photosensitivity response to near-infrared region for those chromophores and good film forming properties, the PCE was still low. The low PCE was incriminated to a less efficient charge separation due to LUMO levels close to the LUMO level of $PC_{61}BM$.

Scheme 69

Similarly to **139**, Hyun et al. have evaluated the photovoltaic properties of thiadiazoloquinoxaline-based units[95] by varying the nature of the π-conjugated backbone as well as the substituents on the quinoxaline moiety (for instance isobutyl and thiophene) (Scheme **70**). The nature of the substituents on the quinoxaline part has a dramatic influence on the final optical properties; from isobutyl to thiophene the absorption onset was shifted from 900 to 1100 nm in the solid state. Device structures with the configuration ITO/PEDOT: PSS/**141-142**: $PC_{71}BM$ (1:3 w/w)/TiOx /Al have been fabricated and the performances evaluated under the AM1.5G conditions. **141**:$PC_{71}BM$ blend films showed better PCE (0.24 %, V_{OC}= 0.42V, J_{SC}= 2.42 mA.cm^{-2}, FF= 0.24) than **142**: $PC_{71}BM$ (0.14%, V_{OC}= 0.38V, J_{SC}= 1.40 mA.cm^{-2}, FF= 0.36) even if **142** possesses a broader absorption up to 1100 nm. The lowest PCE for **142** was attributed to a reduced charge separation and a relatively rougher surface. Compared to its counterpart **139** the lower PCE attained was also due to the weakness of the donor used.

Scheme 70

Scheme 71

Cyano substituents have been introduced along the π-conjugated systems in order to take advantage of additional intramolecular charge transfer to reduce the bandgap and to extend the absorption spectrum of the chromophores (Scheme **71**). Hence, Li et al. have conducted preliminary investigations on compounds **143** bearing two different acceptors namely BX (benzoxadiazole **143a**) and BT (benzothiadiazole **143b**).[96] BX was used to lower the HOMO level of molecular donors, compared to BT, and thus to increase the open-circuit voltage. Devices fabricated with the configuration ITO/PEDOT: PSS/**143**: $PC_{61}BM$/Al showed PCE of 0.33% for **143a** (V_{OC}= 0.58V, J_{SC}= 2.39 mA.cm^{-2}, FF= 0.24) while **143b** exhibited a PCE of 0.50% (V_{OC}= 0.60V, J_{SC}= 2.86 mA.cm^{-2}, FF= 0.29). Interestingly, the introduction of alkoxy side chains on the BT core has a dramatic effect on the photovoltaic properties (**144-145**). The photovoltaic performances were evaluated on devices with the structure ITO/PEDOT: PSS/**144-145**: $PC_{61}BM$ (1:2 ratio, w/w)/Al. The BHJ fabricated with **145**: $PC_{61}BM$ as a blend film provided an impressive PCE of 3.85% (V_{OC}= 1.04V, J_{SC}= 11.20 mA.cm^{-2}, FF= 0.33) while **144**: $PC_{61}BM$ did not exceed 2% (V_{OC}= 0.94V, J_{SC}= 6.33 mA.cm^{-2}, FF= 0.33).[97] The highest PCE was consistent with a deeper low-lying HOMO level induced by the cyano groups and better film morphology compared to **143b**.

To get further insights on molecular design of efficient chromophores Ko et al. have studied the unsymmetrical D-A-D **146** chromophores based on a benzo[1,2,5]thiadiazole central core (Scheme **72**).[98]

Scheme 72

Their photovoltaic performances were assessed with the devices configuration ITO/PEDOT: PSS (35nm)/**146**: $PC_{71}BM$ (55-65nm) (1:5 ratio, w/w)/Al (100nm). Importantly, it was observed that fluorination increased the short-circuit current J_{SC} and the V_{OC} induced by improved hole-mobility and reduced HOMO levels, respectively. The best performance was obtained for **146c** affording a PCE up to 3.24% (V_{OC}= 0.84V, J_{SC}= 9.45 mA.cm^{-2}, FF= 0.41) while **146b** and **146a** afforded 3.05% (V_{OC}= 0.81V, J_{SC}= 9.37 mA.cm^{-2}, FF= 0.40) and 2.70% (V_{OC}= 0.80V, J_{SC}= 9.29 mA.cm^{-2}, FF= 0.38) respectively. In addition, insertion of a thin layer of TiO_x as an optical spacer enhanced the photovoltaic properties by reducing the interfacial resistance between the active layer and the Al metal electrode. Performances were enhanced in all cases reaching a PCE of 4.24% for **146c** (V_{OC}= 0.88V, J_{SC}= 10.76 mA.cm^{-2}, FF= 0.44), 3.73% for **146b** (V_{OC}= 0.85V, J_{SC}= 10.55 mA.cm^{-2}, FF= 0.44) and 3.54% for **146a** (V_{OC}= 0.82V, J_{SC}= 10.52 mA.cm^{-2}, FF= 0.42).

Fused bisthiazole, namely thiazolothiazole, has served to build up D-A-D architectures because it possesses a rigid coplanar structure and the presence of the imine bonds confers to it an electron-accepting character. Thus, linear chromophores **147** flanked with oligothiophenic units have been investigated by Shin et al..[99] The terminal hexyl side chains ensure their solubility in common organic solvents and induce liquid crystalline properties that can be benefit for the supramolecular arrangement in the solid state (Scheme **73**). Solution processed BHJ have been fabricated with the structure ITO/PEDOT: PSS (50nm)/**147**: $PC_{61}BM$ (100nm, 1:1 ratio, w/w)/Al (80-100nm) and evaluated. Reasonably high PCE of 1.57% were achieved (V_{OC}= 0.65V, J_{SC}= 7.85 mA.cm^{-2}, FF= 0.31). Furthermore, increasing the donor: acceptor ratio to 1:2 has not led to an improvement of the efficiency and the device has exhibited a PCE of 1.20% (V_{OC}= 0.42V, J_{SC}= 7.59 mA.cm^{-2}, FF= 0.37).

Scheme 73

To improve the efficiencies of thiazolothiazole-based chromophores, Zhan et al. have used of triphenylamine as end-capped unit associated to different length of the π-conjugated bridge (Scheme **74**).[100] As expected, linear extension of the π-conjugated system, from **148** to **150**, induced a bathochromic shift of the maximum of absorption and an enhancement of the molar absorptivity.

Scheme 74

Organic solar cells were fabricated with the configuration ITO/PEDOT: PSS (35nm)/**148-150**: $PC_{71}BM$ (70-80 nm, 1:2, 1:3 or 1:4 ratio, w/w)/Ca (15nm)/Al (60nm) and tested. The best performances were obtained for a donor: acceptor ratio of 1:4 and thermal annealing at 110°C (**148**, **149**) or 120°C (**150**) affording a PCE of 2.17% (V_{OC}= 0.86V, J_{SC}= 6.08 mA.cm^{-2}, FF= 0.415) for **148**, 3.61% for **149** (V_{OC}= 0.90V, J_{SC}= 9.38 mA.cm^{-2}, FF= 0.428) and 3.89% (V_{OC}= 0.85V, J_{SC}= 9.74 mA.cm^{-2}, FF= 0.47) for **150**. Particularly, the thermal annealing has affected the electron mobility and hole-transport contributing into their balance (for instance for **150** μ_h = 1.70 10^{-6} cm^2 V^{-1} s^{-1} and μ_e = 1.13 10^{-4} cm^2 V^{-1} s^{-1} (μ_e/μ_h = 66.47) and after the thermal annealing μ_h = 1.01 10^{-5} cm^2 V^{-1} s^{-1} and μ_e = 1.89 10^{-5} cm^2 V^{-1} s^{-1} (μ_e/μ_h = 1.89)) and increased the miscibility of $PC_{71}BM$ facilitating the phase separation.

Analogously to **147** Nguyen et al. have designed and synthetized the chromophore **151** having a diketopyrrolopyrrole (DPP) as central electron-withdrawing core (Scheme **75**).[101]

Scheme 75

Replacement of the thiazolothiazole core by DPP has led to a strong red shift of 169 nm in chloroform solution (447 nm to 616 nm). In thin film, **151** exhibited two absorption bands centered at 660 nm and 742 nm shifting the absorption band edge from 1.72eV to 1.51eV. This significant change was ascribed to an improved molecular ordering as evidenced by AFM microphotographs and hole-mobility measurement (μ_h = 3.00 10^{-6} cm^2 V^{-1} s^{-1}). BHJ solar cells were fabricated with the structure ITO/PEDOT: PSS (40nm)/**151**: $PC_{61}BM$ (100 nm, blend ratios 30/70, 50/50, 70/30)/Al (100nm). Photovoltaic performances were evaluated for each donor: acceptor ratios. The best PCE of 2.33% (V_{OC}= 0.67V, J_{SC}= 8.42 mA.cm^{-2}, FF= 0.45) was obtained for a 70:30 ratio without any thermal post-treatment to prevent the BOC group elimination.

Adashi et al. also have investigated mesomorphic DPP-based chromophores, in order to achieve optimized photovoltaic efficiencies taking into account their intrinsic self-organizing properties (Scheme **76**).[102] Effect of the nature of the alkyl chains, with the appropriate ratio, on the photovoltaic performances was studied. As expected, compounds **152** exhibit liquid-crystalline properties and form well-developed nanostructured bulk heterojunction (BHJ) architectures with a fullerene derivative ($PC_{71}BM$). The organic solar cells have been fabricated with the standard device structure ITO/PEDOT: PSS (40nm)/**152**: $PC_{71}BM$ blend (90-120nm, 1:1, 1.5:1, and 2:1 ratios, w/w)/LiF (1nm)/Al (100nm) and evaluated under AM 1.5G illumination. The best performances were achieved with a 1:1 ratio after a thermal annealing at 140°C for **152a**. As evidenced on UV-Vis spectra, upon thermal post-treatment major structural changes were obtained in the solid state for the blend **152a**:$PC_{71}BM$ highlighting the formation of *H*-aggregates at the expense of *J*-aggregates that are predominant for **152b** even after heating. This thermo-responsive organization was fully in agreement with the LC state of **152a** occurring from 117°C upon heating. The self-assembling into ordered domains strongly affects the stacking in the solid state, the charge carriers mobilities and the solar cells performances. As anticipated **152a** exhibited the highest PCE of 4.30% (V_{OC}= 0.93V, J_{SC}= 8.37 mA.cm^{-2}, FF= 0.55) after thermal annealing (at 140°C) without any additives while **152a** gave only a PCE of 1.20% (V_{OC}= 0.93V, J_{SC}= 3.90 mA.cm^{-2}, FF= 0.36) (with a thermal post treatment at 120°C).

Scheme 76

To favor the π-π arrangement and the intermolecular contacts in the solid state DPP **153** end-capped with benzofuran units (Scheme **77**) has been synthetized and tested by Nguyen et al.[103] Thin film properties have been investigated from pure **153** to blends films of **153**: $PC_{71}BM$ at various ratios (30:70, 50:50, 60:40, 30:70) and temperatures (from room temperature to 150°C). From these experiments, it has been shown that changing the annealing temperature one can control and adjust the surface domains sizes for a given blend. These changes in morphologies are fully in agreement with the absorption and XRD experiments and correlated with the charge carrier mobility measured. Hence, from the understanding thin-films properties, the best conditions are obtained for a given donor: acceptor ratio of 60:40 annealed at 110°C. Using these criterions a PCE as high as 4.40% was achieved (V_{OC}= 0.92V, J_{SC}= 10.00 mA.cm^{-2}, FF= 0.48) in BHJ solar cells.

Scheme 77

Pursuing their efforts in structure-properties relationships in the DPP chromophores family, T.-Q. Nguyen et al. have studied the effects of stereoisomerism of **153** on the crystallization properties.[104] Typically, 2-ethylhexyl chains are widely used to improve the solution processability of the synthesized chromophore but possess the disadvantage to present an asymmetric carbon (*R* or *S* configuration) affording a mixture of stereoisomers that induce different solid-state properties. Thus, to elucidate the influence of the nature of the stereocenters on the optoelectrical properties the three stereoisomers, namely **153-*RR***, **153-*SS*** and **153-*RS*** (mesomer), were synthesized and purified by a preparative chiral HPLC. As expected, from crystallographic data **153-*RR*** and **153-*SS*** exhibit the same parameters (as they are enantiomers) while the mesomer **153-*RS*** exhibit two additional structures. In addition, due to its centrosymmetry **153-*RS*** adopt a coplanar structure with a π-π stacking of 3.28Å unlike **153-*RR*** or **153-*SS*** exhibit a twisted structure associated to inferior intermolecular stacking (3.47Å). Among these stereoisomers **153-*RS*** possesses the highest crystallinity and carrier mobility (μ_h = 2.80 10^{-3} cm^2 V^{-1} s^{-1} (after annealing at 100°C for 10 min.), for **153-*RR*** μ_h = 8.60 10^{-4} cm^2 V^{-1} s^{-1} and **153-*SS*** μ_h = 9.10 10^{-4} cm^2 V^{-1} s^{-1}). Unlike to **153**, **153-*RS*** exhibits larger crystalline domain size and better intermolecular contacts demonstrating the significant effect of the isomeric purity on the material's optoelectrical properties that could be benefit to improve the photovoltaic performances.

As seen in the previous sections, the most reported BHJ solar cells combine a small molecule (p-type) and exclusively a fullerene derivative (n-type). However, there still need to develop other n-type materials that can be used as alternatives of fullerene derivatives. For this purpose, Nguyen et al.[105] envisioned to investigate a novel heterojunction based on their DPP chromophores, such as **153** and/or **154**[106] and the dicyanoimidazole **155** (vinazene) acceptor (Scheme **78**).

BHJ solar cells were fabricated with the architecture ITO/PEDOT: PSS/**153** or **154**:**155a** or **155b**/Al. Current-density characteristics were determined with different blend ratios and at different annealing temperatures and compared with devices made from $PC_{61}BM$ as acceptor. As expected, the nature of the alkyl chains on vinazene derivatives **155** influences the optoelectrical properties: the less hindered and bulky hexyl chain led to more favorable morphology than its 2-ethylhexyl counterpart. Upon thermal annealing marginal improvement was observed. Nevertheless the best photovoltaic performances were obtained with a blend **154**:**155a** (1:1 ratio, 80°C) 0.80% (V_{OC}= 1.23V, J_{SC}= 2.30 mA.cm^{-2}, FF= 0.28) and **154**:**155b** (1:1 ratio, 110°C) 1.10% (V_{OC}= 1.08V, J_{SC}= 2.76 mA.cm^{-2}, FF= 0.35). Higher PCE values were achieved when $PC_{61}BM$ was used as acceptor up to 3.72% in the case of the blend **154**: $PC_{61}BM$ (1:1, 110°C, V_{OC}= 0.84V, J_{SC}= 9.26 mA.cm^{-2}, FF= 0.48) but with lower V_{OC}.

Scheme 78

A more deeply structure-properties relationships on **153** analogues have been conducted by Roncali et al. using a combination of benzothiophene or benzofuran with thienyl or furanyl-DPP-based D-A-D molecules (**153**, **156**) as well the replacement of the carbonyl groups of DPP by thioketo (**157**) (Scheme **79**).[107] Interestingly, within the series **156** the composition of the side chains has no effect on the HOMO-LUMO levels as evidenced by the absorption spectroscopy and the cyclic voltammetry. Furthermore and surprisingly using a planar heterojunction device structure ITO/PEDOT: PSS (40nm)/ **153-156** (20nm)/ C_{60} (50nm)/Al (100nm), only molecule **153** gave rise to a reasonable PCE of 2.50% (V_{OC}= 0.72V, J_{SC}= 7.90 mA.cm^{-2}, FF= 0.39) while for the others structures the PCE did not exceed 0.80%. Hence, minor structural modifications may cause dramatic changes on the optoelectrical properties. Additionally, although the replacement of the carbonyl of DPP by thioketo groups produces a significant reduction of the bandgap there is a complete attenuation of the photovoltaic conversion efficiency. The best structure from **153** was then used in a BHJ device structure with $PC_{61}BM$ affording a PCE of 3.13% (V_{OC}= 0.81V, J_{SC}= 10.01 mA.cm^{-2}, FF= 0.35) after a thermal annealing at 70°C.

Scheme 79

To fine tune the device performances Li et al. have investigated and synthesized highly polarizable DPP-based chromophores **158** using thiophene (**158a**), selenophene (**157b**) and/or fused thienothiophene (**158c**) as π-conjugated side-chains (Scheme **80**).[108] Electroptical properties and films properties were analyzed revealing that blends of **158b** and $PC_{61}BM$ exhibited the best film-forming characteristics and **158c** the poorer packing order. ITO/PEDOT: PSS/**158**: $PC_{61}BM$/Ca/Al devices were fabricated and evaluated. Increasing the donor: acceptor ratio (1:1, 2:1, 3:1) leads to an improvement of the photovoltaic performances in all cases. As expected from the solid-state properties analysis the best performance was achieved for **158b** with a PCE of 2.30% (3:1, V_{OC}= 0.86V, J_{SC}= 5.81 mA.cm^{-2}, FF= 0.46) while 160c exhibits the lowest PCE (1.25% (3:1, V_{OC}= 0.79V, J_{SC}= 4.51 mA.cm^{-2}, FF= 0.36).

Scheme 80

To get further insights various terminal modifications have been explored by Frechet et al. in order to promote their solid-state self-assembling via end-to-end π-π interactions (Scheme **81**).[109] End-groups were selected for their tendency to induce strong π-stacks like pyrene (derivatives **161-162**) and compared with non-planar analogues (**159**) and planar ones bearing non-coplanar substituents (**160**). Thin-film BHJ solar cells were fabricated with the following architecture ITO/PEDOT: PSS (30-40nm)/**159-162**: $PC_{71}BM$/Al (100nm). Devices prepared from **159** to **161** where optimized at a 1:4 donor: $PC_{71}BM$ ratio while a blend ratio of 2:1 was used for **162**. Increasing the donor part in the devices comprising compounds **159-161** leads to poorer conversion efficiencies even though an enhancement of the hole-mobilities was gained. In contrast in devices made from **162** higher concentration of donor up to the optimized 2:1 ratio enhanced both the fill factor and the hole-mobilities suggesting that pyrene promotes the molecular packing and film morphology in the solid-state that are favorable to an increase of the PCE. Indeed, the highest PCE of 3.7% (V_{OC}= 0.76V, J_{SC}= 8.30 mA.cm^{-2}, FF= 0.58) was achieved for **162b** after thermal annealing. Interestingly, **161** as only a PCE of 0.70% (V_{OC}= 0.73V, J_{SC}= 3.20 mA.cm^{-2}, FF= 0.29) compared to **162a** (2,40%, V_{OC}= 0.77V, J_{SC}= 5.70 mA.cm^{-2}, FF= 0.55) indicating that photovoltaic performances are strongly dependent both on end-group planarity and symmetry.

Scheme 81

Extension of the π-conjugated system, by the insertion of an acetylene linkage between the pyrene end-group and the DPP (**163**), and its consequences on PCE was investigated by Park et al. (Scheme **82**).[110] The insertion of the linkage favors a more planar geometry of the π-conjugated backbone for derivatives **163**, as supported by DFT calculation. This behavior should be beneficial to increase the PCE relative to **161**. BHJ with the structure ITO/PEDOT: PSS (30-40nm)/ **161** or **163**: $PC_{71}BM$ (7:3 ratio, 130nm)/Al (100nm) were prepared according to reported procedures. The performances of the solar cells were recorded under standard illumination conditions AM1.5 giving a PCE of 2.95% (V_{OC}= 0.85V, J_{SC}= 8.89 mA.cm^{-2}, FF= 0.42) that is almost 6,5 times greater than **161** measured in the same conditions (0.46% (0.70%),[109] V_{OC}= 0.79V, J_{SC}= 2.38 mA.cm^{-2}, FF= 0.27). The improved performances were unambiguously assigned to the acetylene linkage that induced a more planar backbone facilitating the intermolecular contacts and increased absorption.

Scheme 82

Controlling the morphology of the donor/acceptor domains in the active layer is of crucial importance to optimize the performance of the solar cells. Stupp et al. proposed recently an elegant strategy by combining synergistically different weak interactions within the active layer (namely H-bonds and π-π interactions) to control the supramolecular organization of each component upon proper and optimized conditions. Thus, they have combined a *trans*-1,2-diaminocyclohexane building block, that possesses the capability to engender H-bonding, with the DPP chromophore **164** affording the hairpin-shaped chromophore **165** (Scheme **83**).[111] Upon a careful stepwise cooling process associated to a minimal solution stirring led to the formation of a supramolecular nanowire driven by H-bonds and π–π stacking. This supramolecular arrangement should be helpful to improve the electroptical properties. Additionally, the shaped of **165** is also favorable to create cavities allowing better cofacials interfaces between donor and acceptor. Solar cells were fabricated using **165** as donor and $PC_{71}BM$ as acceptor under different conditions (systematically donor: acceptor ratio, temperature and solvent). Hence, a blend of disrupted assembly of **165**: $PC_{71}BM$ affords only a PCE of 1.40 10^{-3}% while a 400-fold greater PCE (0.53%, V_{OC}= 0.66V, J_{SC}= 2.98 mA.cm^{-2}, FF= 0.27) was achieved with devices fabricated with assembled **165** solutions. If **164** is used under the same conditions a PCE of 0.24% (V_{OC}= 0.57V, J_{SC}= 1.43 mA.cm^{-2}, FF= 0.29) was obtained, nevertheless in this case the concentration of the active component is higher attesting *de facto* that the self-assembling contributes significantly to enhance the device performances.

Scheme 83

Besides DPP, other interesting acceptors could be used for the synthesis of novel D-A-D structures. Among them, fluorenone has been widely used in this context. To study the role of fluorenone on photovoltaic performances, symmetrically chromophores bearing different π-conjugated side chains have been synthesized by Demadrille et al. (Scheme **84**).[112] Solar cells were fabricated with the following device structure ITO/PEDOT: PSS/**166-169**: $PC_{61}BM$ (1:2 or 1:1 ratio, 100 ±20nm)/LiF (0.80nm)/Al. As expected the molecules possessing the shortest π-conjugated systems have exhibited the lowest conversion efficiencies. The highest PCE reported for these compounds reaches 1.19%, for **169**, (V_{OC}= 0.82V, J_{SC}= 3.61 mA.cm^{-2}, FF= 0.40) after post-thermal treatment at 70°C at a 1:1 ratio. For compounds **166-168** PCEs are ranged from 0.14% to 0.58% (V_{OC}= 0.72V, J_{SC}= 0.73 mA.cm^{-2}, FF= 0.27 (**166**), (V_{OC}= 0.52V, J_{SC}= 0.91 mA.cm^{-2}, FF= 0.29, (**167**), (V_{OC}= 0.68V, J_{SC}= 2.67 mA.cm^{-2}, FF= 0.32 (**168**)) under the same conditions and without thermal annealing. furthermore, for **166** and **167** increasing the ratio from 1:1 to 1:2 gives to a substantial improvement of the PCE up to 0.37% (V_{OC}= 0.67V, J_{SC}= 1.85 mA.cm^{-2}, FF= 0.30) and 0.42% (V_{OC}= 0.75V, J_{SC}= 1.86 mA.cm^{-2}, FF= 0.30) respectively. Further enhancement can be achieved by thermal annealing at 80°C.

Scheme 84

Encouraged by the results reported on DPP oligothiophenes by Nguyen, isoindigo-based chromophores in conjunction with bithiophene as π-conjugated donor were developed and evaluated by Reynolds et al. (Scheme **85**).[113] Compounds **170** and **171** present remarkable broad spectra in the solid-state with estimated optical band-gaps of 1.67eV and 1.72eV, respectively. BHJ solar cells were made from spin-coated chlorobenzene solution of **170-171**: $PC_{61}BM$ blends onto ITO/PEDOT: PSS glass substrate. Various parameters have been optimized (comprising the solution concentrations, blends ratio, annealing temperature) in order to achieve the highest PCEs. For instance, optimized blend ratios were found to be 1:1 for **170** and 1.5:1 for **171**. After thermal annealing at 100 °C, the device fabricated from **170** showed significant better photovoltaic performances (PCE=1.76%) than the solar cell made from **171** (0.55%) (V_{OC}= 0.74V, J_{SC}= 6.30 mA.cm^{-2}, FF= 0.38 and V_{OC}= 0.66V, J_{SC}= 2.40 mA.cm^{-2}, FF= 0.36, respectively). The higher PCE for **170** was assigned to a better solid-state ordering, greater film morphology and lower energy gap.

Scheme 85

Recently, tetracyanobuta-1,3-diene (TCBD) has been developed as an efficient electron-withdrawing group for the synthesis of NLOphores with improved nonlinear properties and thermal stabilities. Thanks to its intrinsic properties, Roncali et al. have envisioned to use such TCBD for the design of active materials in photovoltaic devices.[114] Thus centrosymmetric and non-centrosymmetric D-A-D structures have been designed and synthesized (Scheme **86**). Compounds exhibit non-planar structures (restricting π -electron delocalization in the TCBD core) associated to good solubility and reduced aggregation in solution, high oxidation potentials and strong absorption properties. Bilayer heterojunction solar cells have been fabricated with the following structure ITO/PEDOT: PSS (40nm)/**172-174** (25nm)/C_{60} (20nm)/Al (100nm) and PCEs were determined under AM1.5 conditions at 90 mW/cm^2. As spin-casted from chloroform solution at 10 mM, chromophore **172** led to a PCE of 1.08% (V_{OC}= 0.97V, J_{SC}= 3.06 mA.cm^{-2}, FF= 0.33) while this PCE is reduced down to 0.56% when the chromophore is deposited by vacuum as a film of 13 nm. These encouraging results demonstrate the interest to use such acceptor for developing BHJ solar cells but improvements have to be pursued.

Scheme 86

D – A – D – A – D

Further improvements can be achieved by inserting additionally D-A π-conjugated chromophores to D-A-D architectures leading to D-A-D-A-D structures that should exhibit higher performances due to the extended π-conjugated backbone. Nevertheless, careful disposition and selection of the D and A have to be taken into account in order to optimize the optoelectrical properties.

Recently, Lee et al. have studied and compared the properties of D-A-D having the bithiazole (**175**) and the fused bithiazole (**176**, analogous of **149**) (Scheme **87**). BHJ solar cells have been fabricated with the following structure ITO/PEDOT: PSS/**175-176**: $PC_{71}BM$ (65-75nm)/Al and evaluated. The best performances, after device optimizations, were found to be 1.30% (1:3 ratio, V_{OC}= 0.97V, J_{SC}= 4.63 mA.cm^{-2}, FF= 0.29) and 2.39% (1:3 ratio, V_{OC}= 0.94V, J_{SC}= 6.49 mA.cm^{-2}, FF= 0.39). These performances might be improved by further optimization of the device morphology using processing additives, annealing, and so on. Additionally, it was speculated that the design of new molecular structures with these thiazole derivatives might also provide better tunings for seeking desirable band gap and energy levels and thereby enable better performance.[115]

Hence, from these thiazolo-based chromophores were designed and synthesized the extended π-conjugated systems **177-179** depicted in the Scheme **87**.[116, 117] Incorporation of fused π-conjugated aromatic units into small molecules have the benefit to stabilize the quinoidal structure and to increase both the rigidity and coplanarity of the molecular backbone. In turn, improved charge transport characteristics, reduction of the bandgap and enhancement of the absorption properties are expected that might all contribute to greater device performances.

Scheme 87

BHJ organic solar cells were prepared as follow glass/ITO/PEDOT: PSS (40nm)/**177-179**: $PC_{71}BM$ (60-70nm)/LiF (0.50nm)/Al (120nm). Compounds **177** and **178** exhibited similar absorption profiles in solution, however in the solid state **177** showed a better well-defined vibronic splitting than **178** indicating a greater efficient π-stacking and strong intermolecular interaction in the film confirmed by thin-film XRD. Furthermore, their electrochemical properties are consistent with their optical properties and molecular structures.

The device performances were evaluated under AM1.5 conditions at different weight ratios (1:1 to 1:4) and using chloroform (CF) or chlorobenzene (CB) as solvents. The best performances resulting from the optimization of the conditions led to a PCE of 1.09% for **177** (1:3 ratio in CF, V_{OC}= 0.81V, J_{SC}= 3.35 mA.cm^{-2}, FF= 0.41) and 1.62% for **178** (1:1 ratio in CF, V_{OC}= 0.76V, J_{SC}= 4.47 mA.cm^{-2}, FF= 0.48). Despite to better solid-state properties of **178**, the greater PCE attained for **179** than **178**, even when similar conditions were used (PCE is only 0.76% for **178** when 1:1 ratio is used), is ascribed to the finest film morphology for **178**. Analogously to **175** and **176**, changing the acceptor from **177** to **179** should lead to enhanced performances in favor of **179**. However, the device characteristics gave for the best BHJ solar cell a PCE of 1.44% (1:2 ratio in CB, V_{OC}= 0.75V, J_{SC}= 5.10 mA.cm^{-2}, FF= 0.38) that is inferior to what is expected and obtained for **178**. Nevertheless under the same conditions, *i.e.* 1:2 ratio in CB, **178** led to a PCE of 0.65% (V_{OC}= 0.73V, J_{SC}= 3.01 mA.cm^{-2}, FF= 0.29) confirming that fused bithiazole is a better acceptor than bithiazole.

Following the same strategy Marks et al have studied the influence of the shape of the naphthodithiophene core, *i.e.* linear (NDT) *vs* zig-zag (zNDT), on the photovoltaic performances of D-A-D-A-D comprising a DPP group as acceptor (Scheme **88**).[118, 119] Interestingly, by changing the shape of the central core from NDT to zNDT, both **180** and **181** exhibit the same optical properties and the same optical bandgap (1.70 eV). However **181** exhibits a predicable reduced oxidation potential compared to **180** that should affect in turn the V_{OC}. BHJ solar cells were fabricated with the structure ITO/PEDOT: PSS/**180**-**181**/$PC_{61}BM$/LiF/Al and evaluated. The device performances after optimizing the donor: acceptor ratio and the thermal annealing (1.5:1, 110°C for **180** and 1.2:1, 140°C for **181**) led to a PCE of 4.00% (V_{OC}= 0.84V, J_{SC}= 11.20 mA.cm^{-2}, FF= 0.43) and 4.40% (V_{OC}= 0.75V, J_{SC}= 11.70 mA.cm^{-2}, FF= 0.50) respectively. The results are consistent with the greater hole-mobility for **181** (μ_h = 1.00 10^{-4} cm^2 V^{-1}s^{-1}) than **180** (μ_h = 2.50 10^{-7} cm^2 V^{-1}s^{-1}) leading to a substantial enhancement of the short-circuit current in favor of **181** due to a more efficient charge separation and reduced recombination process.

Scheme 88

Recently, the indacenodithiophene (IDT) has sparked great interest as donor molecular building block due to its intrinsic properties, for instance a planar rigid structure, beneficial for the fabrication of SMOSCs. Thus, Hou et al have designed and synthesized small IDT-based chromophores with the structure **182** depicted on scheme **89**.[120] The synthesized chromophore presents optoelectronic properties that make it suitable for the fabrication of organic solar cells (E_g= 1.80eV, broad absorption in the visible region, low-lying HOMO energy, high thermal stability).

Hence, BHJ solar cells based on the blend **182**:$PC_{71}BM$ have been fabricated with the following architecture ITO/PEDOT: PSS (30nm)/**182**: $PC_{71}BM$ (80-100nm)/Ca/Al. Several conditions have been tested by varying the donor: acceptor ratio (from 1:1 to 1:4) leading to the highest PCE of 4.25% (V_{OC}= 0.93V, J_{SC}= 9.42 mA.cm^{-2}, FF= 0.48) for a 1:3 ratio. No further improvements have been achieved by the addition of DIO as solvent additive or even by thermal annealing. The results indicated that chromophores based on IDT core are promising materials for the fabrication of SMOSCs.

Scheme 89

Alongside the work of Marks based on NDT derivatives, Lee et al. have design new molecular D-A-D-A-D architectures based on the BDT unit, analogously to those described in scheme **32**. Chromophore **183** has been synthesized following known procedures and evaluated as donor in BHJ solar cells (Scheme **90**).[121] The solar cells based on the blend **183**:$PC_{71}BM$ have fabricated at different weight ratios, from 1:0.5 to 1:4, with the structure ITO/PEDOT: PSS (40nm)/**183**: $PC_{71}BM$ (50-55nm)/LiF (0.5nm)/Al (120nm). The best performance achieved without any post-treatment gave a PCE of 1.18% (V_{OC}= 0.83V, J_{SC}= 4.80 mA.cm^{-2}, FF= 0.29) at a 1:3 weight ratio. Impressive enhancement of the PCE up to 2.83% (V_{OC}= 0.85V, J_{SC}= 7.81 mA.cm^{-2}, FF= 0.39) was produced upon thermal annealing at 180°C due to a higher π-stacking order and increased hole-mobility up to μ_h = 2.70 10^{-6} cm^2 V^{-1}s^{-1} (untreated film μ_h = 1.40 10^{-6} cm^2 V^{-1}s^{-1}) corroborating the solid-state analysis. In addition the alkyloxy side-chains are helpful to ensure good film morphology and phase separation.

Scheme 90

DTS core has also demonstrated to be an important and useful molecular scaffold for the construction of active component for SMOSCs (see for example scheme **32**). To get further insights on the molecular design of new active donors based on the DTS unit, Bazan et al. have synthesized news D-A-D-A-D structures in association with thiadiazolo pyridine (PT) as acceptor and deeply studied the parameters affecting their photovoltaic performances (Scheme **91**).[122] From the solution to the solid-state the chromophore showed a broadening and a red shift of the optical absorption along with the emergence of a vibronic splitting coherent with a more rigid and ordered structure in the film (E_g =1.51eV). Such features lead to greater π-electron delocalization across the molecular backbone and enhanced inter-chromophore interactions. Upon thermal annealing up to and below 110°C the lowest energy absorption peak is enhanced consistent with a better π-stacking. In agreement with the opto-elelectrochemical properties of **184**, SM-BHJ photovoltaic devices were made using a standard device architecture of ITO/Plexcore® OC AQ/**184**: $PC_{71}BM$ (85-105nm)/Al. The active layers were optimized by varying the **184**: $PC_{71}BM$ weight ratios at 3 different thickness layers and thermal annealing 2 min. at 110°C. From this set of experiments the best performance was achieved for a 60:40 ratio with a blend thickness of 85nm leading to a PCE of 3.20% (V_{OC}= 0.70V, J_{SC}= 10.90 mA.cm^{-2}, FF= 0.42). Determination of the hole and electrons mobilities (μ_h = 1.50 10^{-6} cm^2 V^{-1}s^{-1}, μ_e = 5.30 10^{-5} cm^2 V^{-1}s^{-1}, respectively) leads to unbalanced charge carrier transport and may be responsible for the lower fill factor.

Scheme 91

In close collaboration with A.J. Heeger, mechanistic studies have been performed on the effect of solvent additives processed

active layers during the film morphology formation and their impact on the photovoltaic efficiencies.[123, 124] During this study it has been clearly demonstrated that the use of DIO improves, beyond doubts, the interfacial charge transfer between donor and acceptor domains. This effect was also investigated theoretically. It was also demonstrated that Si-based chromophores are more efficient than their carbon counterparts.[125] Carbon analogue of **184** showed only a PCE of 0.2% (as cast, V_{OC}= 0.66V, J_{SC}= 1.00 mA.cm^{-2}, FF= 0.26) and 0.09% (annealed, V_{OC}= 0.50V, J_{SC}= 0.60 mA.cm^{-2}, FF= 0.28) vs a PCE of 0.9% (as cast, V_{OC}= 0.67V, J_{SC}= 3.60 mA.cm^{-2}, FF= 0.29) and 3.3% (annealed, V_{OC}= 0.70V, J_{SC}= 9.90 mA.cm^{-2}, FF= 0.47) respectively for the blend **185**:$PC_{71}BM$ without additives. The lower efficiency for the carbon analogue is assigned to the presence of larger crystalline domains.

Heeger et al. have conducted additional structural modification on chromophore **184**. Thus, chromophore **185** corresponding to an isomer of **184** has been designed and synthesized (Scheme **92**).[126] The difference came only from the position of the N atom on the PT scaffold. Different weight ratios were evaluated and it was found that at a 7:3 ratio a remarkable PCE of 4.52% (V_{OC}= 0.80V, J_{SC}= 12.50 mA.cm^{-2}, FF= 0.45) was achieved for the blend **185**: $PC_{71}BM$ with a device structure ITO/MoOx/**185**: $PC_{71}BM$/Al. Indeed, it has been shown that ITO/PEDOT: PSS/**185**: $PC_{71}BM$/Al is not a suitable structure to test the performance of **185** due to the acidic character of PEDOT: PSS diminishing the conversion efficiencies and in particular a loss in V_{OC}. Interestingly, solar cells processed with 0,25% v/v DIO exhibit significant enhancement of the photocurrent generation leading to a PCE of 6.70% (V_{OC}= 0.78V, J_{SC}= 14.40 mA.cm^{-2}, FF= 0.59). Higher concentrations of additive lead to a decrease of the photovoltaic efficiencies. It is evidenced that through a rational molecular design associated to controlled active-layer processing methodologies it was possible to achieve highly efficient small organic solar cells.

Scheme 92

Scheme 93

The impact of the N atom and its position on **184** analogues was deeply investigated in a further work of Bazan (Scheme **93**) and compared to the non-nitrogen analogue **187**.[127] The position of the N-atom affects the self-assembling properties in the BHJ film and might be correlated to the dipole-dipole induced-orientation in the solid-state. Chromophores **183-186** exhibit similar optical behaviors in solution and in the solid-state with a pronounced vibronic splitting compared to **187**. Optical band gap are determined to be 1.50eV for **185**and **186**, 1.52eV for **184** and 1.58eV for **187**. The small molecules BHJ solar cells were fabricated with the structure of ITO/MoOx/**184-187**: $PC_{71}BM$/Al and tested under the same conditions and same donor: acceptor weight ratios. The devices were evaluated without any treatment giving PCEs of 4.52% for **185** (V_{OC}= 0.80V, J_{SC}= 12.50 mA.cm^{-2}, FF= 0.45), 2.47% for **186** (V_{OC}= 0.75V, J_{SC}= 8.90 mA.cm^{-2}, FF= 0.37), 1.78% for**184** (V_{OC}= 0.73V, J_{SC}= 7.40 mA.cm^{-2}, FF= 0.33) and 0.19% for **187** (V_{OC}= 0.83V, J_{SC}= 0.90 mA.cm^{-2}, FF= 0.26). Using 0.25% v/v DIO as solvent additive an increase of the photovoltaics efficiencies were obtained in most cases leading to the following PCEs 6.70% for **185** (V_{OC}= 0.78V, J_{SC}= 14.40 mA.cm^{-2}, FF= 0.59), 2.47% for **186** (V_{OC}= 0.73V, J_{SC}= 12.70 mA.cm^{-2}, FF= 0.60), 3.16% for **184** (V_{OC}= 0.72V, J_{SC}= 9.80 mA.cm^{-2}, FF= 0.45) and 0.18% for **187** (V_{OC}= 0.78V, J_{SC}= 0.90 mA.cm^{-2}, FF= 0.25). These results imply that the design of new organic materials for SMOSCs needs to consider not only the electronic structure and the nature of the side-chains but to also to take into account other interactions that can enhance/drive the self-assembly in the film.

Further improvement has been achieved by the introduction of a fluorine atom in place of the N-atom (Scheme **94**). This structural modification renders the chromophore less sensitive to acidic medium and may increase its stability. Photovoltaic devices were fabricated using the general structure of ITO/PEDOT: PSS/**188**: $PC_{71}BM$/Ca/Al and evaluated.[128]

Scheme 94

As a cast film without any post-treatment the device delivers a moderate photocurrent with a PCE of 1.80% (V_{OC}= 0.78V, J_{SC}= 6.60 mA.cm^{-2}, FF= 0.36). To improve the above efficiency, post-deposition thermal annealing were investigated and it was shown that heating 10 min. at 130°C gives an increase of the PCE up to 5.80% (V_{OC}= 0.82V, J_{SC}= 10.80 mA.cm^{-2}, FF= 0.65). Encouraged by these results further investigations in order to improve the device performances were pursued notably by using solvent additives. Progressive increase of DIO up to 0.4 v/v% followed by a thermal treatment at 70°C led to an impressive PCE of 7.00% (V_{OC}= 0.81V, J_{SC}= 12.80 mA.cm^{-2}, FF= 0.68).
Interestingly, a non-fullerene acceptor, namely the perylene diimide PDI, has been used for the fabrication of BHJ solar cells in combination with **188** as donor.[129] PDI exhibits complementary absorption spectra to that of **187** leading to a broad coverage of the visible spectrum. Screenings of the parameters that can influence the performances such as blend ratios, solvent additives and thermal annealing have been examined. Optimized devices were obtained for a 1:1 blend ratio dissolved in CB (30 mg.mL^{-1}) with 0.4% v/v of DIO. BHJ solar cells were fabricated with the standard architecture of ITO/PEDOT: PSS (45nm)/**188**: PDI (1:1, 110nm)/Ca (5nm)/Al (100nm) and evaluated. The highest PCE achieved under these conditions was 3.00% (V_{OC}= 0.78V, J_{SC}= 7.40 mA.cm^{-2}, FF= 0.52). Compared to **188**: $PC_{71}BM$ the lower IQE and reduced FF for **188**: PDI arise from the lower hole/electron mobilities and higher charge recombination as evidenced by experiments.

Finally, extended π-conjugated systems of **185** have been investigated regarding their electroptical properties in order to obtain insights into the role of the molecular size on the relevant properties that can be used for the fabrication of SM BHJ solar cells. [130]

Scheme 95

As expected compounds **189** and **190,** that are oligomeric analogues of **185**, exhibit a red-shift absorption spectra in solution and in the solid-state. From the absorption onsets, the optical band-gaps have been determined to be 1.44eV and 1.41eV respectively which agrees with the HOMO (-5.17eV, -5.04eV respectively) and LUMO energy levels determined by cyclic

voltammetry. In addition, the presence of a vibronic fine structure is associated to specific intermolecular interactions resulting from π-π overlaps in the thin film. Moreover, a thermal annealing (100°C) has shown to be benefit for improving the molecular organization as more intense π-π interactions were observed after a thermal treatment, which is more pronounced for **189**. These features are important to ensure efficient charge transport within the film. Hence, relatively high hole-mobilities were measured from the films $\mu_h = 1.00 \cdot 10^{-2}$ cm^2 V^{-1} s^{-1} (**189**) and $\mu_h = 6.00 \cdot 10^{-3}$ cm^2 V^{-1} s^{-1} (**190**) even after thermal treatment beyond 200°C moderate hole-mobilities are maintained $\mu_h = 3.00 \cdot 10^{-3}$ cm^2 V^{-1} s^{-1} at 230°C (**189**) and $\mu_h = 2.60 \cdot 10^{-3}$ cm^2 V^{-1} s^{-1} at 250°C (**190**). Owing to these considerations, BHJ solar cells have been prepared with the standard structure ITO/MoOx/**189** or **190**: $PC_{61}BM$/Al and tested. An optimal weight ratio of 60:40 for **189**: $PC_{61}BM$ blend followed by a thermal treatment at 100°C (10 min.) afford a PCE of 5.80% (V_{oc}= 0.71V, J_{SC}= 13.60 mA.cm^{-2}, FF= 0.60) while a PCE of 6.50% (V_{oc}= 0.66V, J_{SC}= 15.20 mA.cm^{-2}, FF= 0.65) is reached for **190**: $PC_{61}BM$ blend at ratio 50:50 without any post-deposition treatment. Indeed, it is worth noticing that for **190**: $PC_{61}BM$ blends thermal annealing does not affect the photovoltaic performances, which are also quite insensitive to the blend ratio composition. The general trends observed for **189** and **190** will be useful to design other materials with improved performances that can withstand major environmental changes.

Conclusions

The last decade has witnessed a rapid progress of organic photovoltaics boosted by the design and synthesis of novel π-conjugated small donor molecules, the control and optimization of both device processing and fabrication. Although some important progress has been reached, current challenges remain to further improve efficiency, durability and cost-effectiveness in order to compete with silicon-based solar cells. Within this article we aimed at suggesting some guiding principles for designing new efficient and emerging alternatives to π-conjugated polymers that are solution-processable, facile to synthesize, simple to purify and monodisperse for a batch-to-batch reproducibility. To date, efficiencies up to 7% have been reported and important understandings were found. The main approaches consist in either a modification of the photoactive layer itself or addition of extra transport/blocking layers to facilitate the contacts. As the injection and the photovoltage critically depend on the interface, molecular modifications or physical treatments have been proposed to appropriately modulate the injection barriers either at the electron or hole collecting electrodes (for instance, LiF or PEDOT: PSS respectively). As seen, optimized light harvesting material is also required to match with the solar spectrum and to enhance the photoconversion efficiency. Substantial increases of the solar photon harvesting have led to the design and synthesis of suitable organic low band-gaps materials with appropriate side-groups. Another way is to replace the $PC_{61}BM$ by $PC_{71}BM$ or by changing the nature of the acceptor with the aim to increase the absorption range. In addition, novel solutions can be applied to achieve the same effect, for instance the combination of small molecules with complementary absorption spectrum might be tested in the future. More importantly, the nanoscale morphology of the blend dramatically influences the photovoltaic properties. Hence, in order to increase the efficiency it is crucial to improve the miscibility of the mixed materials leading to finer phase segregation. This can be achieved by adding plasticizer additive, choosing the best solvents, controlling the evaporation time, their wettability and surface interactions, applying thermal annealing and varying the D-A composition. It is of crucial interest to develop also new methodologies and concepts to control the nanomorphology of the bulk heterojunction based on our supramolecular chemistry knowledge, crystallisation processes and solid-sate controlled orientation.

Acknowledgment

This work was supported by the Centre National de la Recherche Scientifique, the Ministère de l'Enseignement Supérieur et de la Recherche (MESR and Aix-Marseille Université throughout their financial support. Financial support from ANR program (SAGe III-V project ANR-11-BS10-012) and "Solutions Communicantes Sécurisées" (SCS) competitive cluster are also acknowledged. V.M. thanks also the Ministère de l'Enseignement Supérieur et de la Recherche for its doctoral financial support.

Notes and references

[a] *Centre Interdisciplinaire de Nanoscience de Marseille (CINaM - UMR CNRS 7325), Aix-Marseille Université, 163 Ave de Luminy case 913, 13288 Marseille cedex 09, France. Fax: +33(0) 491 418 916; Tel: +33(0) 629 413 925; E-mail: raimundo@cinam.univ-mrs.fr*

[b] *Institut Matériaux Microélectronique Nanosciences de Provence-(IM2NP, CNRS-UMR 7334, Aix-Marseille Université, Domaine Universitaire de Saint-Jérôme, Service 231, 13 397 Marseille Cedex 20, France. Institut Supérieur de l'Electronique et du Numérique CNRS, (IM2NP UMR CNRS 7334), Maison des Technologies, Place Georges Pompidou, F-83000 Toulon, France. Fax: +33(0) 494 038 951; Tel: +33(0) 494 038 950; E-mail: lionel.patrone@im2np.fr*

1. G. A. Chamberlain, *Sol. Cells*, 1983, **8**, 47–83.
2. C. W. Tang, *Appl. Phys. Lett.*, 1986, **48**, 183–185.
3. N. S. Sariciftci, L. Smilowitz, A. J. Heeger, and F. Wudi, *Science (80-.).*, 1992, **258**, 1474–1476.
4. a) C. Uhrich, R. Schueppel, A. Petrich, M. Pfeiffer, K. Leo, E. Brier, P. Kilickiran, and P. Baeuerle, *Adv. Funct. Mater.*, 2007, **17**, 2991–2999. b) P. Huhomme, *EPJ Photovoltaics*, 2013, **4**, 40401.
5. a) J. Roncali, *Acc. Chem. Res.*, 2009, **42**, 1719–1730; b) B. Walker, C. Kim, T.-Q. Nguyen, *Chem. Mater.*, 2011, **23**, 470-482; c) A. Mishra, P. Bauerle, *Angew. Chem. Int. Ed.*, 2012, **51**, 2020-2067; d) Y. Lin, Y. Li, X. Zhan, *Chem. Soc. Rev.*, 2012, **41**, 4245-4270; e) J. Roncali, P. Leriche, P. Blanchard, *Adv. Mater*, 2014, **26**, 3821-3838; f) J. E. Coughlin, Z. B. Henson, G. C. Welch, G. C. Bazan, *Acc. Chem. Res.*, 2014, **47**, 257-270.
6. a) M. A. Green, K. Emery, Y. Hishikawa, W. Warta, E. D. Dunlop, *Prog. Photovolt: Res. Appl.*, 2013, **21**, 827-837. b) R. F. Service, *Science*, 2011, **332**, 293-293.
7. P. F. Xia, X. J. Feng, J. Lu, S.-W. Tsang, R. Movileanu, Y. Tao, and M. S. Wong, *Adv. Mater.*, 2008, **20**, 4810–4815.
8. W. Zhang, S. C. Tse, J. Lu, Y. Tao, and M. S. Wong, *J. Mater. Chem.*, 2010, **20**, 2182–2189.
9. P. F. Xia, X. J. Feng, J. Lu, R. Movileanu, Y. Tao, J.-M. Baribeau, and M. S. Wong, *J. Phys. Chem. C*, 2008, **112**, 16714–16720.
10. H. M. Ko, H. Choi, S. Paek, K. Kim, K. Song, J. K. Lee, and J. Ko, *J. Mater. Chem.*, 2011, **21**, 7248–7253.
11. N. Cho, J. Kim, K. Song, J. K. Lee, and J. Ko, *Tetrahedron*, 2012, **68**, 4029–4036.

12. J. Kim, H. M. Ko, N. Cho, S. Paek, J. K. Lee, and J. Ko, *RSC Adv.*, 2012, **2**, 2692–2695.
13. H.-W. Lin, L.-Y. Lin, Y.-H. Chen, C.-W. Chen, Y. Lin, S.-W. Chiu, and K.-T. Wong, *Chem. Commun.*, 2011, **47**, 7872–7874.
14. H. Bürckstümmer, E. V. Tulyakova, M. Deppisch, M. R. Lenze, N. M. Kronenberg, M. Gsänger, M. Stolte, K. Meerholz, and F. Würthner, *Angew. Chemie*, 2011, **123**, 11832–11836.
15. A. Leliège, C.-H. Le Régent, M. Allain, P. Blanchard, and J. Roncali, *Chem. Commun.*, 2012, **48**, 8907–8909.
16. V. Jeux, D. Demeter, P. Leriche, and J. Roncali, *RSC Adv.*, 2013, **3**, 5811–5814.
17. A. Leliège, J. Grolleau, M. Allain, P. Blanchard, D. Demeter, T. Rousseau, and J. Roncali, *Chem. Eu. J.*, 2013, **19**, 9948–9960.
18. L.-Y. Lin, Y.-H. Chen, Z.-Y. Huang, H.-W. Lin, S.-H. Chou, F. Lin, C.-W. Chen, Y.-H. Liu, and K.-T. Wong, *J. Am. Chem. Soc.*, 2011, **133**, 15822–15825.
19. S.-W. Chiu, L.-Y. Lin, H.-W. Lin, Y.-H. Chen, Z.-Y. Huang, Y.-T. Lin, F. Lin, Y.-H. Liu, and K.-T. Wong, *Chem. Commun.*, 2012, **48**, 1857–1859.
20. Y.-H. Chen, L.-Y. Lin, C.-W. Lu, F. Lin, Z.-Y. Huang, H.-W. Lin, P.-H. Wang, Y.-H. Liu, K.-T. Wong, J. Wen, D. J. Miller, and S. B. Darling, *J. Am. Chem. Soc.*, 2012, **134**, 13616–13623.
21. H.-W. Lin, H.-W. Kang, Z.-Y. Huang, C.-W. Chen, Y.-H. Chen, L.-Y. Lin, F. Lin, and K.-T. Wong, *Org. Electron.*, 2012, **13**, 1925–1929.
22. S. Roquet, A. Cravino, P. Leriche, O. Alévêque, P. Frère, and J. Roncali, *J. Am. Chem. Soc.*, 2006, **128**, 3459–3466.
23. A. Cravino, P. Leriche, O. Alévêque, S. Roquet, and J. Roncali, *Adv. Mater.*, 2006, **18**, 3033–3037.
24. A. Cravino, S. Roquet, O. Alévêque, P. Leriche, P. Frère, and J. Roncali, *Chem. Mater.*, 2006, **18**, 2584–2590.
25. E. Ripaud, T. Rousseau, P. Leriche, and J. Roncali, *Adv. Energy Mater.*, 2011, **1**, 540–545.
26. O. Kim, A. Fort, M. Barzoukas, M. Blanchard-Desce, and J.-M. Lehn, *J. Mater. Chem.*, 1999, **9**, 2227–2232.
27. D. Deng, S. Shen, J. Zhang, C. He, Z. Zhang, and Y. Li, *Org. Electron.*, 2012, **13**, 2546–2552.
28. Y. Lin, Z.-G. Zhang, H. Bai, Y. Li, and X. Zhan, *Chem. Commun.*, 2012, **48**, 9655–9657.
29. Y. Lin, Z.-G. Zhang, Y. Li, D. Zhu, and X. Zhan, *J. Mater. Chem. A*, 2013, **1**, 5128–5135.
30. S. Shen, L. Gao, C. He, Z. Zhang, Q. Sun, and Y. Li, *Org. Electron.*, 2013, **14**, 875–881.
31. J. Zhang, D. Deng, C. He, Y. He, M. Zhang, Z.-G. Zhang, Z. Zhang, and Y. Li, *Chem. Mater.*, 2011, **23**, 817–822.
32. J. Min, Y. N. Luponosov, T. Ameri, A. Elschner, S. M. Peregudova, D. Baran, T. Heumüller, N. Li, F. Machui, S. Ponomarenko, and C. J. Brabec, *Org. Electron.*, 2013, **14**, 219–229.
33. H. Shang, H. Fan, Y. Liu, W. Hu, Y. Li, and X. Zhan, *Adv. Mater.*, 2011, **23**, 1554–1557.
34. J. Zhang, J. Yu, C. He, D. Deng, Z.-G. Zhang, M. Zhang, Z. Li, and Y. Li, *Org. Electron.*, 2012, **13**, 166–172.
35. L. Gao, J. Zhang, C. He, S. Shen, Y. Zhang, H. Liu, Q. Sun, and Y. Li, *Sci. China Chem.*, 2013, **56**, 997–1003.
36. G. Wu, G. Zhao, C. He, J. Zhang, Q. He, X. Chen, and Y. Li, *Sol. Energy Mater. Sol. Cells*, 2009, **93**, 108–113.
37. C. He, Q. He, Y. Yi, G. Wu, F. Bai, Z. Shuai, and Y. Li, *J. Mater. Chem.*, 2008, **18**, 4085–4090.
38. X. Guo, L. Xiao, W. Tang, B. Liu, R. Cui, and Y. Zou, *J. Mater. Sci.*, 2013, **48**, 5833–5839.
39. Y. Lin, P. Cheng, Y. Li, and X. Zhan, *Chem. Commun.*, 2012, **48**, 4773–4775.
40. J.-Y. Pan, L.-J. Zuo, X.-L. Hu, W.-F. Fu, M.-R. Chen, L. Fu, X. Gu, H.-Q. Shi, M.-M. Shi, H.-Y. Li, and H.-Z. Chen, *ACS Appl. Mater. Interfaces*, 2013, **5**, 972–980.
41. A. Tang, L. Li, Z. Lu, J. Huang, H. Jia, C. Zhan, Z. Tan, Y. Li, and J. Yao, *J. Mater. Chem. A*, 2013, **1**, 5747–5757.
42. Y. Jiang, D. Yu, L. Lu, C. Zhan, D. Wu, W. You, Z. Xie, and S. Xiao, *J. Mater. Chem. A*, 2013, **1**, 8270–8279.
43. Z. Lu, C. Li, T. Fang, G. Li, and Z. Bo, *J. Mater. Chem. A*, 2013, **1**, 7657–7665.
44. D. Ni, B. Zhao, T. Shi, S. Ma, G. Tu, and H. Wu, *ACS Macro Lett.*, 2013, **2**, 621–624.
45. D. Demeter, T. Rousseau, P. Leriche, T. Cauchy, R. Po, and J. Roncali, *Adv. Funct. Mater.*, 2011, **21**, 4379–4387.
46. Y. Liu, X. Wan, B. Yin, J. Zhou, G. Long, S. Yin, and Y. Chen, *J. Mater. Chem.*, 2010, **20**, 2464–2468.
47. B. Yin, L. Yang, Y. Liu, Y. Chen, Q. Qi, F. Zhang, and S. Yin, *Appl. Phys. Lett.*, 2010, **97**, 023303.
48. Y. Liu, X. Wan, F. Wang, J. Zhou, G. Long, J. Tian, J. You, Y. Yang, and Y. Chen, *Adv. Energy Mater.*, 2011, **1**, 771–775.
49. Z. Li, G. He, X. Wan, Y. Liu, J. Zhou, G. Long, Y. Zuo, M. Zhang, and Y. Chen, *Adv. Energy Mater.*, 2012, **2**, 74–77.
50. G. He, Z. Li, X. Wan, Y. Liu, J. Zhou, G. Long, M. Zhang, and Y. Chen, *J. Mater. Chem.*, 2012, **22**, 9173–9180.
51. G. He, Z. Li, X. Wan, J. Zhou, G. Long, S. Zhang, M. Zhang, and Y. Chen, *J. Mater. Chem. A*, 2013, **1**, 1801–1809.
52. J. Zhou, X. Wan, Y. Liu, G. Long, F. Wang, Z. Li, Y. Zuo, C. Li, and Y. Chen, *Chem. Mater.*, 2011, **23**, 4666–4668.
53. Y. Liu, X. Wan, F. Wang, J. Zhou, G. Long, J. Tian, and Y. Chen, *Adv. Mater.*, 2011, **23**, 5387–5391.
54. J. Zhou, X. Wan, Y. Liu, Y. Zuo, Z. Li, G. He, G. Long, W. Ni, C. Li, X. Su, and Y. Chen, *J. Am. Chem. Soc.*, 2012, **134**, 16345–16351.
55. C. Cui, J. Min, C.-L. Ho, T. Ameri, P. Yang, J. Zhao, C. J. Brabec, and W.-Y. Wong, *Chem. Commun.*, 2013, **49**, 4409–4411.
56. D. Patra, C.-C. Chiang, W.-A. Chen, K.-H. Wei, M.-C. Wu, and C.-W. Chu, *J. Mater. Chem. A*, 2013, **1**, 7767–7774.
57. S. Shen, P. Jiang, C. He, J. Zhang, P. Shen, Y. Zhang, Y. Yi, Z. Zhang, Z. Li, and Y. Li, *Chem. Mater.*, 2013, **25**, 2274–2281.
58. J. Huang, C. Zhan, X. Zhang, Y. Zhao, Z. Lu, H. Jia, B. Jiang, J. Ye, S. Zhang, A. Tang, Y. Liu, Q. Pei, and J. Yao, *ACS Appl. Mater. Interfaces*, 2013, **5**, 2033–2039.
59. Y. Lin, L. Ma, Y. Li, Y. Liu, D. Zhu, and X. Zhan, *Adv. Energy Mater.*, 2013, **3**, 1166–1170.
60. Y. S. Choi and W. H. Jo, *Org. Electron.*, 2013, **14**, 1621–1628.
61. L. Zhang, S. Zeng, L. Yin, C. Ji, K. Li, Y. Li, and Y. Wang, *New J. Chem.*, 2013, **37**, 632–639.
62. X. Lin, Y. Tani, R. Kanda, K. Nakayama, and S. Yagai, *J. Mater. Chem. A*, 2013, **1**, 14686–14691.
63. B. Walker, J. Liu, C. Kim, G. C. Welch, J. K. Park, J. Lin, P. Zalar, C. M. Proctor, J. H. Seo, G. C. Bazan, and T.-Q. Nguyen, *Energy Environ. Sci.*, 2013, **6**, 952–962.
64. W. Li, M. Kelchtermans, M. M. Wienk, and R. a. J. Janssen, *J. Mater. Chem. A*, 2013, **1**, 15150–15157.
65. H. Bai, P. Cheng, Y. Wang, L. Ma, Y. Li, D. Zhu, and X. Zhan, *J. Mater. Chem. A*, 2014, **2**, 778–784.
66. K. Schulze, C. Uhrich, R. Schüppel, K. Leo, M. Pfeiffer, E. Brier, E. Reinold, and P. Bäuerle, *Adv. Mater.*, 2006, **18**, 2872–2875.
67. R. Fitzner, E. Reinold, A. Mishra, E. Mena-Osteritz, H. Ziehlke, C. Körner, K. Leo, M. Riede, M. Weil, O. Tsaryova, A. Weiß, C. Uhrich, M. Pfeiffer, and P. Bäuerle, *Adv. Funct. Mater.*, 2011, **21**, 897–910.
68. R. Fitzner, E. Mena-Osteritz, A. Mishra, G. Schulz, E. Reinold, M. Weil, C. Körner, H. Ziehlke, C. Elschner, K. Leo, M. Riede, M. Pfeiffer, C. Uhrich, and P. Bäuerle, *J. Am. Chem. Soc.*, 2012, **134**, 11064–11067.
69. a) S. Haid, A. Mishra, C. Uhrich, M. Pfeiffer, and P. Bäuerle, *Chem. Mater.*, 2011, **23**, 4435–4444; b) N. F. Montcada, B. Pelado, A. Viterisi, J. Albero, J. Coro, P. de la Cruz, F. Langa, E. Palomares, *Org. Electron*., 2013, **14**, 2826-2832.
70. S. Steinberger, A. Mishra, E. Reinold, J. Levichkov, C. Uhrich, M. Pfeiffer, and P. Bäuerle, *Chem. Commun.*, 2011, **47**, 1982–1984.
71. P. Li, H. Tong, J. Ding, Z. Xie, and L. Wang, *J. Mater. Chem. A*, 2013, **1**, 8805–8812.
72. Y. Chen, C. Li, P. Zhang, Y. Li, X. Yang, L. Chen, and Y. Tu, *Org. Electron.*, 2013, **14**, 1424–1434.
73. S. Steinberger, A. Mishra, E. Reinold, C. M. Müller, C. Uhrich, M. Pfeiffer, and P. Bäuerle, *Org. Lett.*, 2011, **13**, 90–93.
74. X. Wan, Y. Liu, F. Wang, J. Zhou, G. Long, and Y. Chen, *Org. Electron.*, 2013, **14**, 1562–1569.

75. S. Steinberger, A. Mishra, E. Reinold, E. Mena-Osteritz, H. Müller, C. Uhrich, M. Pfeiffer, and P. Bäuerle, *J. Mater. Chem.*, 2012, **22**, 2701–2712.
76. J. a Mikroyannidis, M. M. Stylianakis, P. Balraju, P. Suresh, and G. D. Sharma, *ACS Appl. Mater. Interfaces*, 2009, **1**, 1711–1718.
77. G. D. Sharma, P. Suresh, J. a. Mikroyannidis, and M. M. Stylianakis, *J. Mater. Chem.*, 2010, **20**, 561–567.
78. L.-Y. Lin, C. Lu, W. Huang, Y. Chen, H. Lin, and K.-T. Wong, *Org. Lett.*, 2011, **13**, 4962–4965.
79. D. Ye, X. Li, L. Yan, W. Zhang, Z. Hu, Y. Liang, J. Fang, W.-Y. Wong, and X. Wang, *J. Mater. Chem. A*, 2013, **1**, 7622–7629.
80. K.-H. Kim, H. Yu, H. Kang, D. J. Kang, C.-H. Cho, H.-H. Cho, J. H. Oh, and B. J. Kim, *J. Mater. Chem. A*, 2013, **1**, 14538–14547.
81. K. H. Lam, T. R. B. Foong, Z. E. Ooi, J. Zhang, A. C. Grimsdale, and Y. M. Lam, *ACS Appl. Mater. Interfaces*, 2013, **5**, 13265–13274.
82. C. He, Q. He, Y. He, Y. Li, F. Bai, C. Yang, Y. Ding, L. Wang, and J. Ye, *Sol. Energy Mater. Sol. Cells*, 2006, **90**, 1815–1827.
83. W. Li, C. Du, F. Li, Y. Zhou, M. Fahlman, Z. Bo, and F. Zhang, *Chem. Mater.*, 2009, **21**, 5327–5334.
84. H. Shang, H. Fan, Q. Shi, S. Li, Y. Li, and X. Zhan, *Sol. Energy Mater. Sol. Cells*, 2010, **94**, 457–464.
85. Q. Hou, Y. Chen, H. Zhen, Z. Ma, W. Hong, G. Shi, and F. Zhang, *J. Mater. Chem. A*, 2013, **1**, 4937–4940.
86. D. Deng, Y. Yang, J. Zhang, C. He, M. Zhang, Z.-G. Zhang, Z. Zhang, and Y. Li, *Org. Electron.*, 2011, **12**, 614–622.
87. J. Zhang, G. Wu, C. He, D. Deng, and Y. Li, *J. Mater. Chem.*, 2011, **21**, 3768–3774.
88. Y. Lin, P. Cheng, Y. Liu, X. Zhao, D. Li, J. Tan, W. Hu, Y. Li, and X. Zhan, *Sol. Energy Mater. Sol. Cells*, 2012, **99**, 301–307.
89. Y. Lin, P. Cheng, Y. Liu, Q. Shi, W. Hu, Y. Li, and X. Zhan, *Org. Electron.*, 2012, **13**, 673–680.
90. a) Q. Liu, Z. Du, W. Chen, L. Sun, Y. Chen, M. Sun, and R. Yang, *Synth. Met.*, 2013, **178**, 38–43. b) W. Ying, F. Guo, J. Li, Q. Zhang, W. Wu, H. Tian, J. Hua, *ACS Appl. Mater. Interfaces*, 2012, **4**, 4215-4224.
91. H.-Y. Wang, J. Gao, L.-J. Gu, J.-H. Wan, W. Wei, and F. Liu, *J. Mater. Chem. A*, 2013, **1**, 5875–5885.
92. S. Song, T. Kim, H. Park, Y. Jin, I. Kim, J. Y. Kim, and H. Suh, *Synth. Met.*, 2013, **183**, 16–23.
93. M. Sun, L. Wang, X. Zhu, B. Du, R. Liu, W. Yang, and Y. Cao, *Sol. Energy Mater. Sol. Cells*, 2007, **91**, 1681–1687.
94. M. Sun, L. Wang, B. Du, Y. Xiong, R. Liu, and Y. Cao, *Synth. Met.*, 2008, **158**, 125–129.
95. V. Tamilavan, M. Song, S.-H. Jin, and M. H. Hyun, *Bull. Korean Chem. Soc.*, 2013, **34**, 661–664.
96. S. Zeng, L. Yin, X. Jiang, Y. Li, and K. Li, *Dye. Pigment.*, 2012, **95**, 229–235.
97. S. Zeng, L. Yin, C. Ji, X. Jiang, K. Li, Y. Li, and Y. Wang, *Chem. Commun.*, 2012, **48**, 10627–10629.
98. S. Paek, N. Cho, K. Song, M.-J. Jun, J. K. Lee, and J. Ko, *J. Phys. Chem. C*, 2012, **116**, 23205–23213.
99. M. Nazim, S. Ameen, M. S. Akhtar, Y.-S. Lee, and H.-S. Shin, *Chem. Phys. Lett.*, 2013, **574**, 89–93.
100. P. Cheng, Q. Shi, Y. Lin, Y. Li, and X. Zhan, *Org. Electron.*, 2013, **14**, 599–606.
101. A. B. Tamayo, B. Walker, and T.-Q. Nguyen, *J. Phys. Chem. C*, 2008, **112**, 11545–11551.
102. W. Shin, T. Yasuda, G. Watanabe, Y. S. Yang, and C. Adachi, *Chem. Mater.*, 2013, **25**, 2549–2556.
103. B. Walker, A. B. Tamayo, X.-D. Dang, P. Zalar, J. H. Seo, A. Garcia, M. Tantiwiwat, and T.-Q. Nguyen, *Adv. Funct. Mater.*, 2009, **19**, 3063–3069.
104. J. Liu, Y. Zhang, H. Phan, A. Sharenko, P. Moonsin, B. Walker, V. Promarak, and T.-Q. Nguyen, *Adv. Mater.*, 2013, **25**, 3645–3650.
105. B. Walker, X. Han, C. Kim, A. Sellinger, and T.-Q. Nguyen, *ACS Appl. Mater. Interfaces*, 2012, **4**, 244–250.
106. C. Kim, J. Liu, J. Lin, A. B. Tamayo, B. Walker, G. Wu, and T.-Q. Nguyen, *Chem. Mater.*, 2012, **24**, 1699–1709.
107. E. Ripaud, D. Demeter, T. Rousseau, E. Boucard-Cétol, M. Allain, R. Po, P. Leriche, and J. Roncali, *Dye. Pigment.*, 2012, **95**, 126–133.
108. J. Huang, H. Jia, L. Li, Z. Lu, W. Zhang, W. He, B. Jiang, A. Tang, Z. Tan, C. Zhan, Y. Li, and J. Yao, *Phys. Chem. Chem. Phys.*, 2012, **14**, 14238–14242.
109. O. P. Lee, A. T. Yiu, P. M. Beaujuge, C. H. Woo, T. W. Holcombe, J. E. Millstone, J. D. Douglas, M. S. Chen, and J. M. J. Fréchet, *Adv. Mater.*, 2011, **23**, 5359–5363.
110. J.-W. Mun, I. Cho, D. Lee, W. S. Yoon, O. K. Kwon, C. Lee, and S. Y. Park, *Org. Electron.*, 2013, **14**, 2341–2347.
111. A. Ruiz-Carretero, T. Aytun, C. J. Bruns, C. J. Newcomb, W.-W. Tsai, and S. I. Stupp, *J. Mater. Chem. A*, 2013, **1**, 11674–11681.
112. F. Lincker, N. Delbosc, S. Bailly, R. De Bettignies, M. Billon, A. Pron, and R. Demadrille, *Adv. Funct. Mater.*, 2008, **18**, 3444–3453.
113. J. Mei, K. R. Graham, R. Stalder, and J. R. Reynolds, *Org. Lett.*, 2010, **12**, 660–663.
114. A. Leliège, P. Blanchard, T. Rousseau, and J. Roncali, *Org. Lett.*, 2011, **13**, 3098–3101.
115. P. Dutta, W. Yang, S. H. Eom, and S.-H. Lee, *Org. Electron.*, 2012, **13**, 273–282.
116. P. Dutta, H. Park, W.-H. Lee, I.-N. Kang, and S.-H. Lee, *Org. Electron.*, 2012, **13**, 3183–3194.
117. P. Dutta, W. Yang, W.-H. Lee, I. N. Kang, and S.-H. Lee, *J. Mater. Chem.*, 2012, **22**, 10840–10851.
118. S. Loser, C. J. Bruns, H. Miyauchi, R. P. Ortiz, A. Facchetti, S. I. Stupp, and T. J. Marks, *J. Am. Chem. Soc.*, 2011, **133**, 8142–8145.
119. S. Loser, H. Miyauchi, J. W. Hennek, J. Smith, C. Huang, A. Facchetti, and T. J. Marks, *Chem. Commun.*, 2012, **48**, 8511–8513.
120. W. Yong, M. Zhang, X. Xin, Z. Li, Y. Wu, X. Guo, Z. Yang, and J. Hou, *J. Mater. Chem. A*, 2013, **1**, 14214–14220.
121. P. Dutta, J. Kim, S. H. Eom, W.-H. Lee, I. N. Kang, and S. Lee, *ACS Appl. Mater. Interfaces*, 2012, **4**, 6669–6675.
122. G. C. Welch, L. a. Perez, C. V. Hoven, Y. Zhang, X.-D. Dang, A. Sharenko, M. F. Toney, E. J. Kramer, T.-Q. Nguyen, and G. C. Bazan, *J. Mater. Chem.*, 2011, **21**, 12700–12709.
123. L. G. Kaake, G. C. Welch, D. Moses, G. C. Bazan, and A. J. Heeger, *J. Phys. Chem. Lett.*, 2012, **3**, 1253–1257.
124. J. J. Jasieniak, B. B. Y. Hsu, C. J. Takacs, G. C. Welch, G. C. Bazan, D. Moses, and A. J. Heeger, *ACS Nano*, 2012, **6**, 8735–8745.
125. N. D. Eisenmenger, G. M. Su, G. C. Welch, C. J. Takacs, G. C. Bazan, E. J. Kramer, and M. L. Chabinyc, *Chem. Mater.*, 2013, **25**, 1688–1698.
126. Y. Sun, G. C. Welch, W. L. Leong, C. J. Takacs, G. C. Bazan, and A. J. Heeger, *Nat. Mater.*, 2012, **11**, 44–48.
127. C. J. Takacs, Y. Sun, G. C. Welch, L. A. Perez, X. Liu, W. Wen, G. C. Bazan, and A. J. Heeger, *J. Am. Chem. Soc.*, 2012, **134**, 16597–16606.
128. T. S. van der Poll, J. A. Love, T.-Q. Nguyen, and G. C. Bazan, *Adv. Mater.*, 2012, **24**, 3646–3649.
129. A. Sharenko, C. M. Proctor, T. S. van der Poll, Z. B. Henson, T.-Q. Nguyen, and G. C. Bazan, *Adv. Mater.*, 2013, **25**, 4403–4406.
130. X. Liu, Y. Sun, L. a Perez, W. Wen, M. F. Toney, A. J. Heeger, and G. C. Bazan, *J. Am. Chem. Soc.*, 2012, **134**, 20609–20612.

Thiophene-based push-pull chromophores for small molecule organic solar cells (SMOSCs).

Volodymyr Malytskyi,[a, b] Jean-Jacques Simon [b], Lionel Patrone*[b] and Jean-Manuel Raimundo*[a]

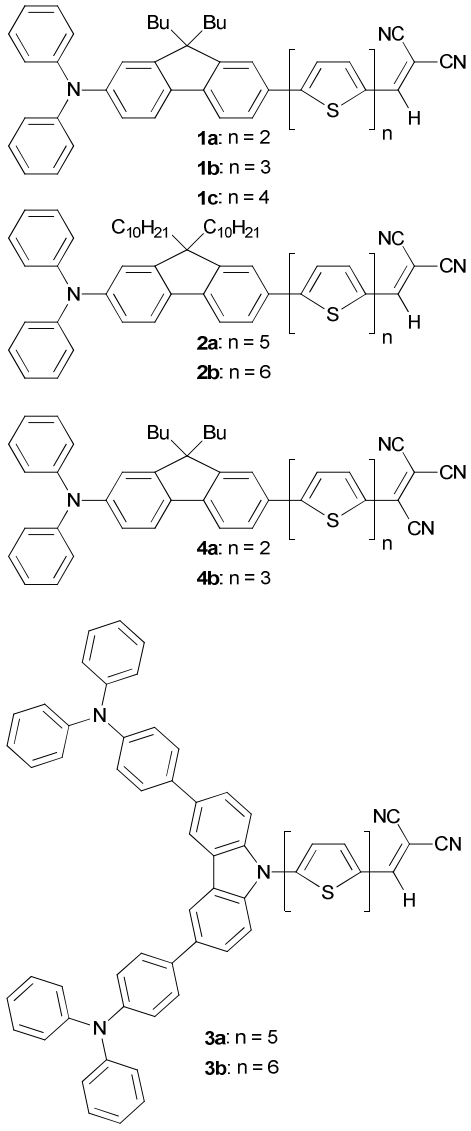

Scheme 1

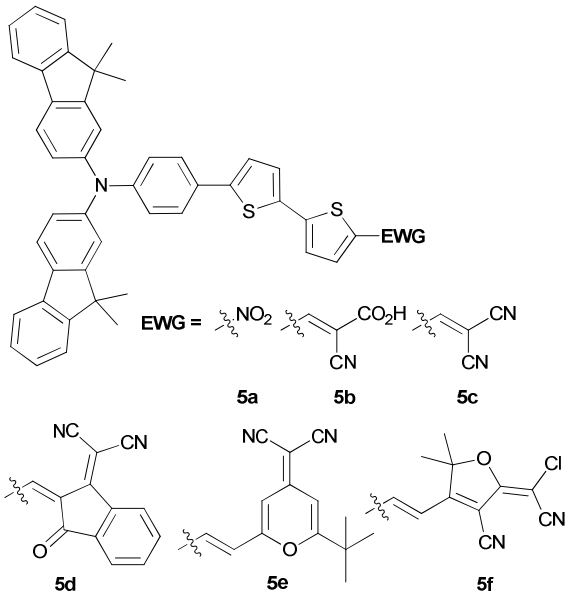

Scheme 2

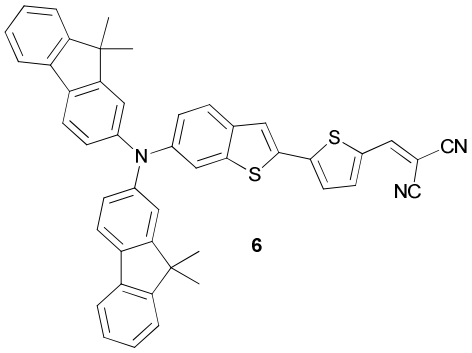

Scheme 3

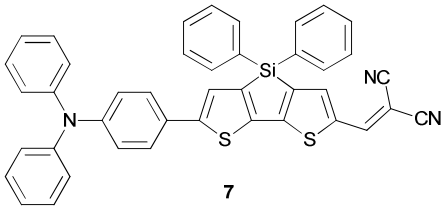

Scheme 4

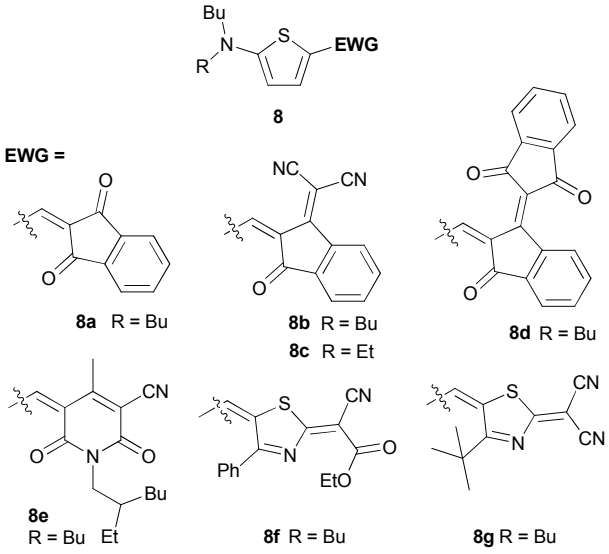

Scheme 5

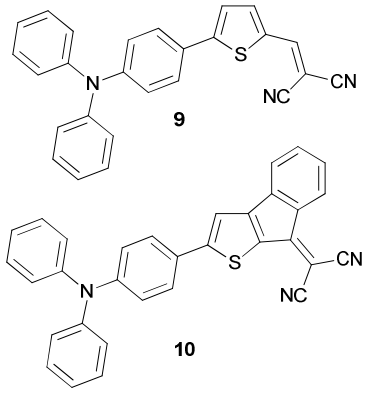

Scheme 6

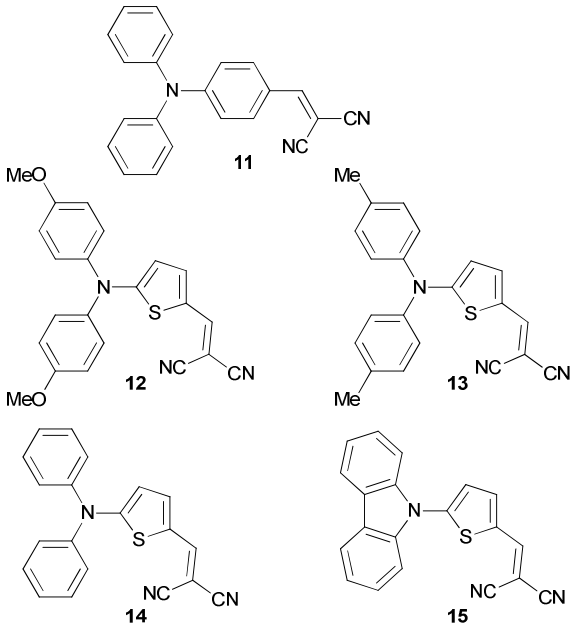

Scheme 7

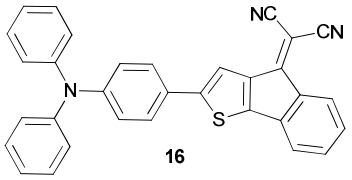

16

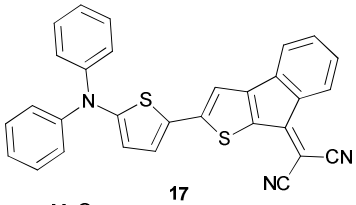

17

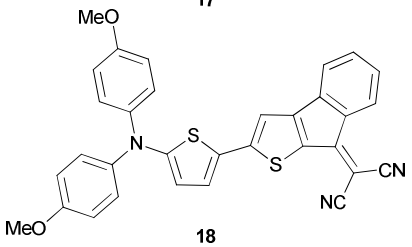

18

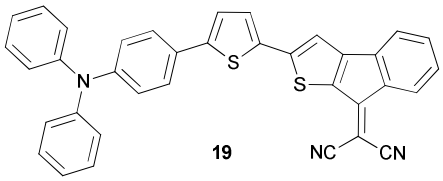

19

Scheme 8

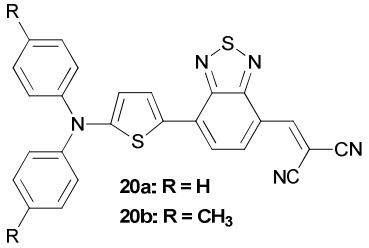

20a: R = H
20b: R = CH_3

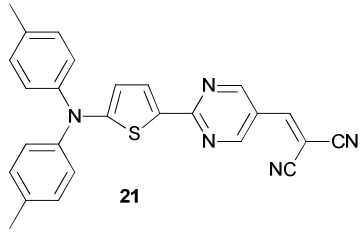

21

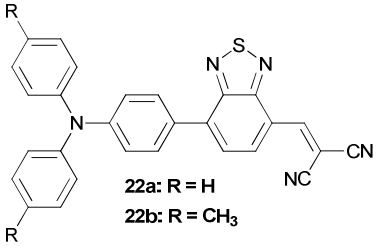

22a: R = H
22b: R = CH_3

Scheme 9

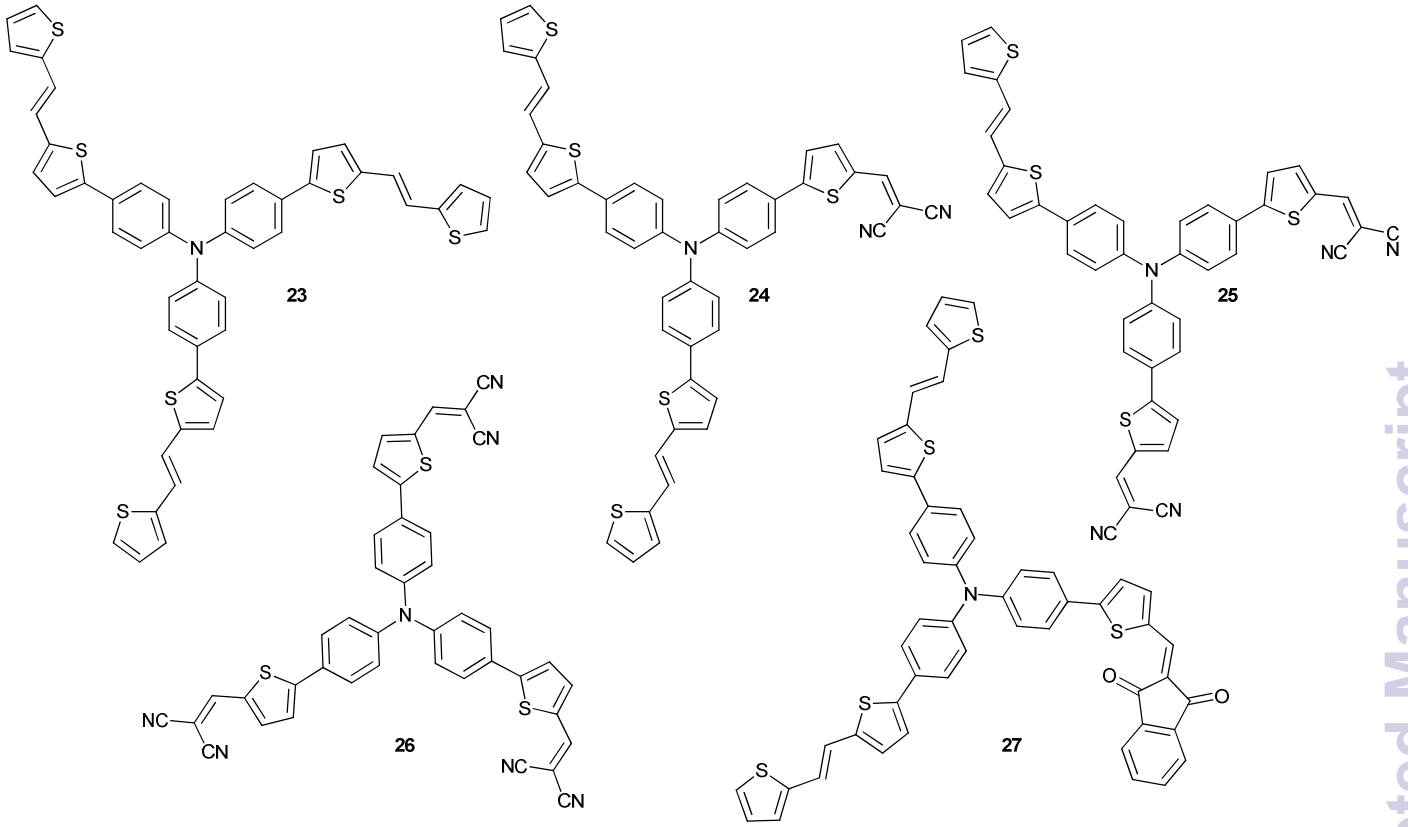

Scheme 10

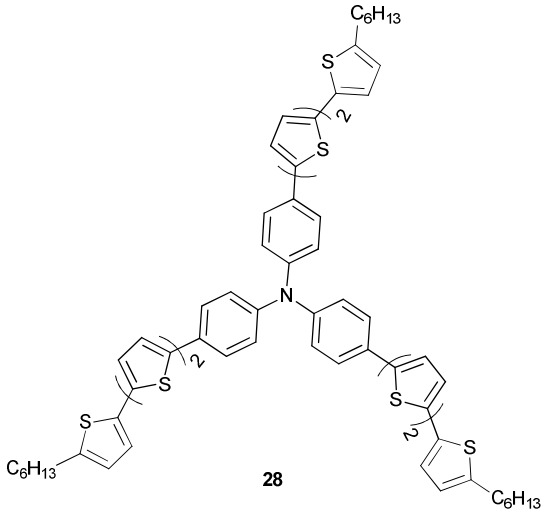

Scheme 11

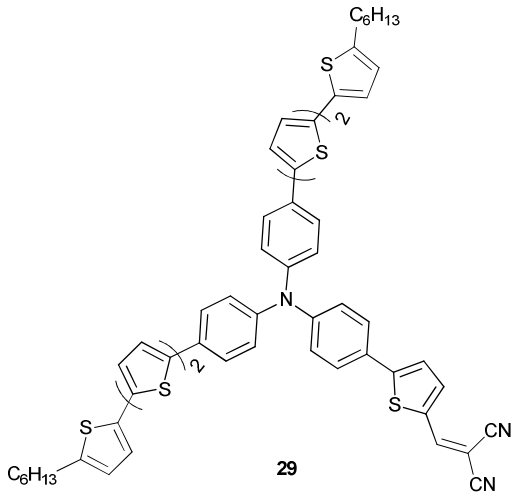

29

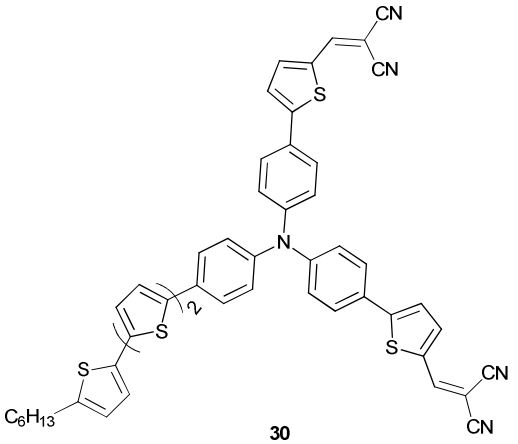

30

Scheme 12

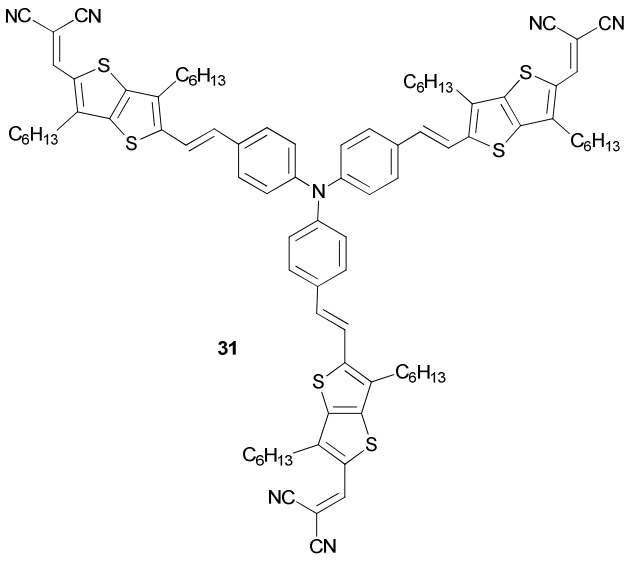

31

Scheme 13

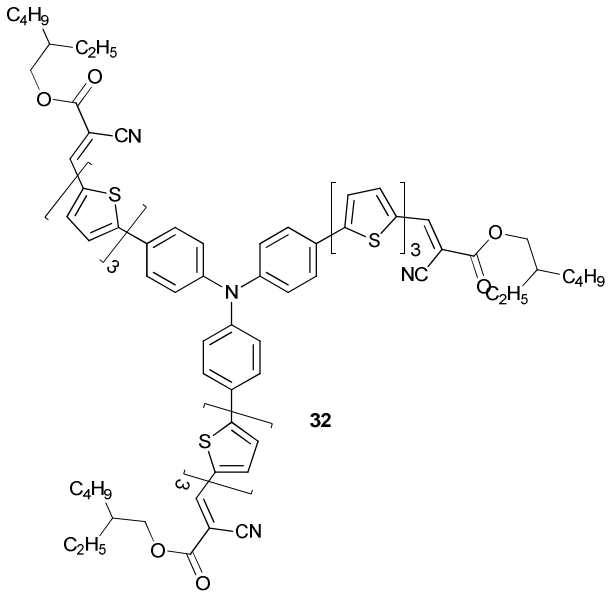

32

Scheme 14

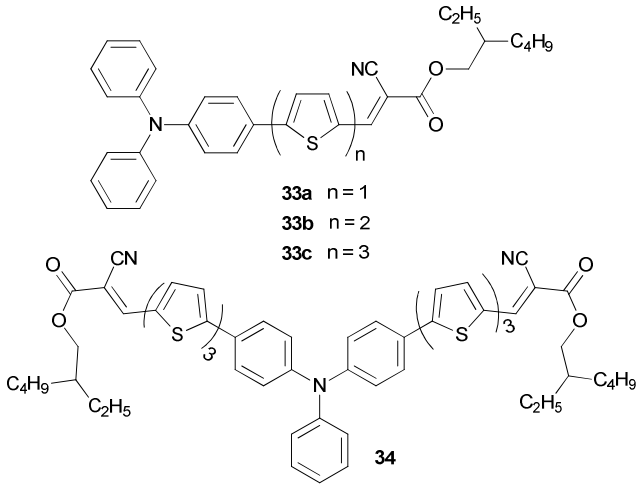

33a n = 1
33b n = 2
33c n = 3

34

Scheme 15

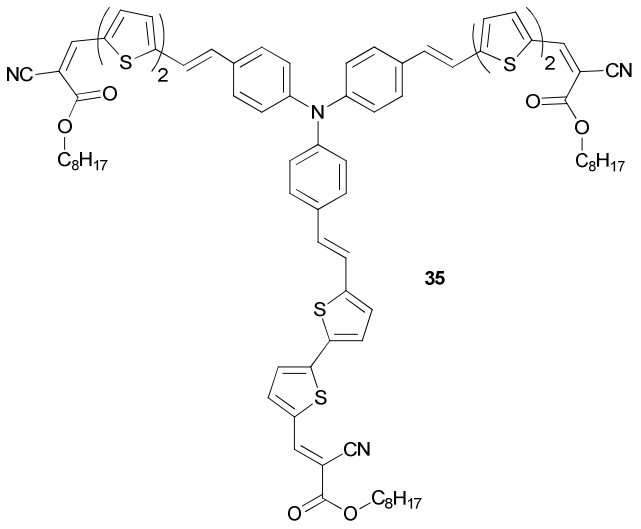

35

Scheme 16

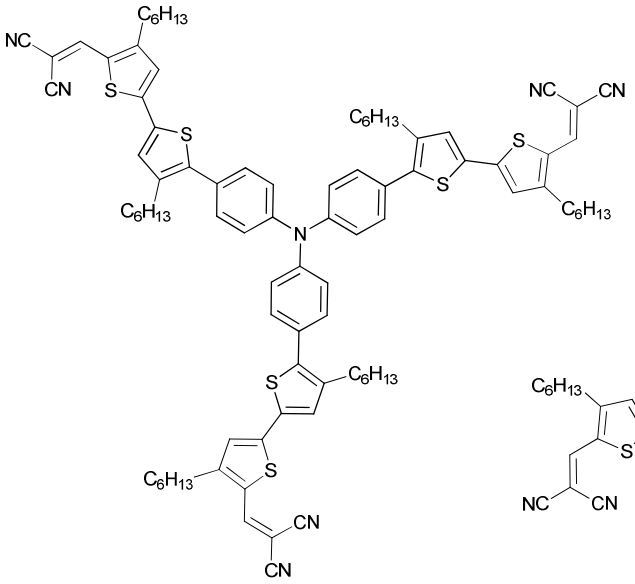

36

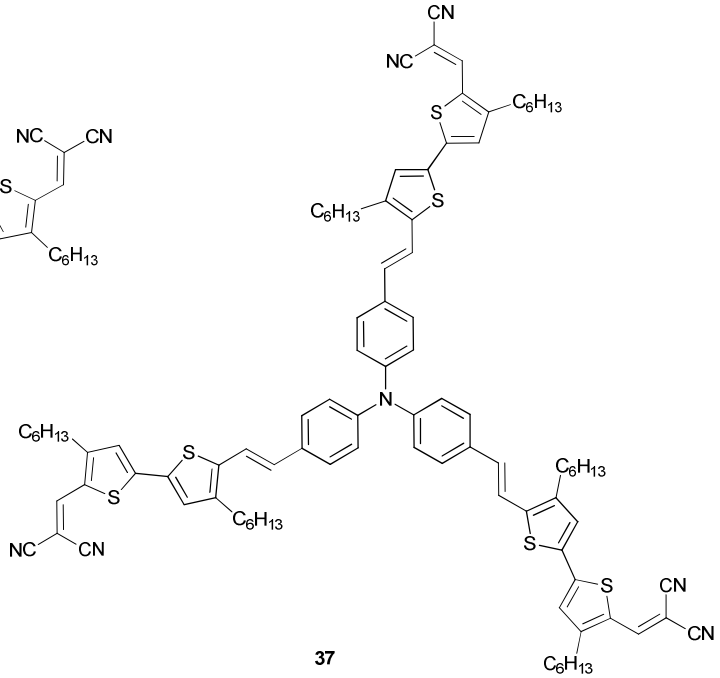

37

Scheme 17

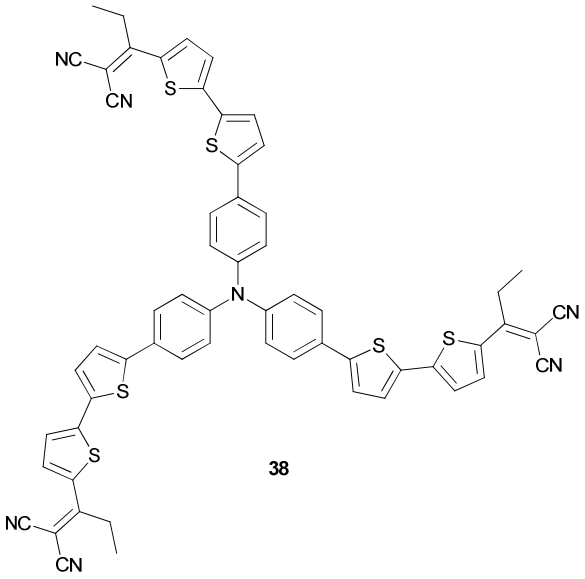

38

Scheme 18

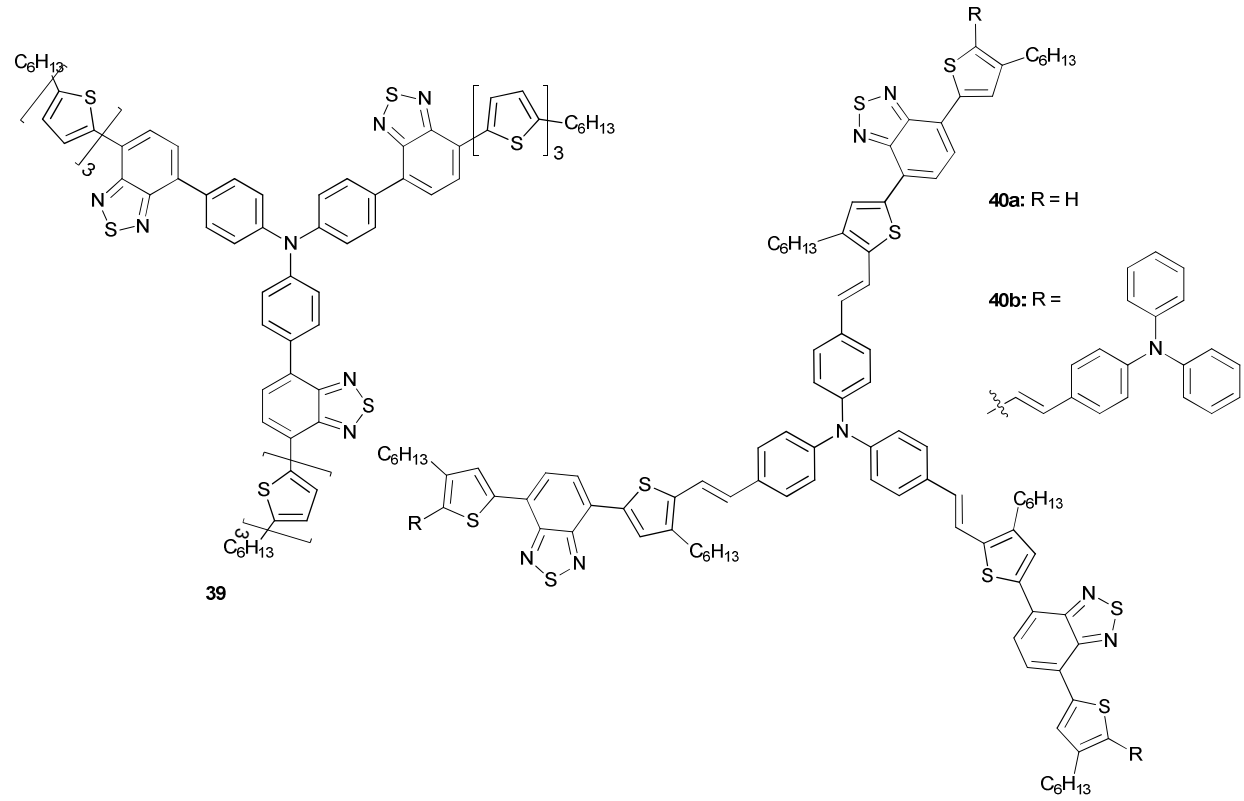

Scheme 19

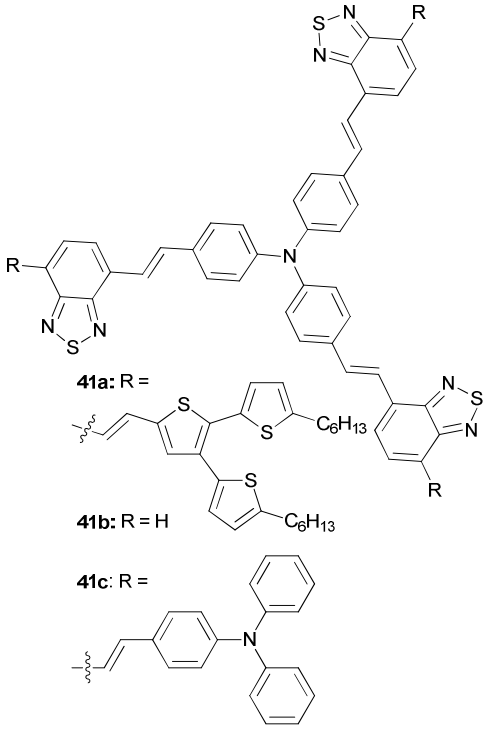

Scheme 20

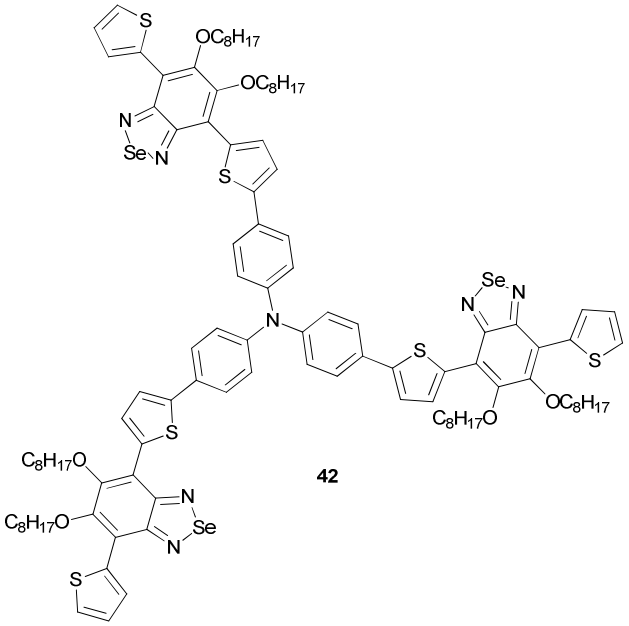

42

Scheme 21

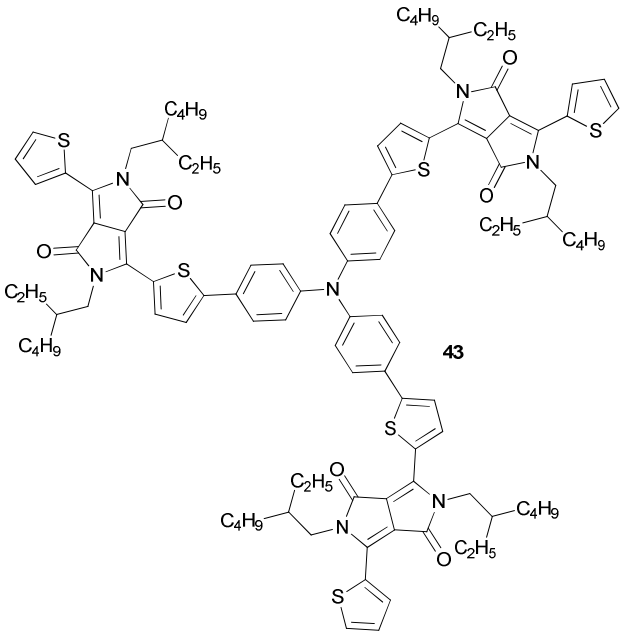

43

Scheme 22

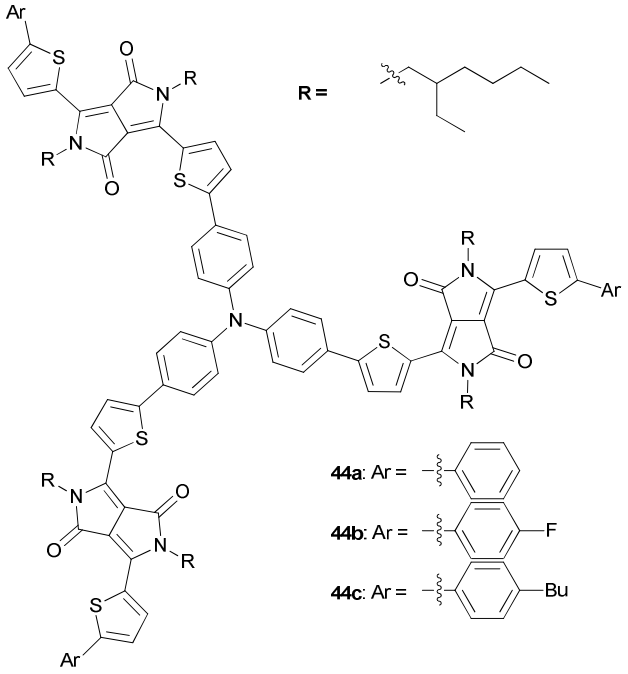

Scheme 23

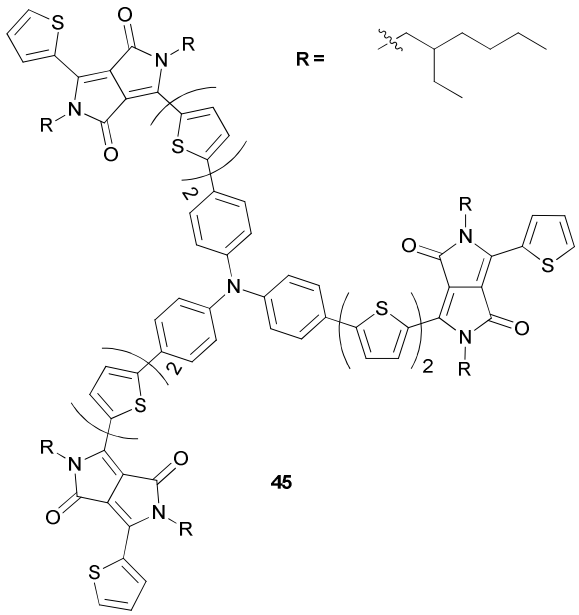

Scheme 24

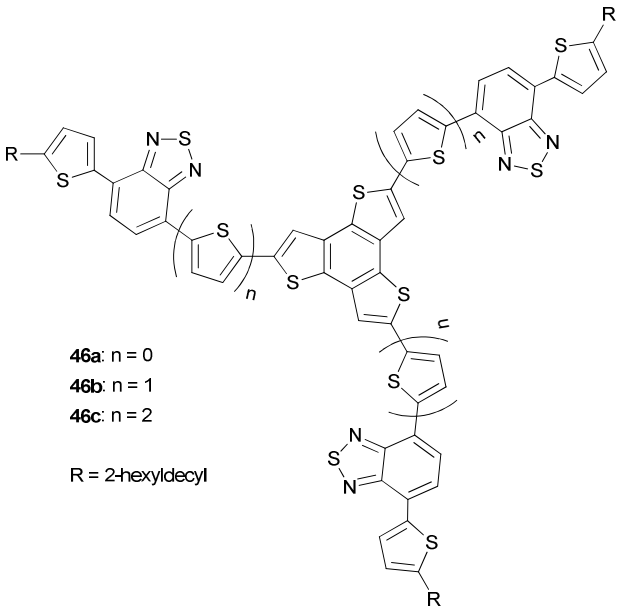

Scheme 25

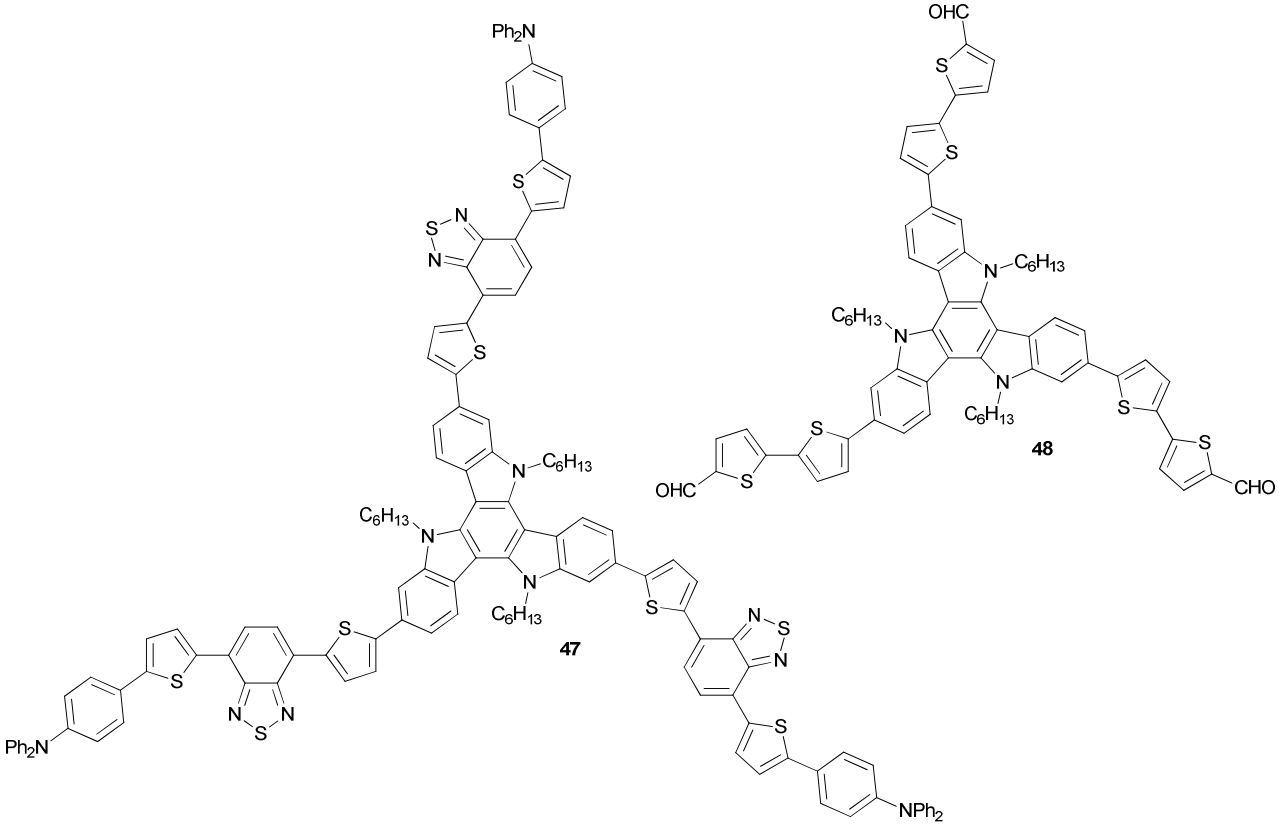

Scheme 26

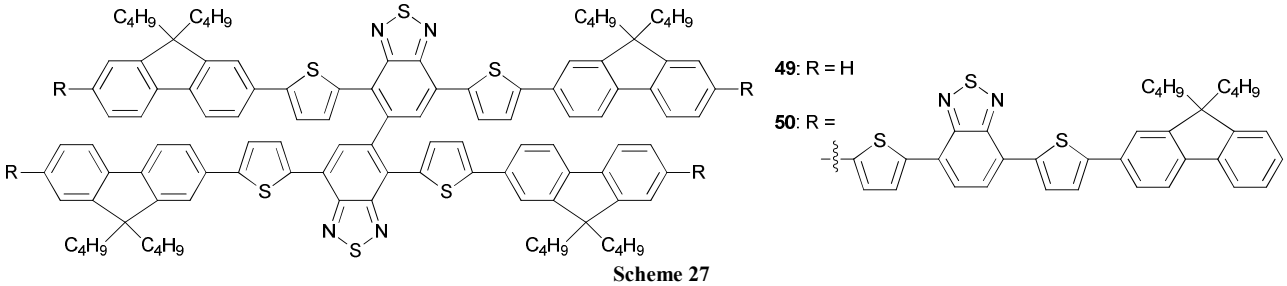

Scheme 27

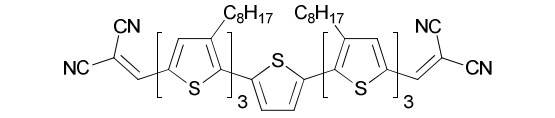

51

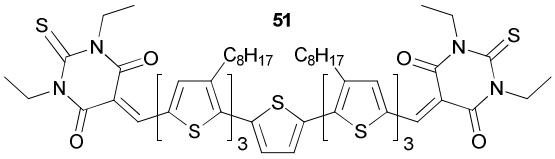

52

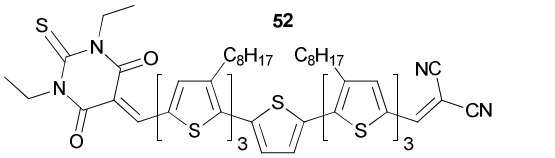

53

Scheme 28

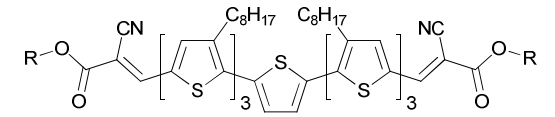

54a **54b** **54c**

R =

Scheme 29

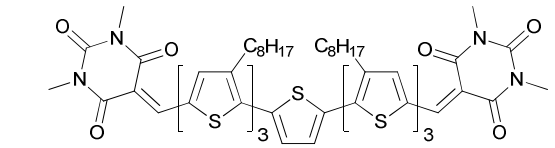

55

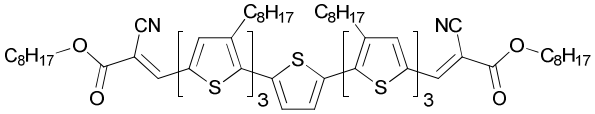

56

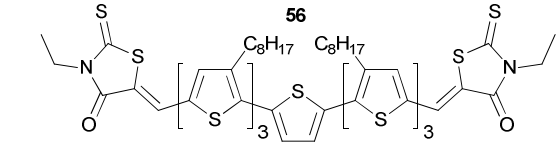

57

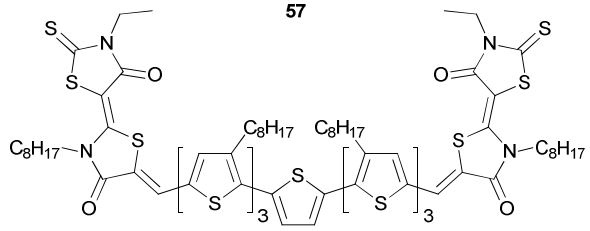

58

Scheme 30

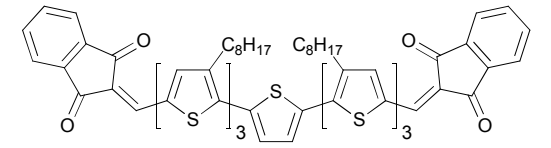

59

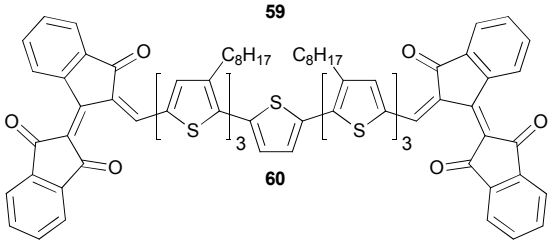

60

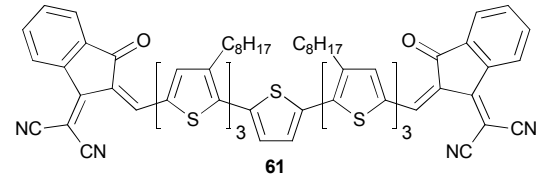

61

Scheme 31

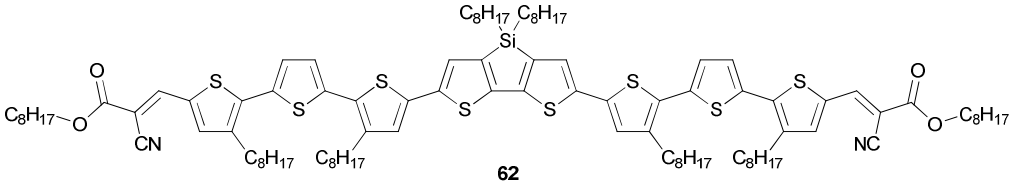

62

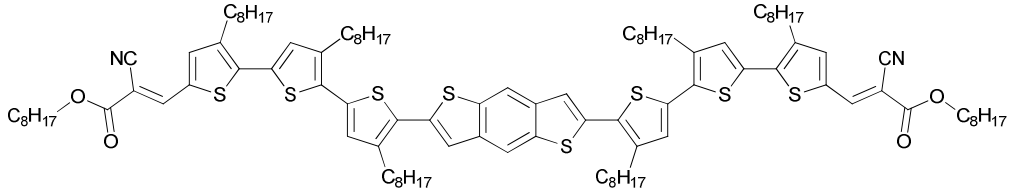

63

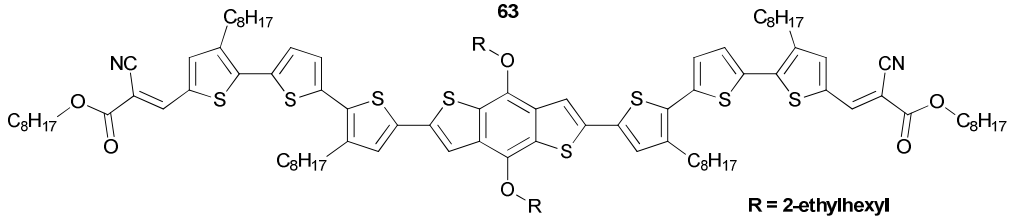

R = 2-ethylhexyl

64

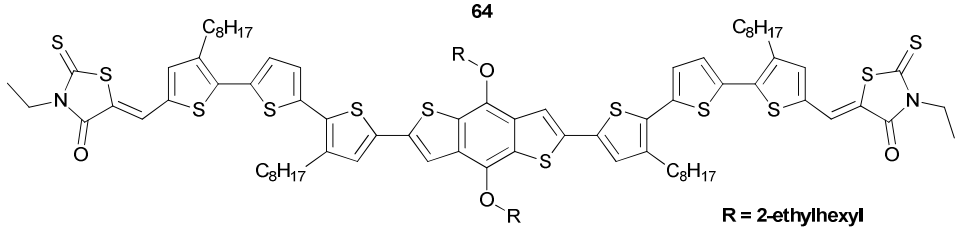

R = 2-ethylhexyl

65

Scheme 32

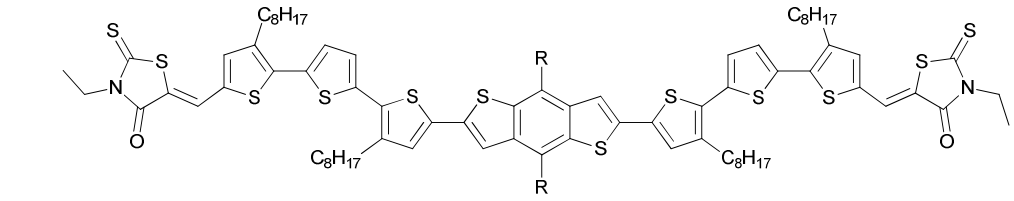

66a : R = 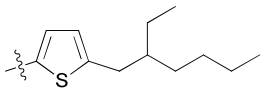 **66b : R =** 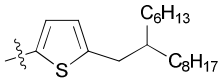 **66c : R =** 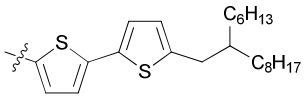

Scheme 33

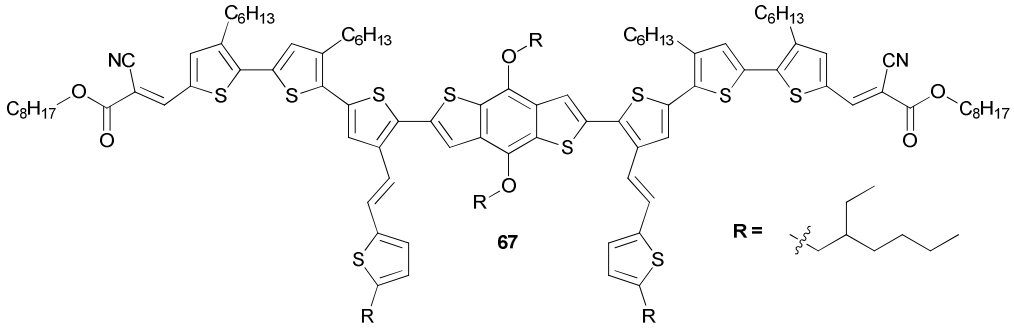

67 **R =**

Scheme 34

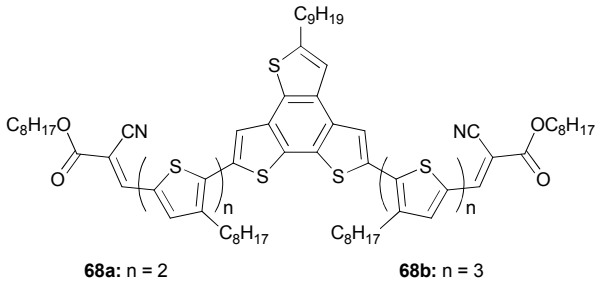

68a: n = 2 **68b:** n = 3

Scheme 35

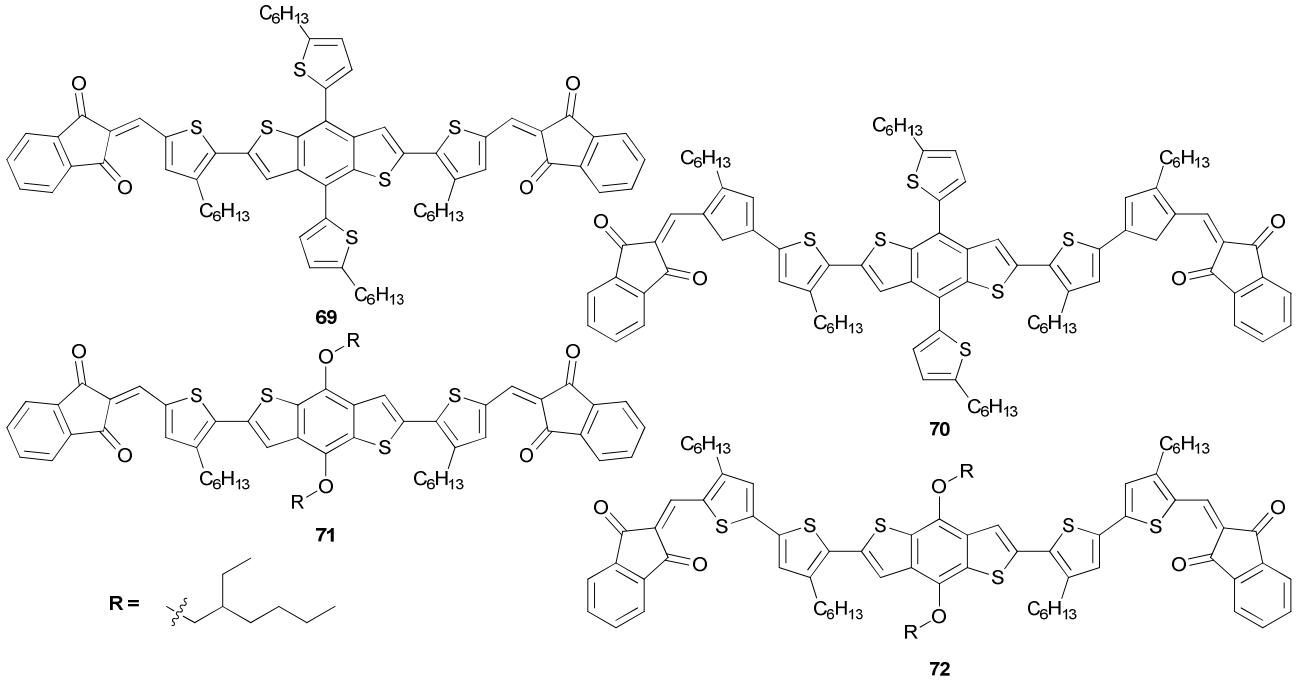

69 **70** **71** **72**

R =

Scheme 36

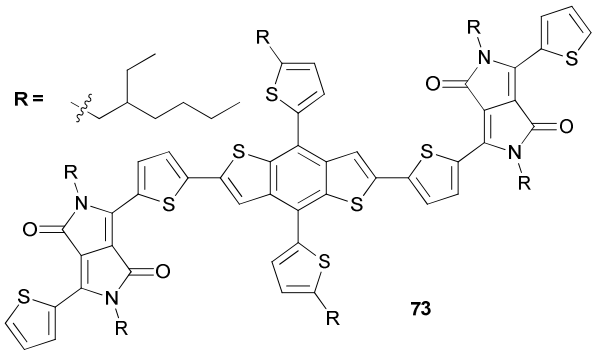

Scheme 37

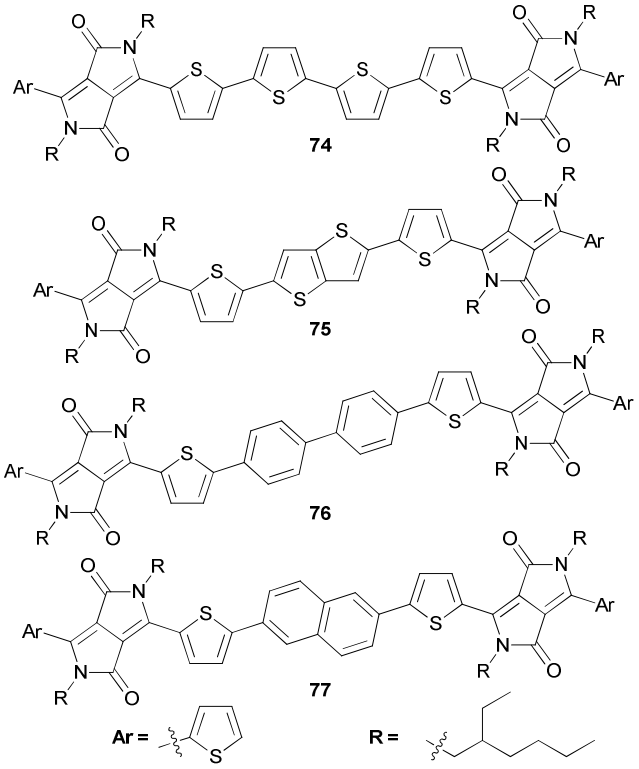

Scheme 38

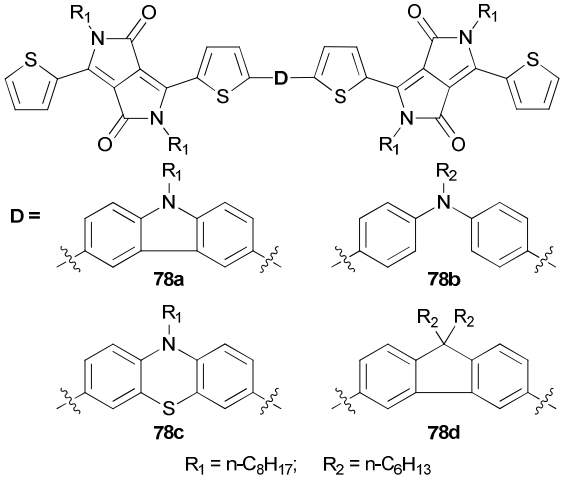

Scheme 39

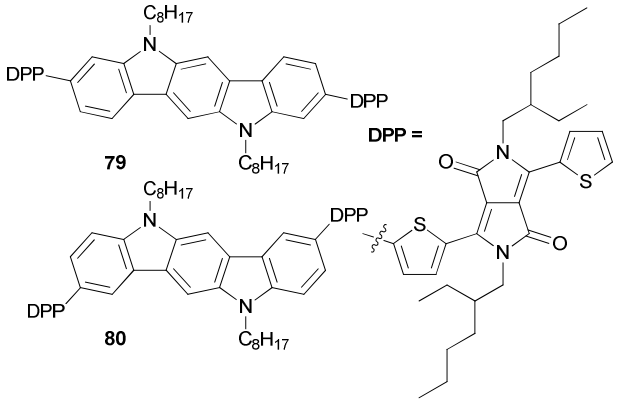

Scheme 40

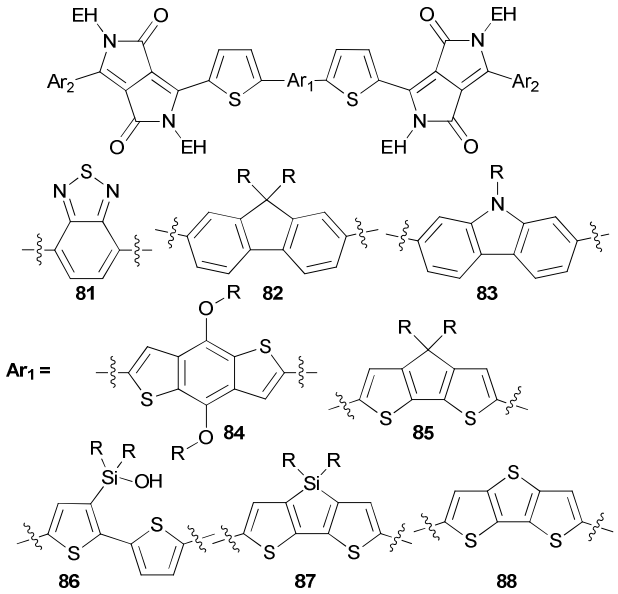

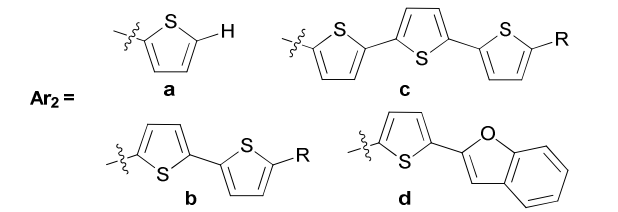

Scheme 41

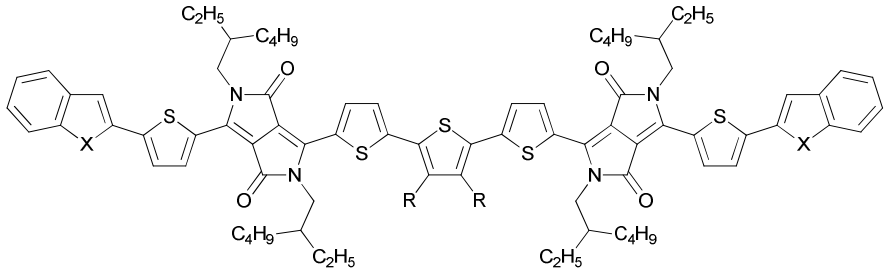

89a: X = S, R = H **89b:** X = S, R = CH_3

89c: X = O, R = H **89d:** X = O, R = CH_3

Scheme 42

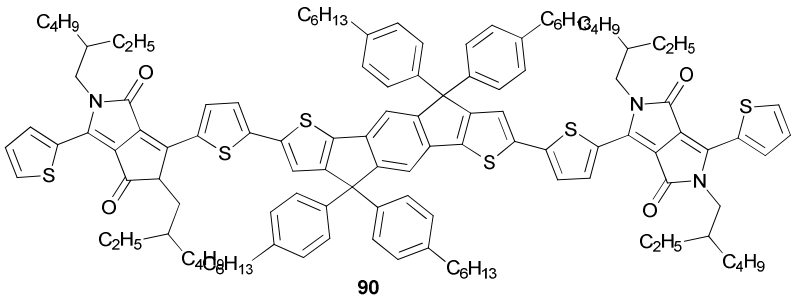

90

Scheme 43

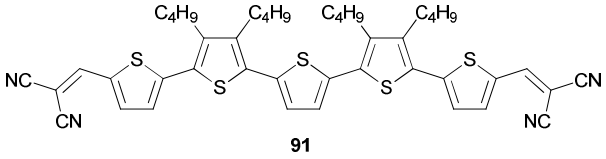

91

Scheme 44

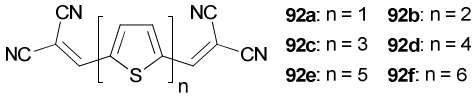

92a: n = 1 **92b**: n = 2
92c: n = 3 **92d**: n = 4
92e: n = 5 **92f**: n = 6

Scheme 45

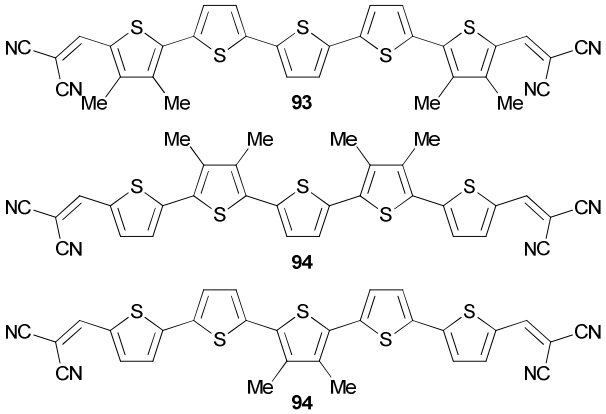

93 **94** **94**

Scheme 46

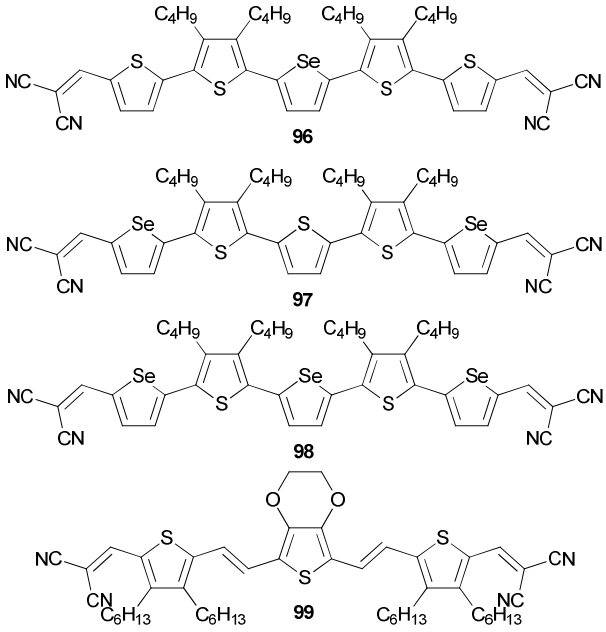

96 **97** **98** **99**

Scheme 47

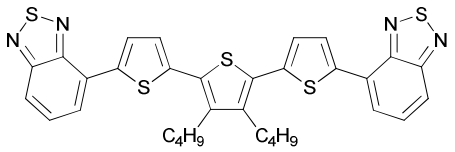

100

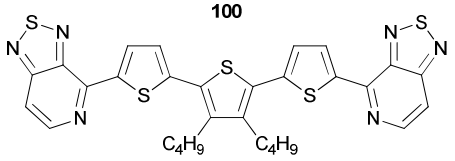

101

Scheme 48

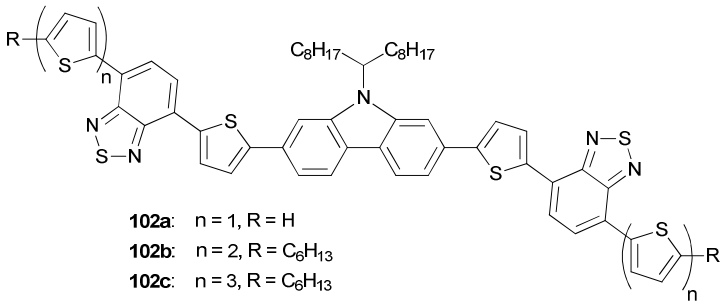

102a: n = 1, R = H
102b: n = 2, R = C_6H_{13}
102c: n = 3, R = C_6H_{13}

Scheme 49

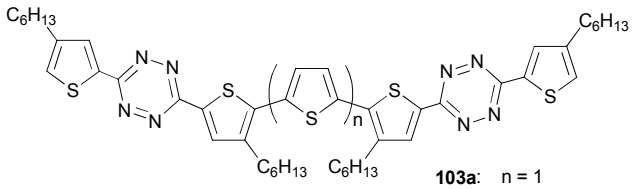

103a: n = 1
103b: n = 2
103c: n = 3

Scheme 50

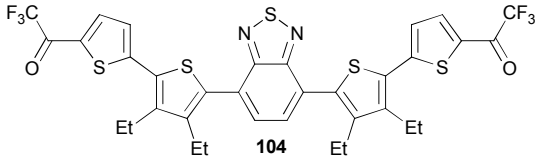

104

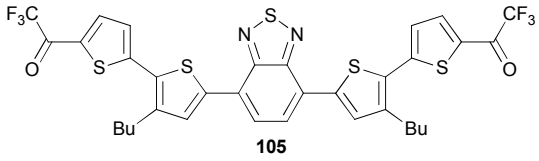

105

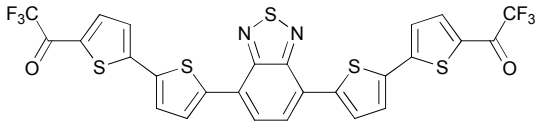

106

Scheme 51

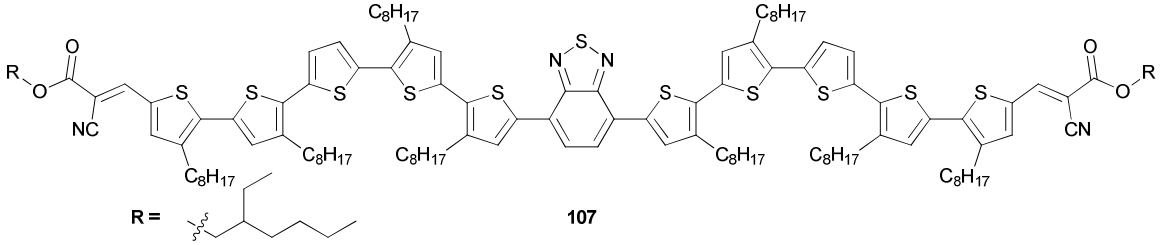

107

Scheme 52

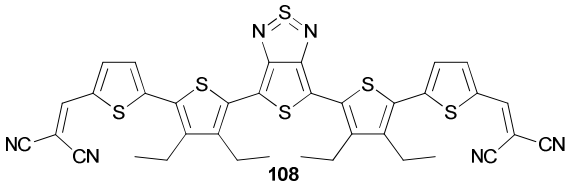

108

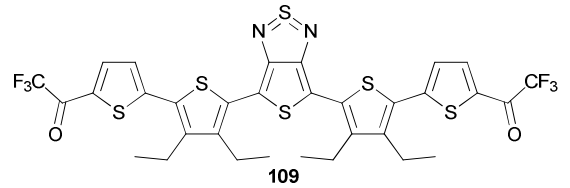

109

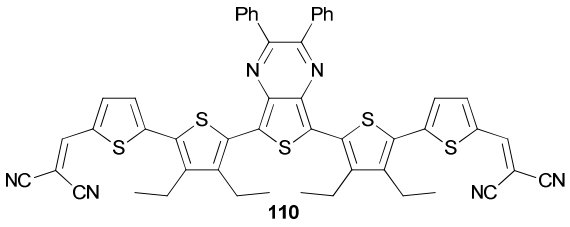

110

Scheme 53

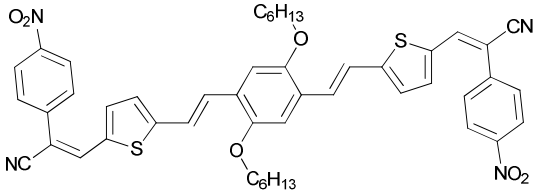

111

Scheme 54

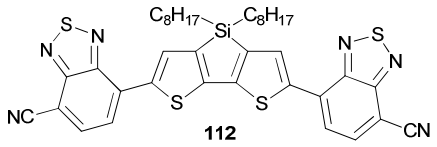

112

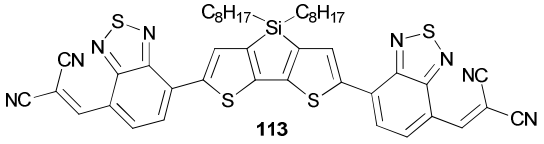

113

Scheme 55

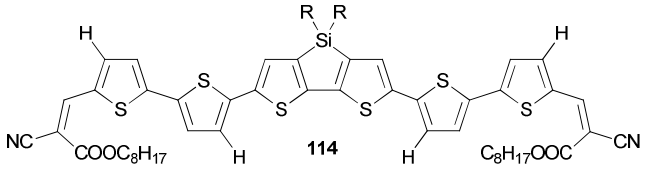

114

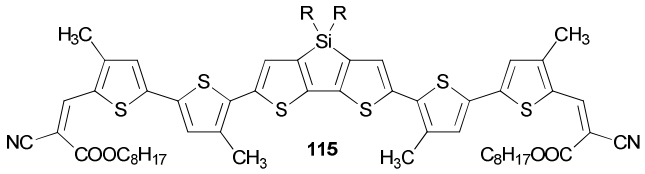

115

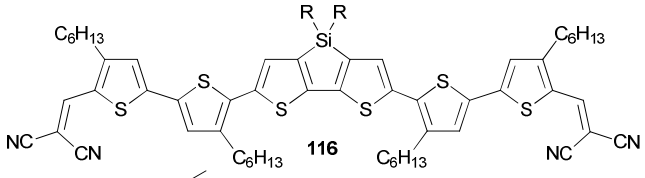

116

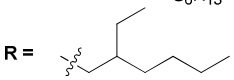

Scheme 56

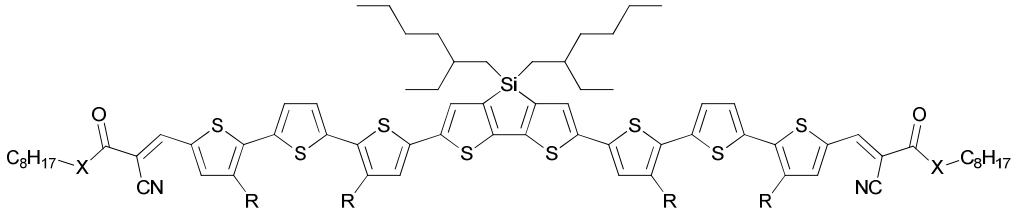

117a: X = O R = *n*-octyl
117b: X = O R = *n*-decyl
117c: X = O R = 2-ethylhexyl

118a: X = NH R = *n*-octyl
118b: X = NH R = *n*-decyl
118c: X = NH R = 2-ethylhexyl

Scheme 57

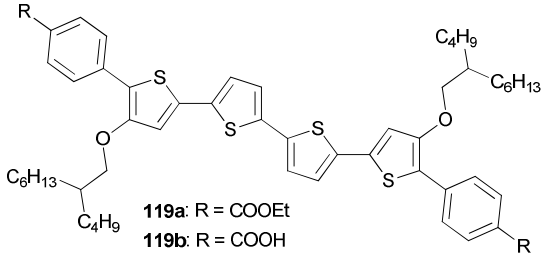

119a: R = COOEt
119b: R = COOH

Scheme 58

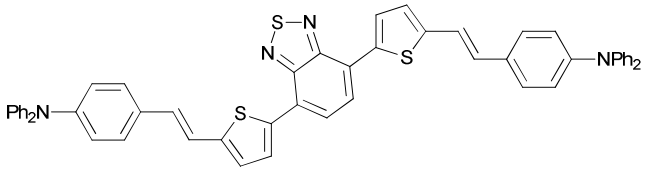

120

Scheme 59

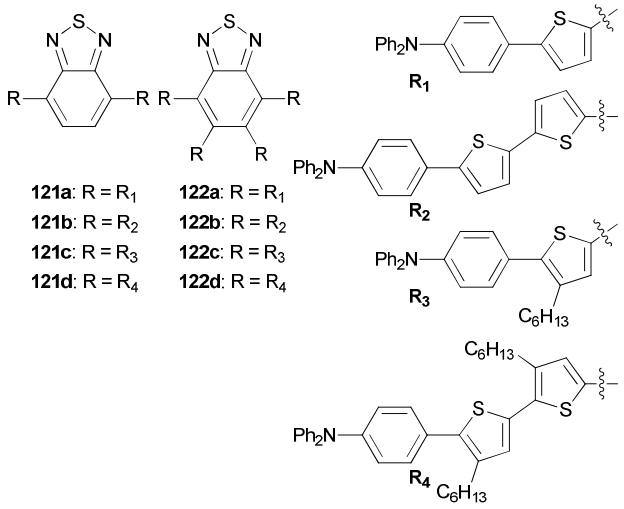

Scheme 60

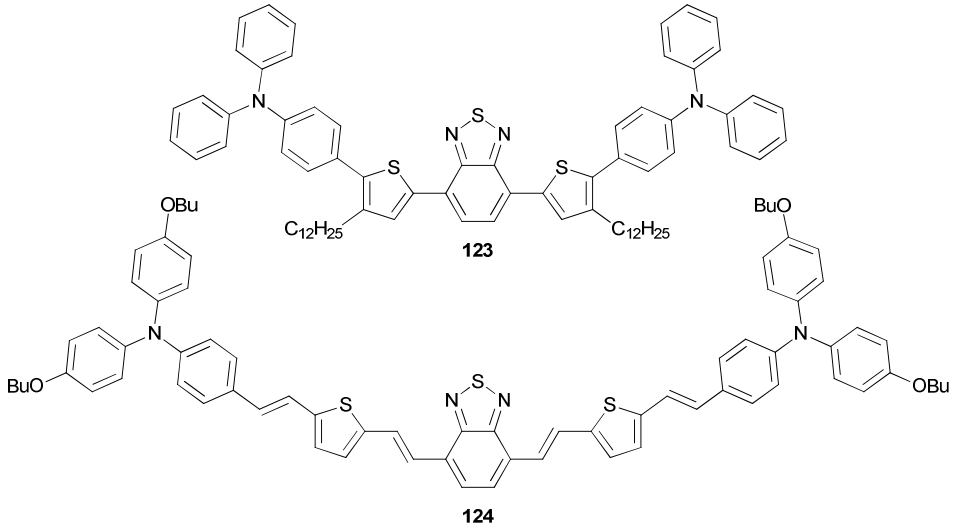

Scheme 61

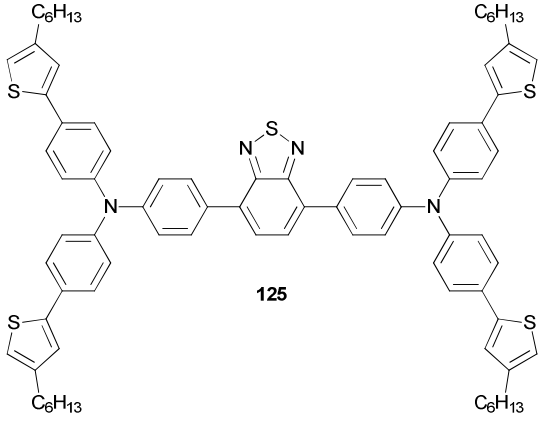

Scheme 62

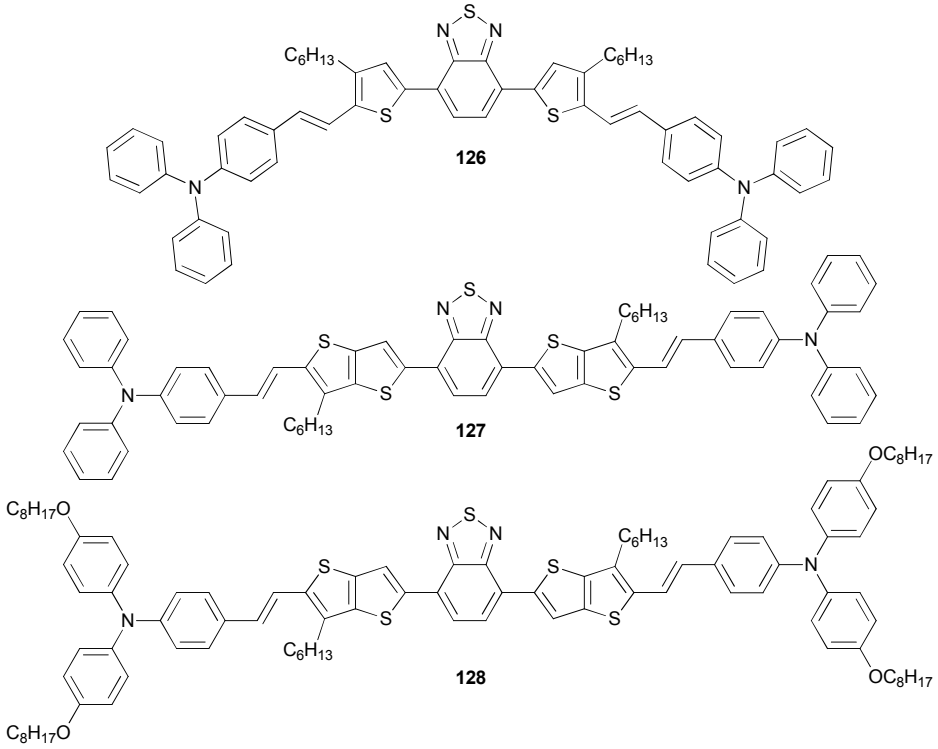

Scheme 63

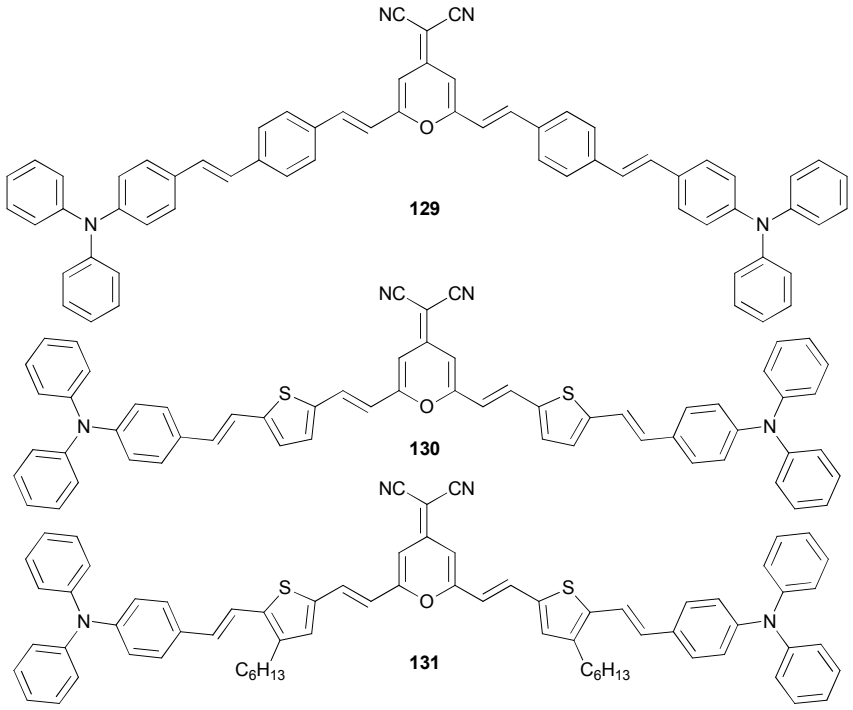

Scheme 64

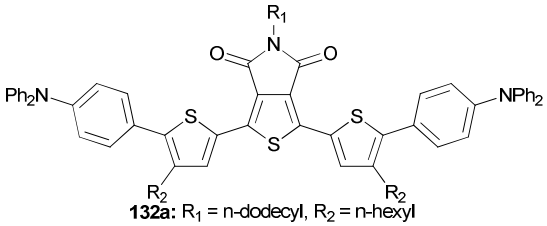

132a: R_1 = n-dodecyl, R_2 = n-hexyl
132b: R_1 = n-dodecyl, R_2 = H
132c: R_1 = 2-ethylhexyl, R_2 = H

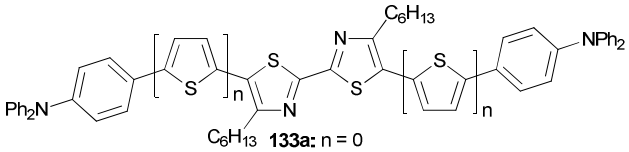

133a: n = 0
133b: n = 1
133c: n = 2

Scheme 65

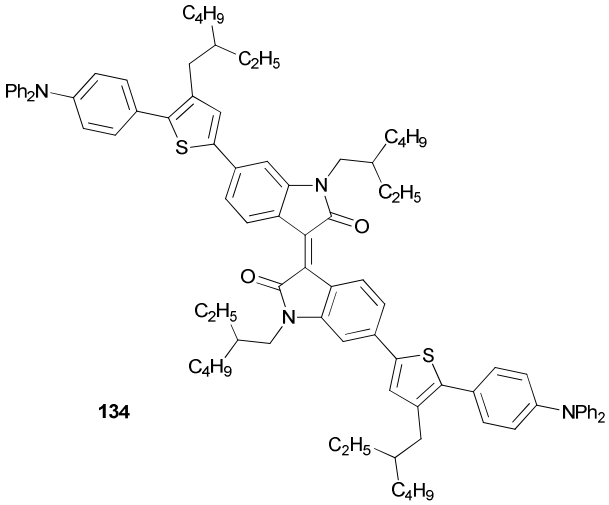

134

Scheme 66

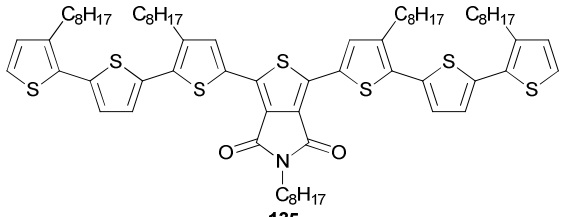

135

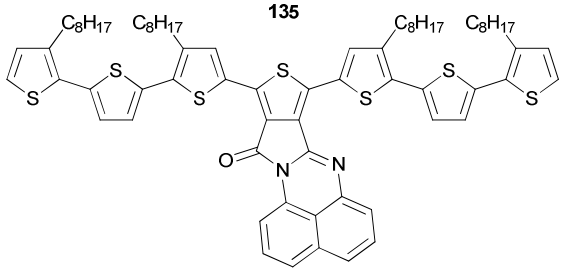

136

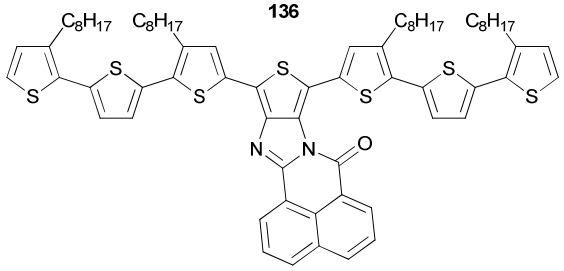

137

Scheme 67

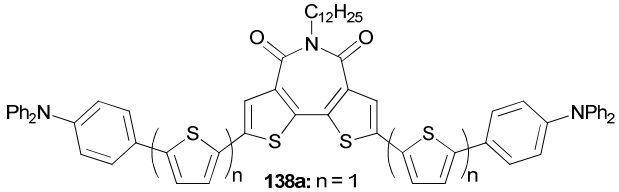

138a: n = 1

138b: n = 2

Scheme 68

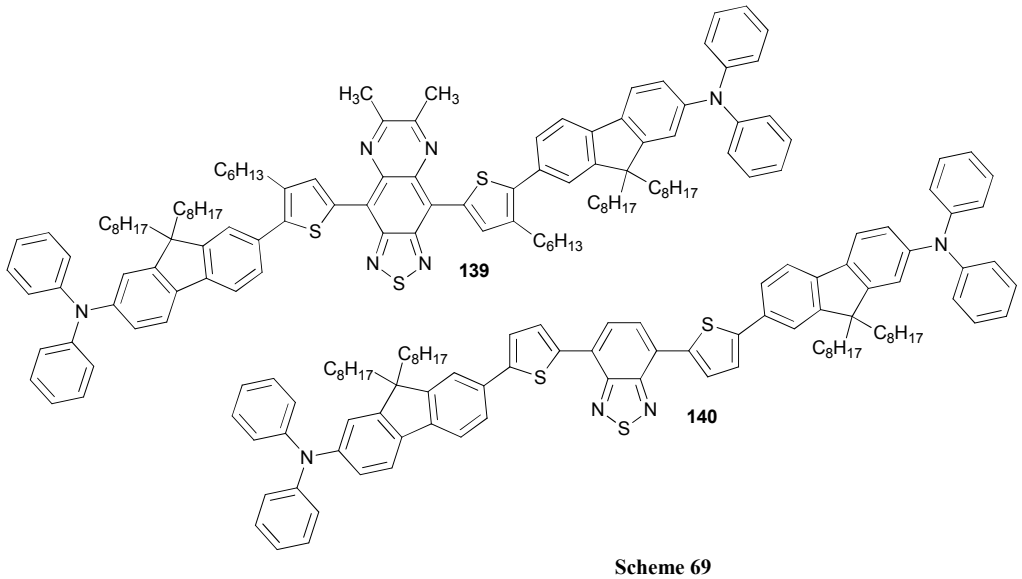

139

140

Scheme 69

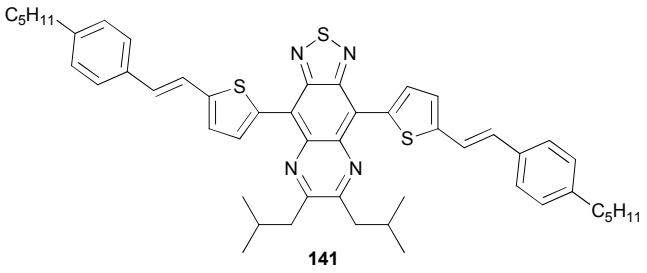

141

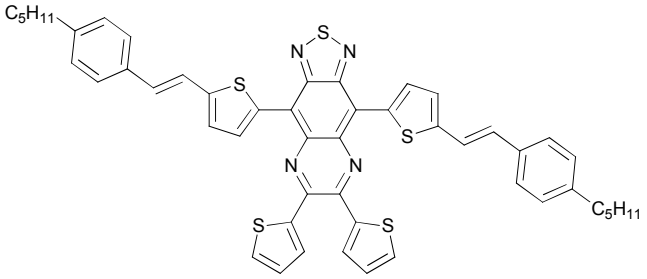

142

Scheme 70

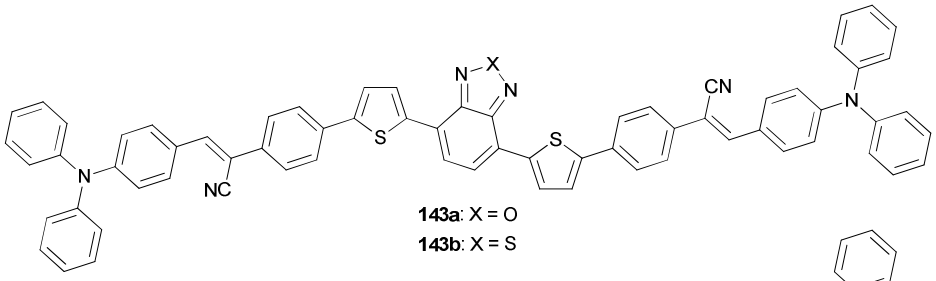

143a: X = O
143b: X = S

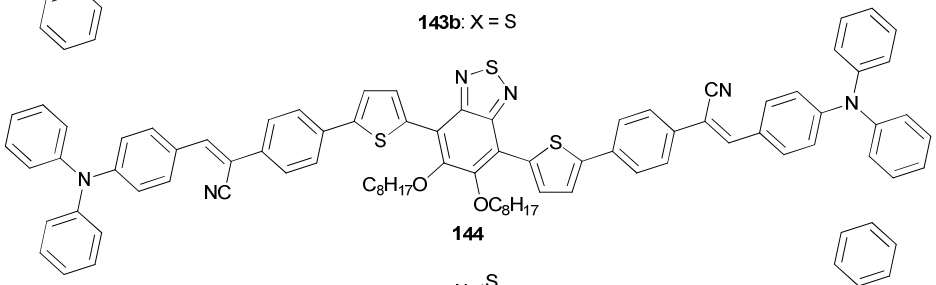

144

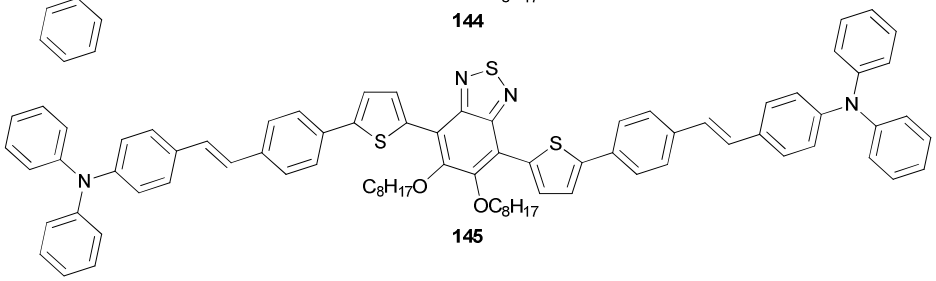

145

Scheme 71

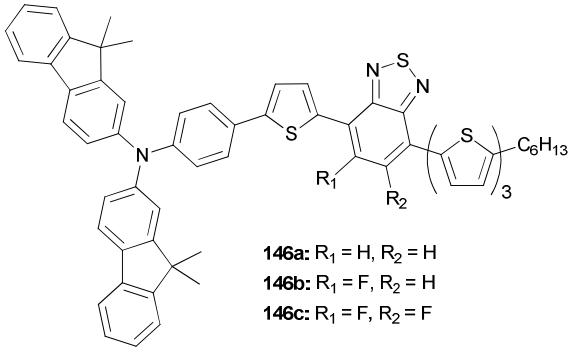

146a: R_1 = H, R_2 = H
146b: R_1 = F, R_2 = H
146c: R_1 = F, R_2 = F

Scheme 72

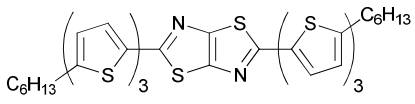

147

Scheme 73

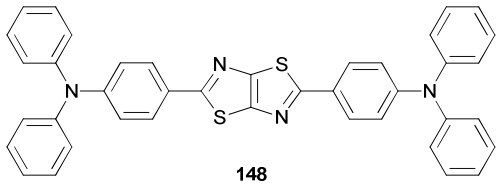

148

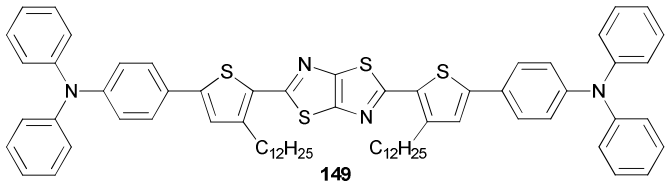

149

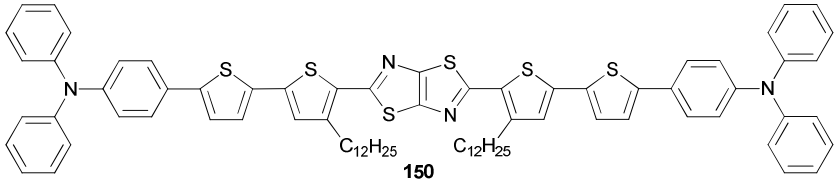

150

Scheme 74

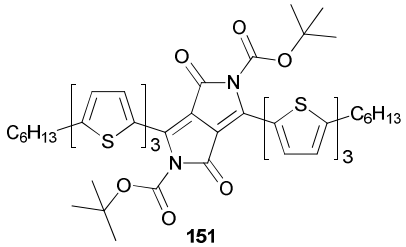

151

Scheme 75

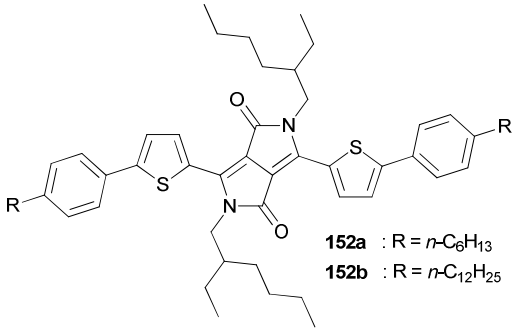

Scheme 76

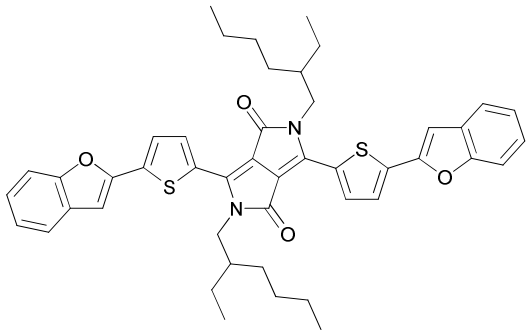

153

Scheme 77

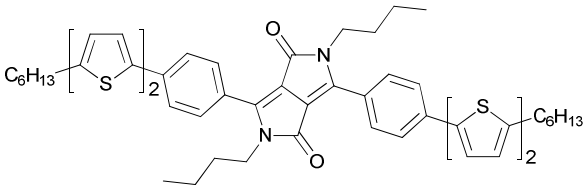

154

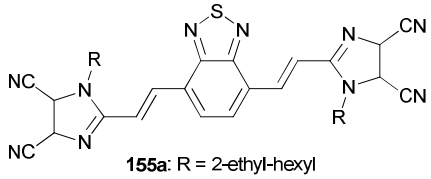

155a: R = 2-ethyl-hexyl
155b: R = hexyl

Scheme 78

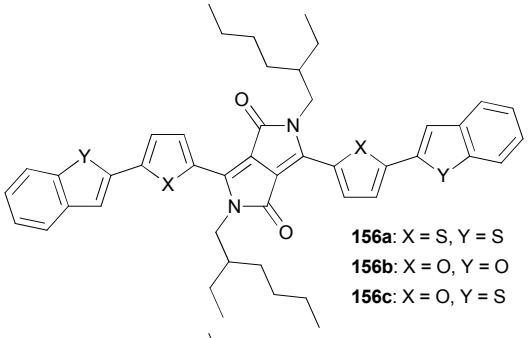

156a: X = S, Y = S
156b: X = O, Y = O
156c: X = O, Y = S

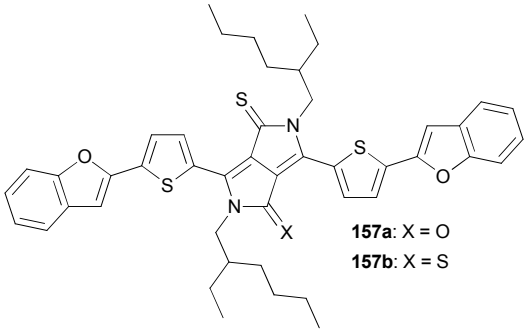

157a: X = O
157b: X = S

Scheme 79

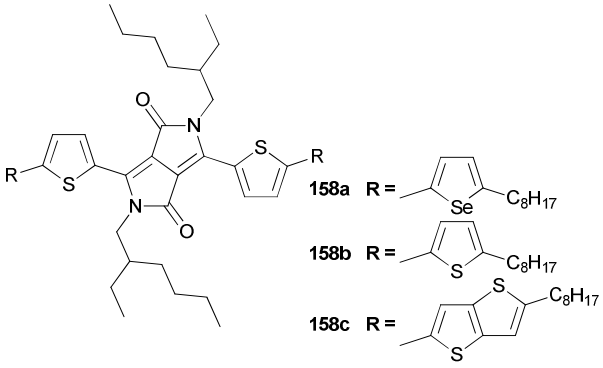

158a R =
158b R =
158c R =

Scheme 80

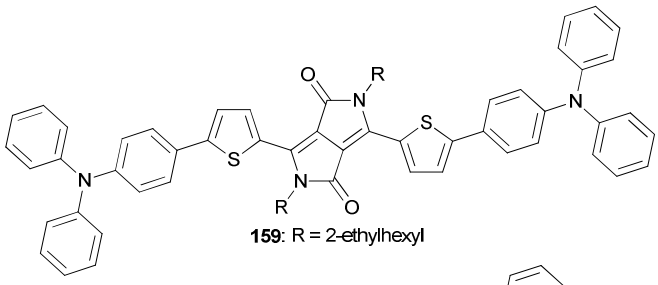

159: R = 2-ethylhexyl

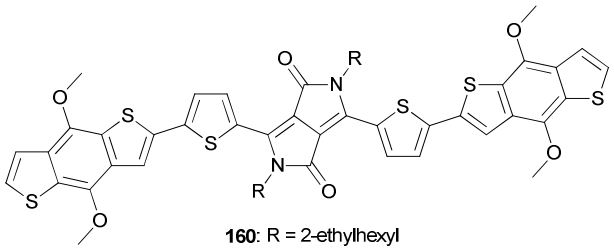

160: R = 2-ethylhexyl

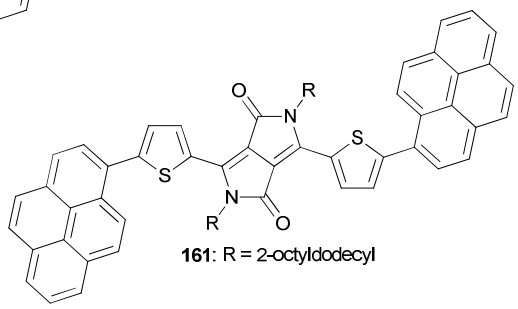

161: R = 2-octyldodecyl

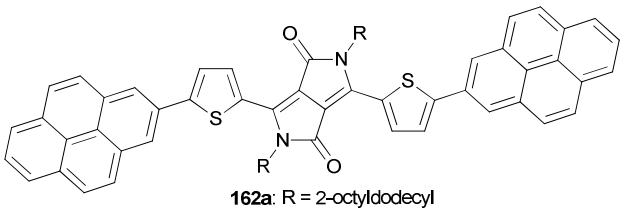

162a: R = 2-octyldodecyl
162b: R = 2-hexyldecyl
162c: R = 2-butyloctyl
162d: R = 2-ethylhexyl

Scheme 81

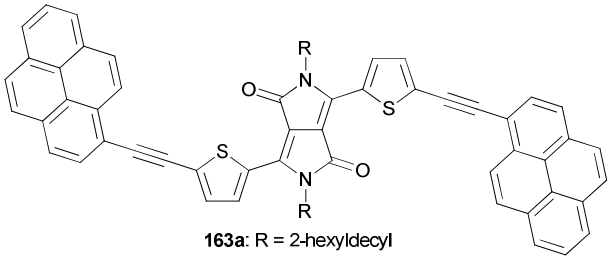

163a: R = 2-hexyldecyl
163b: R = 2-octyldodecyl

Scheme 82

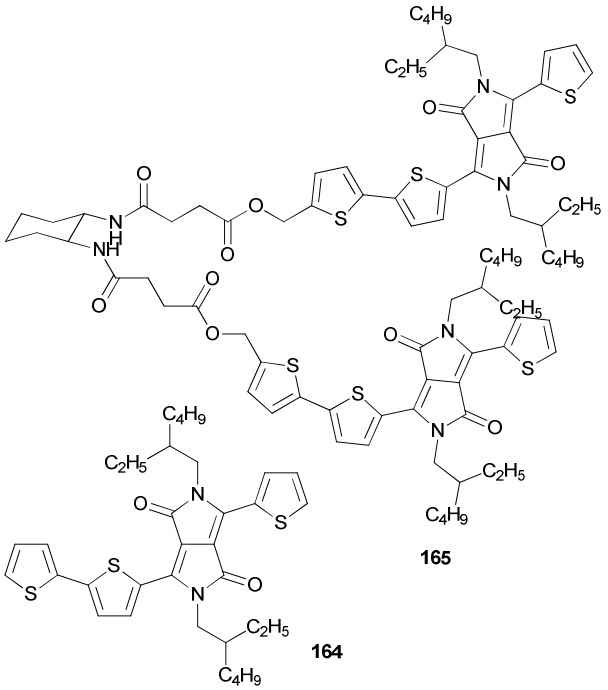

165

164

Scheme 83

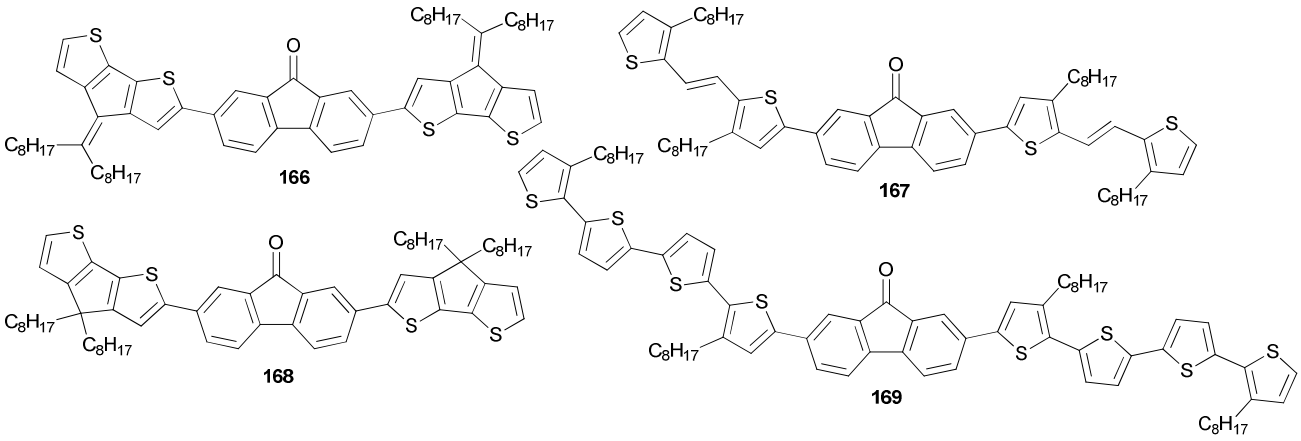

Scheme 84

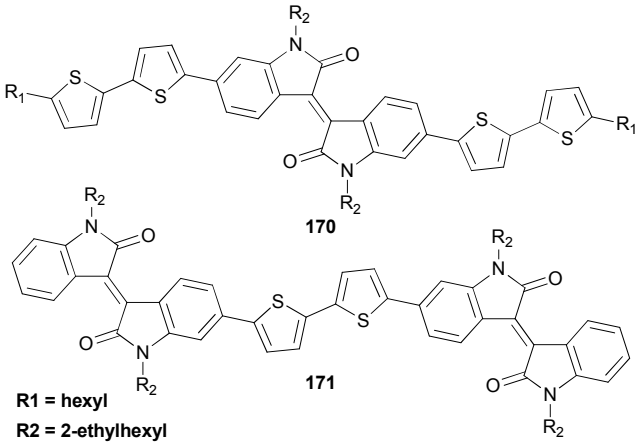

Scheme 85

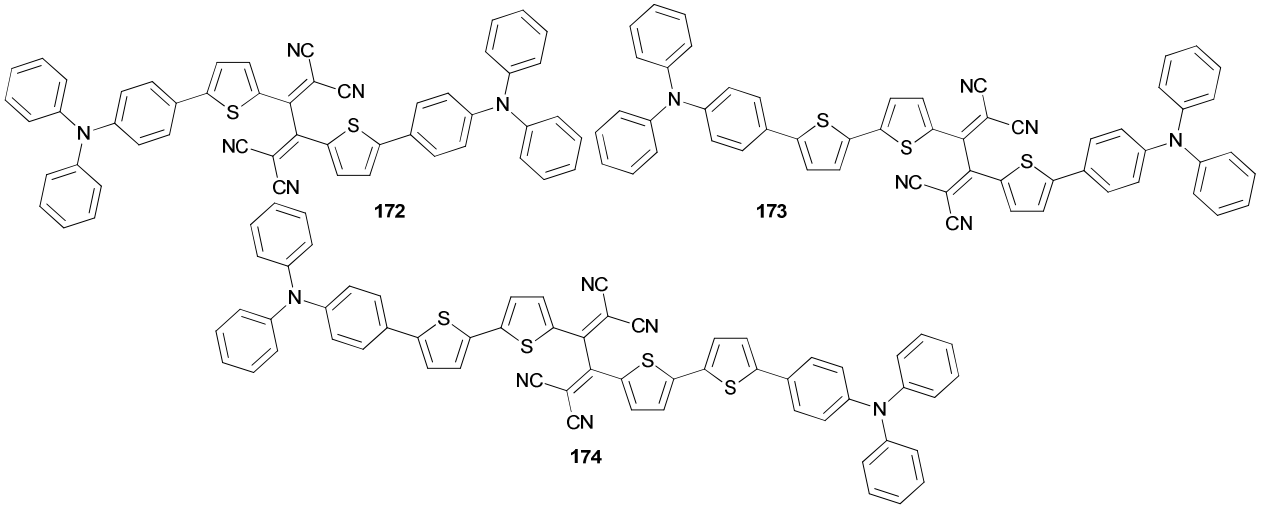

Scheme 86

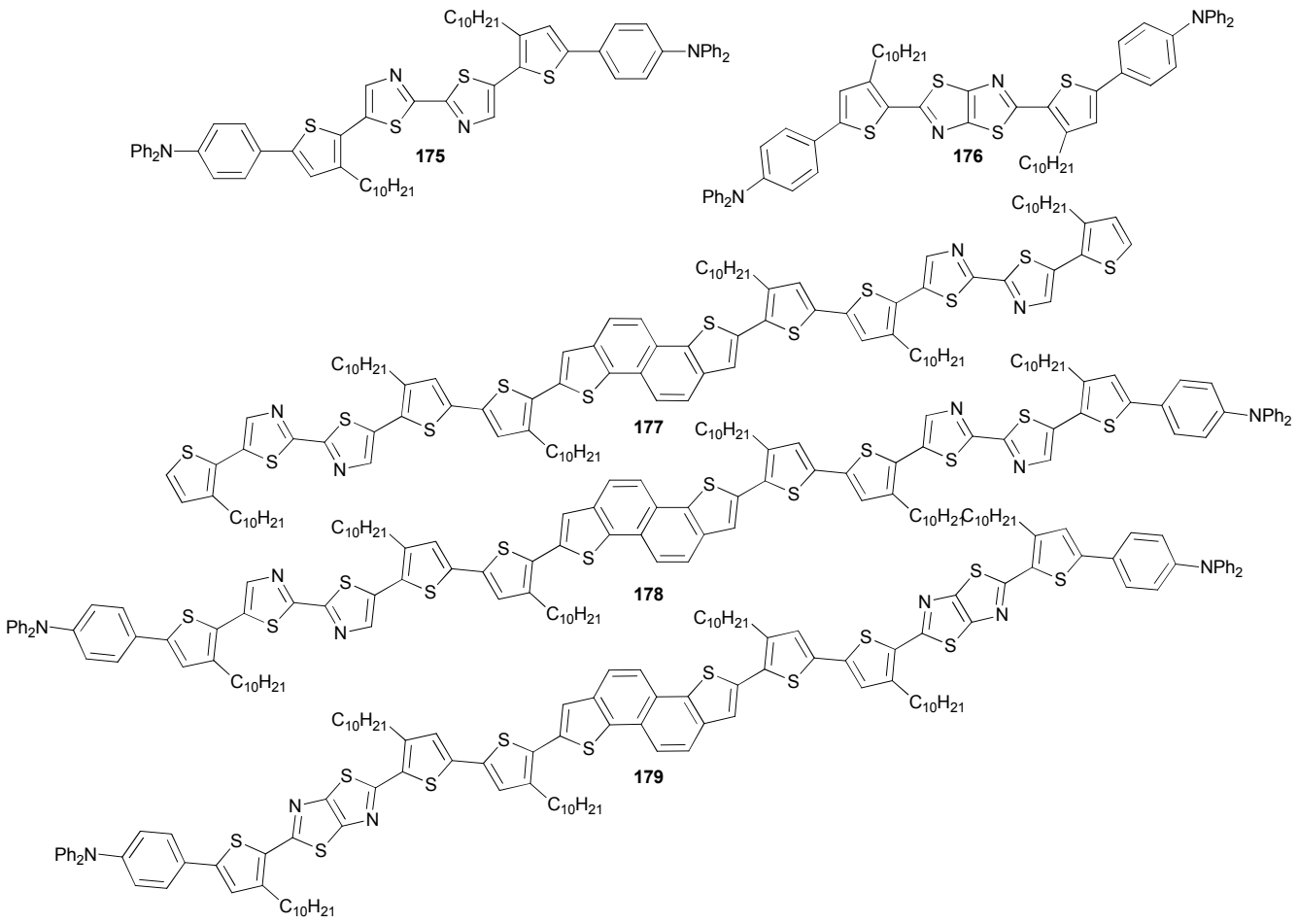

Scheme 87

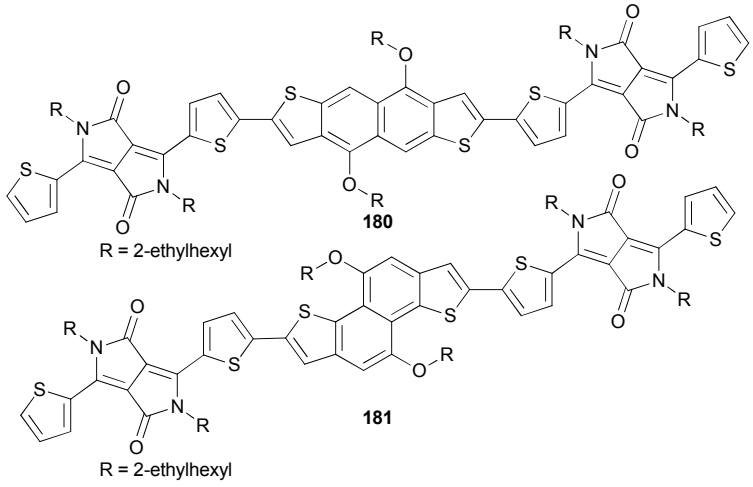

Scheme 88

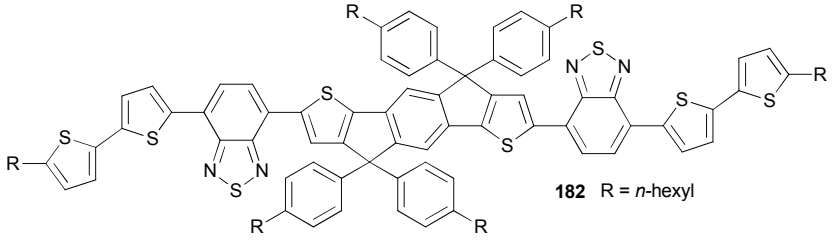

Scheme 89

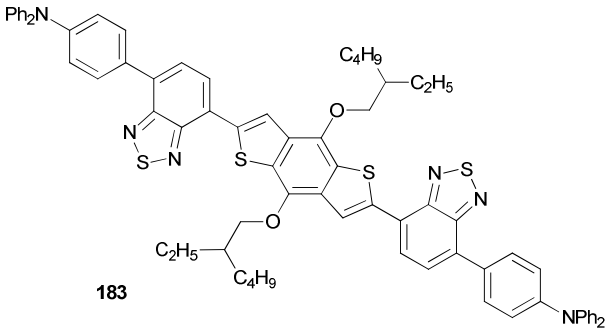

183

Scheme 90

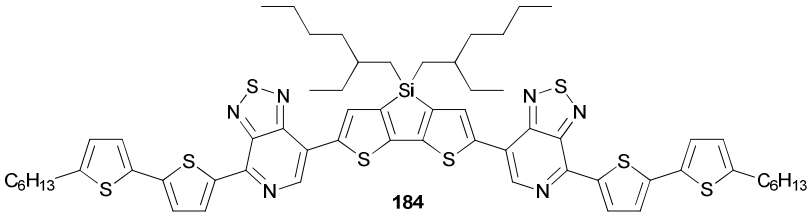

184

Scheme 91

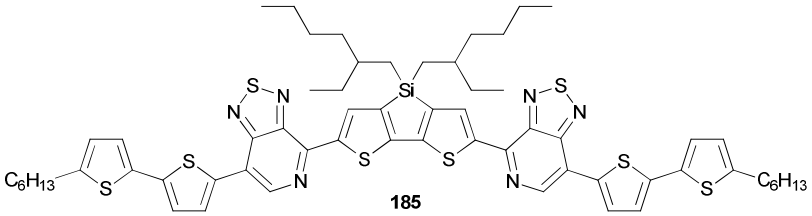

185

Scheme 92

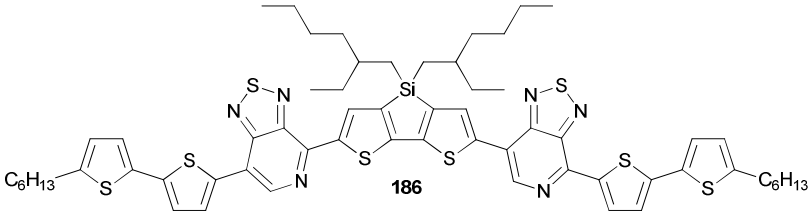

186

Scheme 93

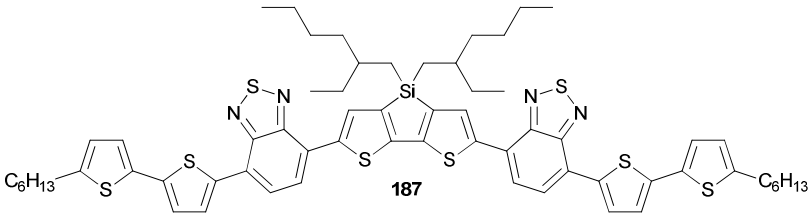

187

Scheme 94

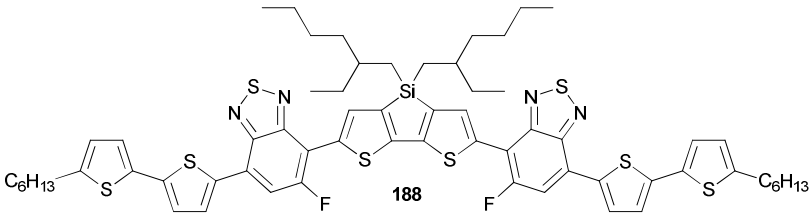

188

Scheme94

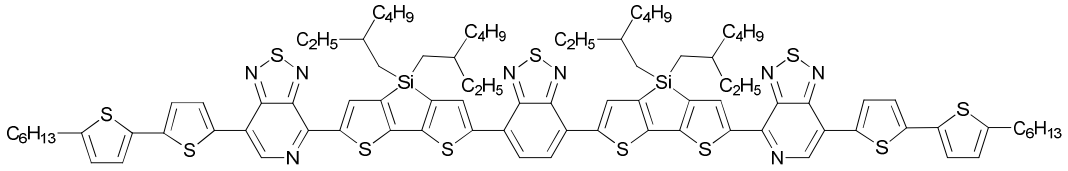

189

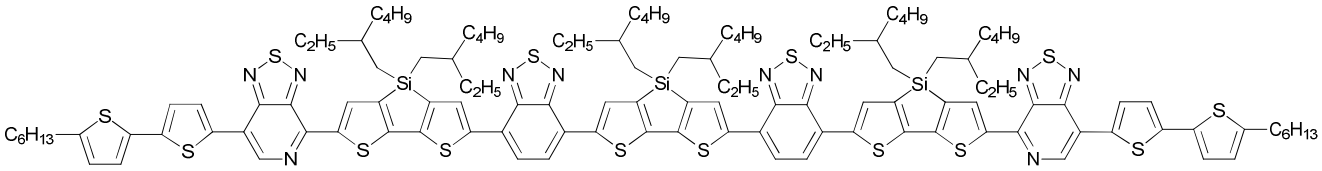

190

Scheme95